POLITECNICO DI TORINO
DEPARTMENT OF MANAGEMENT AND PRODUCTION ENGINEERING
DIGEP

VINÍCIUS DE FREITAS PACHECO

Benchmarking in additive manufacturing systems with photopolymers through part quality analysis

TURIN
2020

VINÍCIUS DE FREITAS PACHECO

Benchmarking in additive manufacturing systems with photopolymers through part quality analysis

Graduation work presented to Politecnico di Torino
in order to achieve the title of Master of Science
(Laurea Magistrale) in Mechanical Engineering.

Supervisors: Prof. Paolo Minetola
Prof. Flaviana Calignano

TURIN

2020

This work is dedicated to the Italian people, who welcomed me into their home and taught me so much over the years that I was in their country. It is also dedicated to my parents, with admiration, gratitude, and affection for the support they have always given me on my journey.

ACKNOWLEDGEMENTS

A grateful acknowledgement to Professor Paolo Minetola for welcoming me in the elaboration of the thesis, and providing all the support and equipment necessary for the research. I am also greatly thankful to Giovanni Marchiandi from Politecnico di Torino's RMLAB, for supporting the experimental development of the thesis and helping me in the most diverse obstacles.

To Politecnico di Torino and the Department of Management and Production Engineering (DIGEP), I am grateful for the opportunity of taking the Mechanical Engineering Master's of Science course, in a Double Degree partnership with the University of São Paulo.

ABSTRACT

PACHECO, Vinícius de Freitas. Benchmarking in additive manufacturing systems with photopolymers through part quality analysis. 2020. Thesis (Master of Science degree in Mechanical Engineering) – Politecnico di Torino, Turin, 2020.

Additive manufacturing, or 3D printing, has attained a widespread popularity as machines and equipment necessary for fabrication have become more accessible. These manufacturing processes, however, have each their own limitations and capabilities. For instance, every machine to its own process will be able to fabricate a similar product, with different errors and accuracies. As a result, it is important that a machine's capabilities are known prior to utilization, so that the automated operations of the additive manufacturing (AM) system are capable of producing a part with the desired dimensions and geometries. In this study, a benchmarking analysis is conducted among three different AM systems for processes involving photopolymers. Accuracy is evaluated in terms of ISO IT grades and standards of geometric dimensioning and tolerancing, in order to compare machines that produced the same reference artifact in stereolithography (SLA), digital light processing (DLP) and PolyJet.

Keywords: 3D printing; SLA; DLP; PolyJet; ISO IT grades; Additive manufacturing.

LIST OF FIGURES

LIST OF TABLES

LIST OF ABBREVIATIONS

AM	.....	Additive Manufacturing
CAD	.....	Computer Aided Design
DLP	.....	Digital Light Processing
DUC	.....	Digital Ultrasonic Cleaner
DIGEP	.....	Dipartimento di Ingegneria Gestionale e della Produzione
DSPC	.....	Direct production casting
EWL	.....	Effective working length
FDM	.....	Fused Deposition Modelling
GD&T	.....	Geometric dimensioning and tolerancing
ISO	.....	International Standardization Organization
IPA	.....	Isopropyl Alcohol
LOM	.....	Laminated object manufacturing
MPE	.....	Maximum permissible error
POLITO	.....	Politecnico di Torino
PJ	.....	PolyJet manufacturing systems
RMLAB	.....	Rapid Prototyping and Rapid Manufacturing Laboratory
RMS	.....	Root Mean Squared
SLS	.....	Selective laser sintering
STL	.....	Standard Tessellation Language
SLA	.....	Stereolithography
TPM	.....	Tripropylene Glycol Monomethyl Ether
UCB	.....	Ultrasonic Curing Box
UV	.....	Ultraviolet
USP	.....	University of São Paulo / Universidade de São Paulo

TABLE OF CONTENTS

1. INTRODUCTION

Throughout the years, society has repeatedly evolved in its ways of producing items and goods. Recalling to Sir Isaac Newton's much popularized metaphor: "If we've seen further, it is by standing on the shoulders of giants [1]". In its purest and earliest form, manufacturing, or the production of objects for use or sale, saw commencement through artisanship, hand-production methods, and a rural-based creation of items. By means of steadily improving technology and a necessity of attending demands from flourishing populations, mechanization and new manufacturing processes would emerge in Europe and the United States in the 18th century with the Industrial Revolution [2]. Handwork and manual crafting would lose space and product creation would transition into processes based in the usage of machinery and large chemical operations. This can be categorized as the beginning of an "era of power", where human labor was incapable of being akin to the performance of steam or water powered machinery. In the 19th century, with yet a second Industrial Revolution, work and energy resources would once again migrate from its present state of affairs, into methods based in combustible fuels and electricity. And finally, in the 20th century, robotics, automation and electronics would make space for new, ground-breaking technologies [3].

Manufacturing methods would mature within this time, and eventually allow for newly processed materials and the possibility of creating modernized products and goods. This evolution can be comparatively observed through specific processes, such as injection molding, for instance. The first machine of its type is a contemporary to the second Industrial Revolution: an apparatus for pyroxiline manufacturing dating back to 1872 [4]. In contrast, by the second half of the 20th century, plastic production had overtaken that of steel, and screw injection machines would account for the vast majority of all injection molding machines – an unforeseen technological scenario in earlier centuries. A synchronous, yet more accelerated comparison can be made for another manufacturing method: in 1950, Raymond F. Jones conceptualized a manufacturing procedure based on a "molecular spray" for a science fiction publisher [5]. Only two decades later, the concept of polymerizing liquid monomers in a layer-by-layer fashion to form solid objects was approached by David Jones, in a column from 1974 for a journal of scientific content [6]. And this is the time frame and conjuncture in which additive manufacturing processes would ultimately emerge.

Additive manufacturing is yet another technological advancement made possible through society's gathering of knowledge and expertise over time. It is a transformative method in which computer-aided machines are capable of fabricating objects by means of material

deposition, usually in individual layers [7]. The first manifestations of additive manufacturing emerged at around 1987, when the use of stereolithography (SLA) – a process of light-sensitive liquid resin polymerization – became patented and commercially available. In the early '90s alternative additive manufacturing processes would arise and also be commercialized, such as laminated object manufacturing (LOM, 1991), fused deposition modelling (FDM, 1991), selective laser sintering (SLS, 1992) and direct production casting (DSPC, 1993) [8]. Some of these processes, such as SLA and SLS are still very prevalent in today's market, and FDM itself is responsible for the popularization of "3D printing" as a concept and as a readily available hobby-grade manufacturing process [9]. The ideation of new additive manufacturing processes is constantly moving forward, and a timeline with the year in which these had emerged can be seen in Figure 1 below.

Figure 1 – Timeline with a select amount of additive manufacturing processes, based on patenting dates.

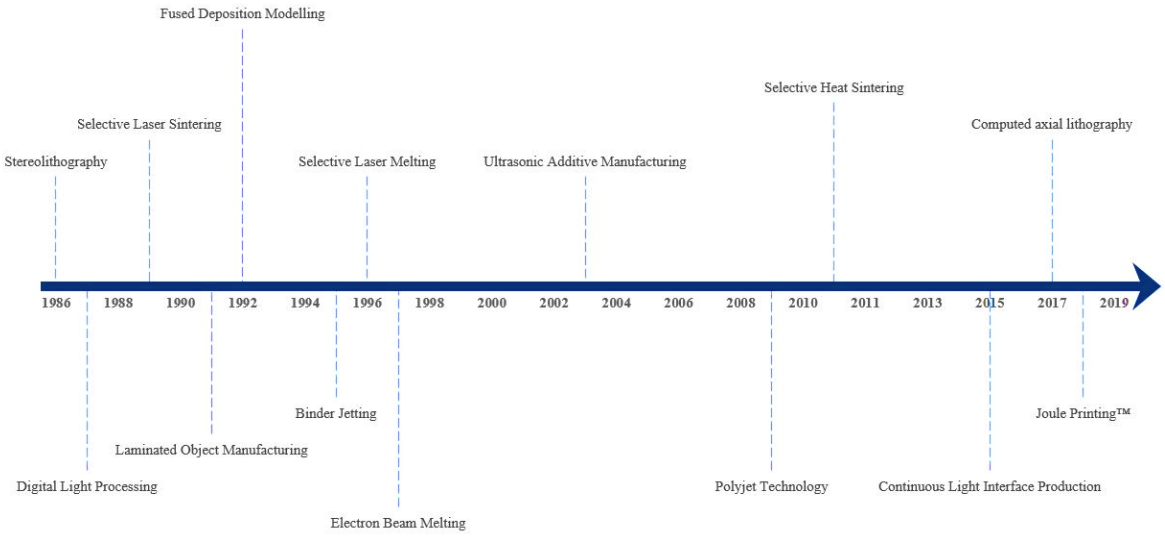

Source: [10]–[15]

Products made in 3D printing procedures such as FDM are known to be very accessible, however, at the cost of some possibly problematic characteristics of the part, such as mechanical resistance, material temperature traits or finishing quality. By opting to produce a part through alternative additive manufacturing processes, it may be possible to achieve better results within the selected attributes of the project. And that is where the field of fabrication benchmarking becomes relevant. Ever so similar, each additive manufacturing procedure, equipment or even configuration parameters will produce parts with individually distinctive

resulting characteristics. Therefore, it is important to carry out experimental observations of objects fabricated and their attributes, in order to predict the results that can be obtained in a specific manufacturing process.

In this dissertation, different machines and manufacturing processes available at Politecnico di Torino (Turin, Italy) will be evaluated with regards to their capability of producing parts with dimensional and geometric accuracy comparable to the CAD designs that are presented for fabrication. Machines of three different manufacturing processes will be evaluated within this study: stereolithography (SLA), digital light processing (DLP) and PolyJet manufacturing processes. All of these processes are based on liquid resin photopolymers that are cured in layers by the emission of ultraviolet light, in order to form a three-dimensional object. A single test artifact model will be designed according to the boundary conditions of the analysis, and manufactured in every machine. It is interesting to include in this test part a range of different dimensions and basic geometric features.

According to Minetola *et. al*, when dealing with accuracy and tolerances, a convenient method of analysis is that which is proposed by the standard International Tolerance (IT) grades, proposed by the International Organization for Standardization (ISO) [16]. These serve as a comparison reference for Geometric Dimensioning and Tolerancing (GD&T) of different processes, and are capable of summarizing results of a benchmarking study for rapid prototyping or additive manufacturing machines. After inspection of the replicas produced, it will be possible to discriminate a measurable indicator for each machine, and therefore establish which of the equipment at Politecnico di Torino is capable of producing a more accurately correct three-dimensional object.

2. OBJECTIVE

The main objective of the dissertation at hand is to evaluate the dimensional and geometric accuracy and manufacturing overall performance of three distinct additive manufacturing machines available at Politecnico di Torino's Rapid Prototyping and Rapid Manufacturing Laboratory (RMLAB). The main constraint to the study is that each of the manufacturing apparatuses analyzed must refer to a fabrication method based in the use of photopolymers and resin-based curing of a 3D part. Within the direction of academic intent, this thesis will commit to a detailed description of each manufacturing method approached by the equipment available.

In order to create a GD&T benchmarking analysis of each machine, a reference study of existing test artifacts must be conducted. This is done in order to ensure an efficient part design that will allow for extraction of relevant fabrication parameters, and an overall understanding of how engineering benchmarkings are structured for manufacturing processes. As a concluding objective of the dissertation, the experimental data collected must be evaluated with the intent of classifying each machine and process available at RMLAB with respect to the relevant fabrication attributes selected.

3. ARTIFACT DEVELOPMENT

Accuracy performance of additive manufacturing and rapid prototyping machines is evaluated through the dimensional and geometric accuracy of their manufactured parts. Therefore, the process of selecting a part to be produced occupies an important role in benchmarking studies of manufacturing equipment.

In this section, an in-depth analysis of existing reference parts and accuracy-related topology will be conducted. Subsequently, the most feasible artifact solution is to be used in the accuracy benchmarking study for the referred machines and processes.

3.1 Formerly proposed test artifacts

Various reference parts and artifact specimen have been proposed in previous literature in an attempt to standardize and ensure completeness of benchmarking studies. Throughout the years, researchers would add new geometric features and qualities to test parts in order to compare the capabilities of various processes [17]. A group of diverse benchmarking artifacts is analyzed below in order to determine which existing artifacts are interesting starting points for working with SLA and other processes with photopolymers.

3.1.1 User Part Based Models

Some early approaches to additive manufacturing benchmarks would use a test specimen called the “user part”. It is one of the first parts used for qualitative and quantitative assessment of accuracy in stereolithography systems, proposed by Gargiulo [18] in the first European conference of Rapid Manufacturing. The design (Figure 2) was conceived in 1990 with the intent of evaluating more elementary qualities of machines, such as accuracy within a specified XY plane of reference. Unlike other contemporary models, such as the 1991 Kruth model [19], the User Part was simple enough to be standardized and used as a foundation for all-process benchmarking models.

Figure 2 – User part CAD model.

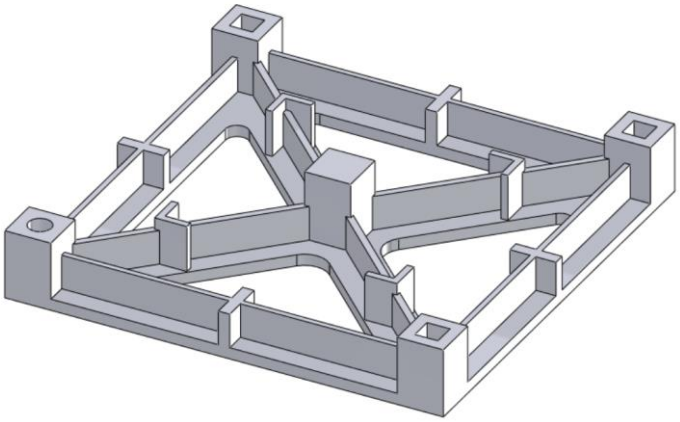

Source: [18]

This part has been used in benchmarks for stereolithography for as early as 1995 with Ippolito *et. al* [20], and the results of this analysis in the field have been used as a reference for International Tolerance (IT) Grades for years.

Since then, various user part based models have been proposed with the intention of progressing its quality of analysis in manufacturing systems. The Mahesh *et. al* model [21] is one of the more interesting ones within a 10 year time frame, in which 6 early models – including Kruth, Gargiulo, and Ippolito – are studied before part proposal.

Figure 3 – Mahesh part CAD model.

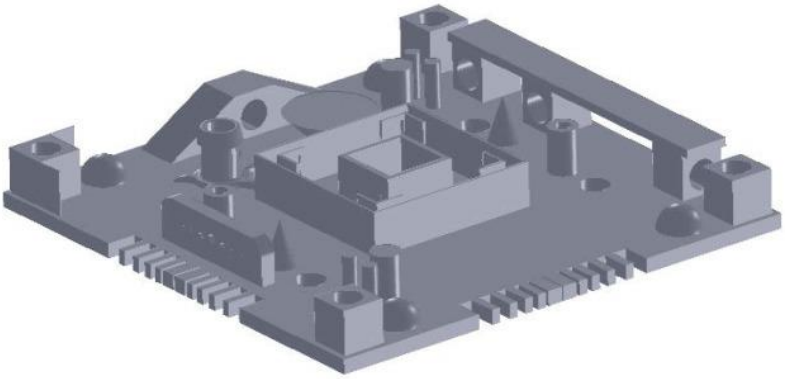

Source: [21]

The Mahesh model (Figure 3, above) focuses on introducing new geometric features to a user part's planar and standardizable layout. Whereas the user part would evaluate only planar geometries, the inclusion of cubes, beams, cylinders, spheres, and cones in both

solid and hollow configurations would corroborate completeness in geometric analysis. In order to make the part standardizable, existing references of straightness (ISO 12780), roundness (ISO 12181), flatness (ISO 12781), cylindricity (ISO 12180) and CMM standards were used in the proposal.

The inclusion of multiple geometries became a tendency in artifact design, where there was an approach of using standard 3D library features (such as spheres, cylinders, prisms, cones, etc.). Part designers would be influenced by previous work and a common set of "rules" seen in the field (see Section 3.1.2), and layouts would then preserve a rectangular or square base with features that attempt to reproduce "real" geometries [17].

3.1.2 Moylan Based Models and Rules for Artifact Design

In 2012, Moylan *et. al* from the National Institute of Standards and Technology (NIST - Gaithersburg, USA) reviewed existing test parts with the intention of proposing a new artifact for standardization. The purpose of the study was to consolidate methodology that would corroborate and facilitate the adoption of additive processes in functional and industrial applications [17]. Therefore, working towards analyzing part accuracy, surface finish, process speed and material proprieties can be kickstarted through standardizing a test part.

Throughout their work, Moylan *et. al* describe a set of "rules" for test artifact design. Their analysis accounts for various considerations made in prior work, such as standards proposed by Richter & Jacobs, Kruth and Byun. According to Moylan *et. al*, test artifact design should [17]:

- Consider part sizing in order to test performance discrepancies near the edges of the build platform as well as near its center;
- Have a substantial number of small, medium, and large features. If possible, should attempt to determine a minimum feature size attainable;
- Not take too long to build;
- Not consume a large quantity of material;
- Be easy to measure;
- Emulate many features of a "real" part (e.g., thin walls, flat surfaces, holes, etc.);
- Include features along various different axes;
- Have simple geometrical shapes, allowing perfect definition and easy control of the geometry;

- Require minimal post-treatment or manual intervention if possible (i.e.: no support structures);
- Allow repeatability measurements;

These “rules” consist of recommendations and good practices in order to allow for analysis completeness. In some cases, however, it is optimal to observe different scenarios to which a part is subjected, allowing for design flexibility in this subject.

Moylan *et. al* developed an artifact based on 8 items of primary importance: straight features, parallel and perpendicular features, circular and arced features, fine features, and freeform ones. Features should be included as both holes (negatives or cavities) and bosses (solid, standing structures) in various planes and the correct locations and orientations. The design can be seen in Figure 4 below.

Figure 4 – Moylan et. al CAD model (modified).

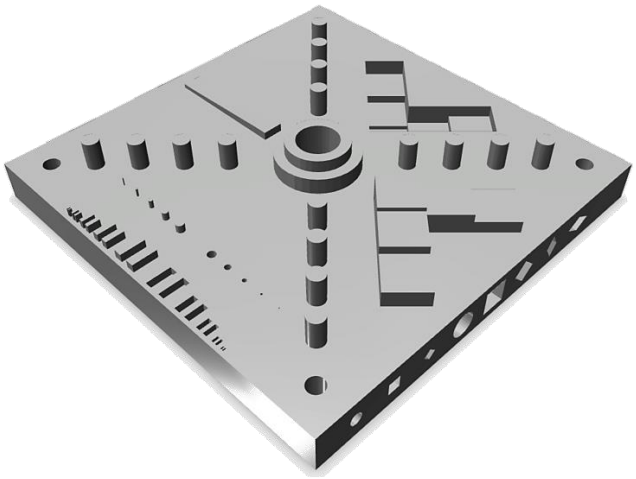

Source: [22]

This design has been used as a reference since it was conceived, however, the study in hand focused on the accuracy evaluation of SLS processes. Thus, it was opted to evaluate some qualities through indirect measurement analyses. Directly spherical and tapering geometries are not present throughout the part. Also, some geometries are included as lateral features, which may not be an optimal procedure for some processes that may deal with resin material.

The Cruz Sanchez *et al.* benchmarking study from 2014 attempted to include more geometries such as hemispheres and inclines in an accuracy evaluation for FDM open-source 3D printers [23]. The design (

Figure **5**) is a modified version of the Moylan et al. 2012 standardized part, that includes 15 different family groups labeled through a lettering system (A-O) and a number for each individual geometry.

Figure 5 – Cruz Sanchez et al. CAD Model with identification ID's.

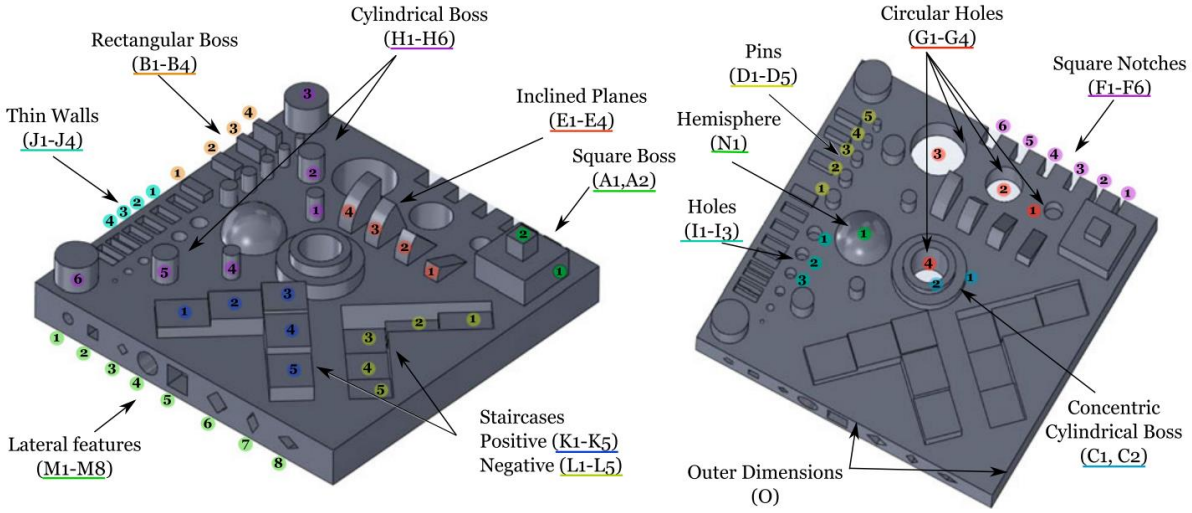

Source: [23]

Within a different configuration setup, Minetola's benchmarking study for additive manufacturing systems uses a similar concept to that of Cruz Sanchez and Moylan. A planar base is used in a square or rectangular setup with the inclusion of various geometries (Figure 6). It is very interesting to observe how efficiently Minetola *et al.* places each elements within the available space. Cruz Sanchez and Minetola attempt to create a special configuration that would satisfy the good practices of minimizing material waste – through an efficient geometries-over-area ratio – while still contemplating CMM limitations [16].

Minetola's approach to improving geometry allocation also uses a concept of element division into a negative (hollow half), and positive half (bosses). This is noticeable in geometries such as hemispheres (SP_i) and horizontal cylinders (CL_i), where the same space that would be occupied by a full feature is optimized into containing two versions of a measurable element. This is a functioning method due to the fact that CMM measurements are results of interpolated measurement data, and therefore a full feature is not indispensable – only enough points of interpolation are mandatory [24]. It is also interesting to notice how tilted planes can be found in almost every derivative feature of the part (TP_i).

Figure 6 – Minetola et al. CAD Model with identifications.

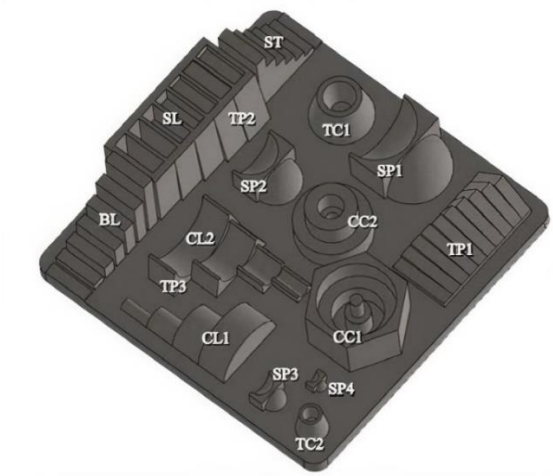

Source: [16]

3.1.3 Other Test Artifacts

A contemporary analysis to that of Moylan *et al.* is the Fahad & Hopkinson study also performed in 2012 [25]. In this research, various existing parts are analyzed and compared in terms of their principal functionalities and benchmarking results. Among others, the mentioned models of Kruth, Mahesh and Ippolito are observed as adequate, however each with correlated limitations. An interesting analyzed model is that of Juster & Childs [26], where the concept of free-form geometries is included, as seen in Figure 7. However, due to difficult standardization, symmetry and repeatability, this concept can be seen as a limitation to model designs.

Figure 7 – Juster & Childs CAD Model.

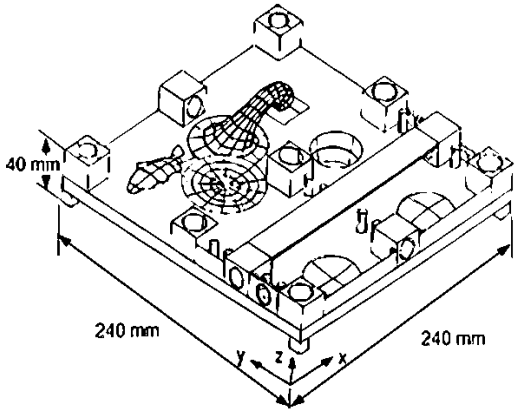

Source: [25]

The final artifact proposed by Fahad & Hopkinson presents itself on thin a rectangular base with small scale geometries (Figure 8). It is a benchmarking part that includes all necessary features in a compact manner, and prioritizes accuracy evaluation through repeatability of features by incorporating geometries in a symmetrical arrangement. This design is suited for fabrication within different additive manufacturing processes such as Fused Deposition Modelling, Stereolithography and Selective Laser Sintering.

Figure 8 - Fahad & Hopkinson CAD Model.

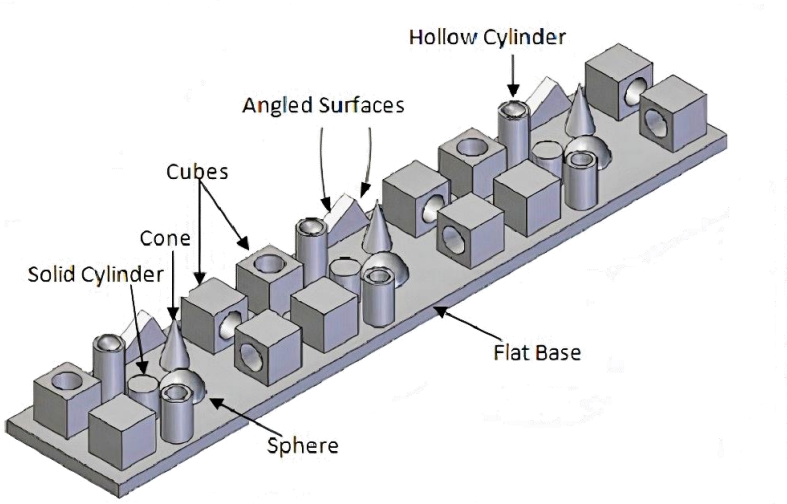

Source: [25]

3.2 Design Points of Interest

After conducting a case study of previous work and existing artifacts it is important to establish criteria and key points of interest to the specific benchmarking work in progress. The 5 following design points were indexed in order to evaluate the particularities of the study at hand:

- Benchmarking type considerations;
- Machine and process considerations;
- Measurement and post-processing equipment considerations;
- Geometries, features and part characteristics desired;
- Process error listing and analysis.

All key points will be analyzed with regards to Chapter 3.1.2, where Moylan *et. al* “rules” and good practices for artifact design were introduced.

3.2.1 Benchmarking Type Considerations

A benchmark is a comparison of performance in similar yet different organized structures (such as companies machines, equipment, processes etc.). Such comparison requires a reference standard with regards to which structural aspects are being observed. In mechanical engineering, benchmarkings can be used to contrast material proprieties, manufacturing accuracy, finishing, repeatability, geometrical resolution and even design or working conditions of parts [25]. According to Mahesh *et al.*, benchmarkings in additive manufacturing can be classified within three categories:

- Process Benchmark: used to establish process related parameters (part orientation, support structures, layer thickness, speed, etc.).
- Mechanical Benchmark: used to analyze the mechanical properties (tensile strength, compressive strength, creep, etc.);
- Geometric Benchmark: used to measure the geometric features of a part (i.e. tolerances, accuracy, repeatability and surface finish);

Within this dissertation, a geometric benchmarking will be realized in order to evaluate the accuracy and tolerances of parts produced by additive manufacturing processes and machines in stereolithography (SLA), digital light processing (DLP) and PolyJet equipment. Therefore, the test part's design should focus on optimizing observability of characteristics such as finishing, tolerances and geometric accuracy.

3.2.2 Stereolithography (SLA) machine used

The first machine benchmarked in this study will be the Sharebot Antares. Sharebot is an Italian based company that offers AM technology services in FDM, resin-based manufacturing and powder sintering. The Antares is one of their older product models in photosensitive resin-based manufacturing. The printer is categorized as a high-precision professional SLA working tool for large model fabrication. Further details about the machine can be found in **Table 1** below.

Table 1 – Sharebot Antares printer specifications.

ANTARES TECHNICAL DETAILS	
Materials	PR-S, PR-T
Printing Volume	250 x 250 x 250 mm
XY resolution Layer	±0.1 mm (100 micron)
Layer thickness	> 0,05 mm
Laser Power	150 mW
Wavelength	405 nm
Dimensions	500 x 500 x 1.400 mm
Weight	120 kg
Slicing software	Included

Source: [27]

At first, it is important to be aware of the machine's size. Since the print volume is of $250\ x\ 250\ x\ 250\ mm$ and the Sharebot Antares is a fairly large machine (Figure 9), dimensional limitations are not very concerning in terms of artifact design. As observed by Moylan *et al.* existing test artifacts have considerable size variations, however the largest observed part was of $240\ x\ 240\ mm$ in a square-based XY area [17].

Figure 9 - Sharebot Antares SLA printer.

Source: [28]

3.2.3 Digital Light Processing (DLP) machine used

For this study, the equipment observed will be the Sharebot Rover DLP Printer (Figure 10). The Sharebot Rover is a machine that proposes compact desktop manufacturing. Therefore, this machine contains a small scale printing plate of only $62\ x\ 115\ x\ 100\ mm$ [29], which is a relevant parameter in order to define the maximum admissible build volume for a test artifact. Further details about the Sharebot Rover can be found in Table 2 below.

Table 2 – Sharebot Rover printer specifications.

ROVER TECHNICAL DETAILS	
Materials	ASTM, S-Series
Printing area XY	62 x 115 x 100 mm
XY resolution Layer	47 micron
Layer thickness	20 - 100 micron
Matrix 2K	1440 x 2560 pixels
Wavelength	405 nm
Dimensions	460x353x200 mm
Weight	15 kg
Slicing software	Included

Source: [29]

Figure 10 – Sharebot Rover DLP printer.

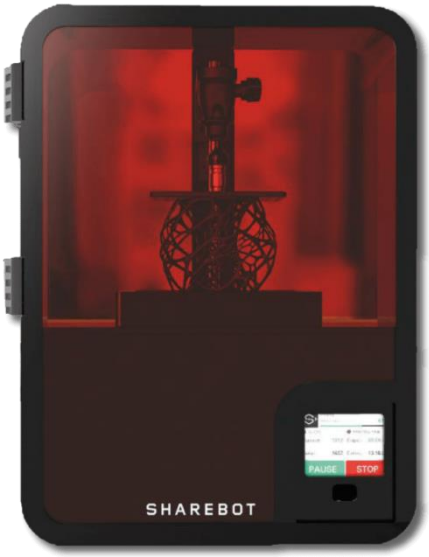

Source: [29]

3.2.4 PolyJet technology machine used

For the benchmark in hand, the equipment in study for PolyJet manufacturing is the Stratasys Objet30 Prime (Figure 11). The Objet30 Prime is a small scale machine designed for both beginner prototyping or professional applications in engineering teams. It is also designed for use of resins that encompass characteristics ranging from material strength to aesthetics and transparency [30].

Figure 11 – Stratasys Objet30 Prime PolyJet printer.

Source: [30]

The Objet30 Prime has a maximum build size of $294\ x\ 192\ x\ 148.6\ mm$ (XYZ; approximately $8.3\ L$ of total build volume). Therefore, this is one of the larger machines in the study and the build area is not a major concern.

The expected accuracy of the machine, however, is of $0.1\ mm\ (100\ \mu m)$ or $\pm 0.06\%$ length if greater. Such value varies depending on part geometry, size, orientation, material, and post-processing method. Also, layering can be set to use heights of 16 or 28

microns, which will also influence the final part precision [31]. Further information about the printer is summarized in Table 3 below.

It is also worth noting that this machine will be able to manufacture the test part without the use of supports. Therefore, the need for a non-measured expendable support surface would not be a concern within artifact design in PolyJet.

Table 3 – Objet30 Prime PolyJet printer specifications.

OBJET30 TECHNICAL DETAILS	
Materials	Vero Series and multi-compatibility with other resins
Support Material	SUP705/6
Maximum Build Size (XYZ)	294 x 192 x 148.6 mm
System Size and Weight	82.5 x 62. 59 cm; 106kg
Resolution (XYZ)	600 x 600 x 1600 dpi
Accuracy	0.1 mm + variation for geometry, size, orientation etc.
Minimum Layer Thickness	16 microns; 28 microns for Tango materials
Build Modes	Draft (36µm), High Speed (28µm), High Quality (16µm)
Software	Windows XP/7/8
Operating Conditions	Temperature: 18 - 25°C; Relative humidity: 30-70%
Power Requirements	50-60 Hz, Single Phase (100-200V, 7A) or (200-240V, 3.5A)

Source: [30]

3.2.5 Measurement equipment and design parameters

Coordinate measuring machines, or CMMs, are devices that evaluate height, depth, width, and overall geometries of a part through using a probing tool onto an inspected surface. Today, probing can be done in various manners, such as physical contact, optical based measuring, and even white light emission. These machines can be manually operated or have numerical control systems similar to automatic CNC manufacturing machines [32].

By means of probing various points of a part for data collection, these machines are capable of interpolating discrete Cartesian positions into geometric parameters and GD&T specifications. This procedure can be categorized as a “virtual” or indirect measurement method, where virtual points, lines and geometric references are created through data acquisition. This type of evaluation can be difficult with other measuring machines, but it is made possible through the use of 3D coordinate system CMM machines. A typical contact CMM measuring machine is composed of four elements, as presented in Figure 12. The most important element is the probing tool (Figure 12– B) or stylus, where a high hardness material is used in a spherical configuration to approximate to the measured part. The most common materials for probe tips

are ruby and zirconia. This tip is generally attached to an aculeiform rod that allows for further reach into specific bodies and geometries.

Figure 12 – Generic Coordinate Measuring Machine Representation.

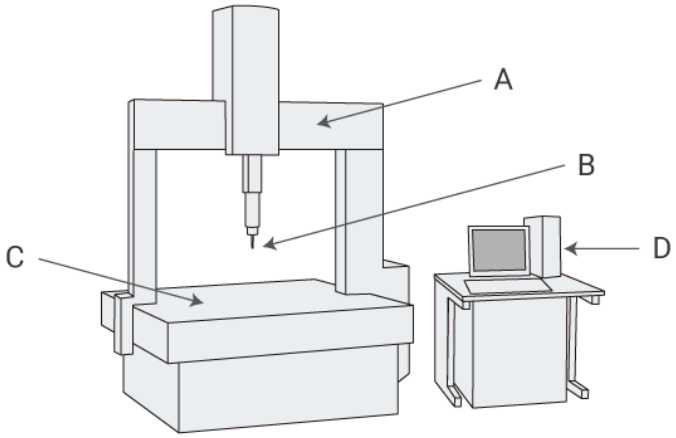

Source: [32]

The moving bridge (A) and stage (C) are the structural elements of the machine. Whereas the moving part of the CMM can be either the table or the probe-attached structure, depending on the model available for use. In general, the bridge is the mobile component , since it facilitates positional processing and calibration. Compressors are used for pressurized air in order to drive the machine and relieve weight for measuring procedures. The stage, on the other hand, is often a heavy surface of plate made of stone, such as granite, so that highly accurate measurements and machine stability becomes possible. This also affects calibration and long-term use of the machine since the material is not easily subject to strain, distortion, and scratching.

Finally, the control and processing unit (D) is where CMM software is stored and results are presented. Modern machines are capable of using computer-based storage units, where data can be stored and processed simultaneously. To the contrary of earlier designs, manual annotation, and post-interpolation of gathered data is generally not necessary. The CMM software can improve usability is various manners, such as measuring time, quality control, man-to-machine interfacing and even CAD data incorporation for comparisons. Therefore, working with different CMM software can largely influence results.

The key working points of a contact based CMM have been reviewed since the measurement machine available for this dissertation is very similar to that which was described. The equipment that will be used is a manually operated Poli Light Man measuring machine.

Figure 13 – Poli Light Man CMM Machine.

Source: [33]

The Poli Light Man is one of the older models from its product line, and therefore does not necessarily have advantages available in more modern machines [33]. According to the manufacturer and the international standard defined in ISO 10360-2:2009 [34], the Poli Light Man machine has the capability of performing measurements with a MPE 5 + 10*L accuracy. This is a statement of the machine's maximum permissible error (MPE) length of measurement. Therefore, it is expected that the Poli Light Man's length measurement errors (E_l) will not exceed the maximum permissible error of length measurement, and $E_l < 5 + 10L$ [µm]. Further detail and information about the machine can be found in Table 4 below.

Table 4 – Poli Light Man specifications.

POLI LIGHT MAN DETAILS	
Operation Type	Manual CMM
Movement Type	Air pressure sliding
Positioning Method	Mechanical locks and micrometric adjustment on axes
Coordinates (XYZ)	300 x 280 x 250 mm
Accuracy	MPE 5 + 10 * L (ISO 10360-2:2009)
Default Probe	Renishaw 1mm
Measurement Software	Poli 3D GEOSOFT
Machine Base	Black Granite

Source: [33]

Another measurement parameter of the CMM that is relevant for part design is that of the stylus to be used. Styli are the tips of probing tools in contact coordinate measuring machines, where a measuring rod with a spherical head attached to its extremity makes physical contact to the component under measurement [35].

Choosing a stylus is of paramount importance for artifact design in terms of geometric and dimensional decision making. General stylus selection practices recommend short non-jointed styli with spherical sizing specific to the type of analysis in hand. The length of a stylus influences in errors due to material deflection. A longer stylus is prone to deflection or bending, inducing errors that can be minimized through the usage of a shorter stylus overall length. The same principle can be applied to jointed styli, where builds that contain joints or extensions can induce deflection points and localized movement error. Finally, the diameter of the probing sphere influences how contact affects readings. Larger spheres maximize clearance from the part, reducing false triggering, while a smaller probe will maximize the impact of surface finishing and imprecision. A general overview of relevant stylus parameters can be seen in Figure 14 below, such as its threading (A), effective working length (B), overall length (L) and diameter (D).

Figure 14 – Stylus dimensions for terminology.

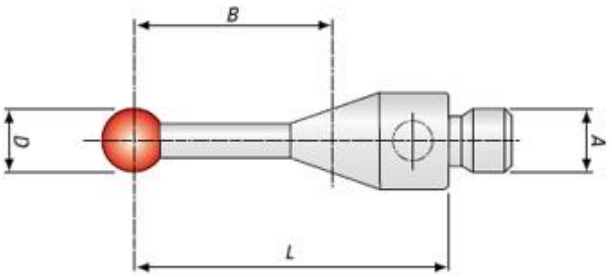

Source: [35]

For a benchmarking study that assesses dimensional precision and geometric accuracy, and especially one within additive manufacturing, it is important to use a small enough spherical probing tip. This will allow for examination of the parts inaccuracies due to surface roughness, building precision, layering, among other factors. Therefore, the preeminent parameters of the stylus to be evaluated are its diameter and effective working length.

Each stylus has an Effective Working Length (EWL, represented as “B” in Figure 14), which is expected the working length of the stylus, regarding its possible penetration into part geometries [24]. This length is measured as that to which the tip can achieve before the

stylus shaft can contact the component, as seen in Figure 15. However, this dimension includes the tapered cone frustrum used in the shaft, and for very small parts, it may be more relevant to consider only the stylus' rod length.

Figure 15 – Effective working length of a measuring probe.

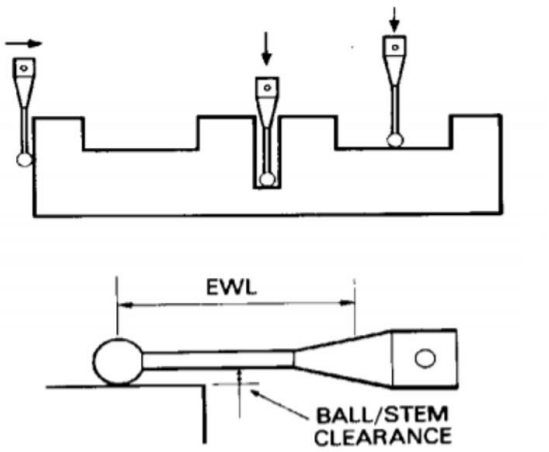

Source: [24]

The stylus available at Politecnico di Torino for this study is a ruby-point 1mm Renishaw spherical probe, as referenced earlier in Table 4. It has an EWL of 12 mm, composed by a 7 mm rod and tapered cone. Therefore, artifact design should consider a maximum depth of the rod length for geometries in the vertical Z axis.

Figure 16 – Renishaw 1mm probing tool at Politecnico di Torino.

3.2.6 Geometries, features and part characteristics

As seen in the references study, a manufacturing benchmark will use a reference part with specific geometries that evaluate different types of machine characteristics. Geometries will vary from simple, linear shapes, to those that are composed of tapered or free-form elements. In this chapter, the geometries seen in past work will be analyzed as to their

purposes, limitations and what are the expected analytical results that each element will offer to an additive manufacturing benchmark.

It is also important to note that some benchmarking attributes are not necessarily geometries, but a derivative of the interaction between equal geometries or diverging ones. A clear example can be that of parallelism. This is a part characteristic that is evaluated through a specific hypothetically perfect reference. Concentricity is another characteristic that also demands a referencing circumference, and is associated to geometrical elements such as circular holes and embossed cylinders. This type of part characteristic is useful for manufacturing benchmarking, however, is not generally be considered as a geometric element, but a featured by-product.

The geometries, features and part characteristics that will be evaluated for inclusion in the artifact of this study have been summarized in Table 5 below:

Table 5 – Geometries, features and part characteristics evaluated.

Geometries, features and part characteristics	
Planes	Planes, Inclines, Circular Rings, Edges
Cylinders	Cylinder Boss, Concentric Cylinder Boss, Pins, Holes, Horizontal Cylinders, Vertical Cylinders
Cones	Cones, Truncated Cones, Tapering
Spheres	Spheres, Hemispheres
Prismatic features	Rectangular Boss, Square Boss, Prismatic Boss, Staircase, Lateral Features, Fine Features, Brackets, Hollow Prismatic Features
Derivative Characteristics	Parallelism, Straightness/Flatness, Concentricity, Roundness, Perpendicularity, Slope (or 3D Contour), Surface Roughness, Porosity, Layering

3.2.6.1 Planes

A plane is one of basic concepts in geometry. In accordance to the Encyclopedia of Mathematics, a plane can be defined as a flat two-dimensional surface, and can be regarded as

a set of points, a set of straight lines, a combination of a point to an axis, among other mathematical axioms and definitions. In practice, however, a plane will be defined as a finite surface that will likely contain imperfections and inaccuracies, such as a natural roughness and meager curvature.

As seen in formerly examined bibliography, in terms of manufacturing benchmarks, planes are an important feature that will be present in most formerly proposed artifact elements, and naturally derive off of other geometries as well. Therefore, a plane will be seen as a geometric configuration that is capable of evaluating secondary derivative attributes such as flatness, parallelism, perpendicularity, sloping, and general features involving angularity. As will be further detailed in Chapter 4, planar features are also an important element for CMM calibration.

In artifact design, planes may be presented in various configurations, such as the contrast between a standard vertically oriented feature to a horizontal one. In terms of form, planes may be present in different geometries, due to the nature of prismatic elements, which will be listed in the upcoming chapters. A plane will naturally derive off of geometric extrusions, being available for evaluation atop of embossed features, walls, hollow features, and holes.

3.2.6.2 Cylinders

Cylindricity is an important feature to be evaluated in manufacturing benchmarkings. Physicist Eric Weisstein defines the term “cylinder” as effective for either a mathematical surface that is bound within two planes, and a solid that would be enclosed by this very generalized cylinder [36]. This last definition can also be categorized as a prism in itself. However, in practice, cylinders can be presented in various forms: different orientations, embossed, hollow, holes, among, quarter cylinders, etc. As presented Table 5, there are many possible configurations to a cylindric geometry, and for practical reason, a cylinder will be categorized as a general geometry formed by means of a hypothetical integral displacement of a circumference, filled or in contours.

The objective of a cylindric feature in a manufacturing benchmark is that of evaluating the machines capability of producing cylinders and circular features. A feature’s cylindricity (“circular straightness”) can be used to evaluate error and alignment within the machines axes. Other factors such as roundness, axial positioning, capability of producing radii, coaxiality and repeatability can all be evaluated through the use of cylinders and combined circular features.

3.2.6.3 Cones

According to ISO 3040:2016 cones are a product of a right-angle rotated triangle, where any intersection by a plane perpendicular to the axis of the nominal cone is a circle [37]. The truncated cone that is represented by the standard is characterized by a finite length that connects a point (or cone tip) to its base circumference, with the largest possible radius in the feature.

Cones are an interesting feature to be analyzed since they are largely subject to different types of errors that may occur in additive manufacturing, such as the "staircase effect" and "missing features" effect (further detail in Chapter 5.3.1). This feature, however, is not largely evaluated in prior bibliography in terms of its performance in IT Grades.

3.2.6.4 Spheres

Some industries are interested in fabricating spherical parts or components with spherical features in additive manufacturing, such as businesses related to roller bearings that may be concerned about weight, tolerances, or material performance [38]. Spheres can be defined as "a solid figure that is completely round, with every point on its surface at an equal distance from the center", according to the Oxford dictionary [39].

For the purpose of a benchmarking, there is little research on the evaluation of accuracy for spherical features in additive manufacturing. This feature can be used for the definition of precision in circular dimensions for IT Grades, and can evaluate how likely the machine or process is to produce a three-dimensional spherical object. This geometry can be included in artifact design as a probe-like supported sphere or truncated sphere, and in the latter case the approach used by Minetola et. al of including hemispheres or quarter-spheres is recommended for conciseness and optimization of base area.

3.2.6.5 Prismatic Features

Prismatic features can be understood as "a solid figure with ends that are parallel and of the same size and shape, and with sides whose opposite edges are equal and parallel". Therefore, this feature encompasses extrusions such as: rectangular bosses, square bosses,

triangular bosses, solid cylinders (circular boss), and other features that would only require the protrusion of a basic shape.

These features can be utilized in order to evaluate flatness, circularity, parallelism, the capability of producing parts with correct heights, and the capacity of creating small or fine features. Thus, this is an interesting feature to be included in artifact design, since various data points can be extracted from a single feature in measurement and analysis.

3.2.6.6 Derivative Characteristics

As mentioned in Chapter 3.2.1 manufacturing benchmarkings can evaluate various capabilities of a machine or process. Characteristics such as part strength, repeatability, time until fabrication, etc. are evaluated in this type of study, and in a geometric benchmarking the inclusion of specific geometries and features enables the inspection of derivative characteristics that depend on one or more features.

Parallelism can be evaluated between opposing planes and can indicate how consistent the process is in terms of fabricating a part with correctly oriented geometries. Similarly, flatness and straightness can be evaluated in terms of how accurate the production of planes and lines are, respectively. And in identical fashion, quality of layering and the surface roughness obtained are important parameters for manufacturers. In terms of circular features, concentricity and roundness can be evaluated in features that have radii as their primary dimensional parameter. Finally, sloping and angularity are characteristics that are interestingly observed in benchmarkings, due to recurrent errors in additive manufacturing such as the "staircase effect".

3.2.7 Error listing and analysis

In rapid prototyping there are various characteristics of fabrication that may affect part accuracy. According to a classification by W. Cheng et al. there are six sources of errors during the building of a part: Tessellation; Missing feature errors; Overcure; Distortion and shrinkage; The "container effect"; and the "staircase effect" [40].

Tessellation – the initial source of errors listed – is an effect caused by the conversion of a computerized model into a fabricated part. Most CAD packages generally construct parts using mathematical representation, which allows for continuity, but slicing software creates layers based on an approximated triangulation of mesh data in STL files. This

problem can be alleviated by using other file formats. “Missing feature” is an effect related to constant slicing thickness and fabrication over a singular layer height. Since elements may not be multiples of layer thickness, this effect amounts to potential negligence of geometrical features of the part, and hence results in a loss of control over the accuracy of the manufactured part [41]. Overcure, also known as cure-through or the “back-side effect”, refers to errors caused by unaccounted-for light propagation, that may cause undesired curing in incorrect zones [42]. Distortion and shrinkage are related to material proprieties, topology of the fabricated part and the usage of support structures. The “container effect” is related to surface tension generated around an enclosed region, which would not allow for draining of retained material [43]. And finally, the “staircase effect” is a source that can appear along inclined surfaces in layer manufacturing techniques [44]. It is a decrease in accuracy that is attributed to the contrasting geometries of the original part and that which is layered in fabrication, as per Figure 17 below.

It is important to be aware of these potential errors in order to design the benchmarking analysis that will be conducted. The presence of these errors will be observed as results in Chapter 5.3.

Figure 17 - Staircase effect in layer manufacturing using variable layer thickness.

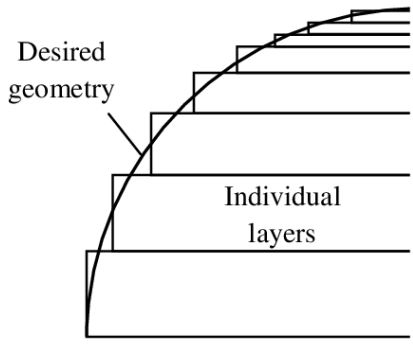

Source: [45]

3.3 The Proposed Part

The artifact was designed considering the points of interest and considerations presented in Chapter 3.2, and an overview illustration is presented in Figure 15 below. Its dimensions, geometry and global features will be justified within the subsequent sections. The main existing references for the designed artifact are those of Minetola et al. [16] and the Cruz Sanchez et al. design [23].

Figure 18 – Proposed artifact part.

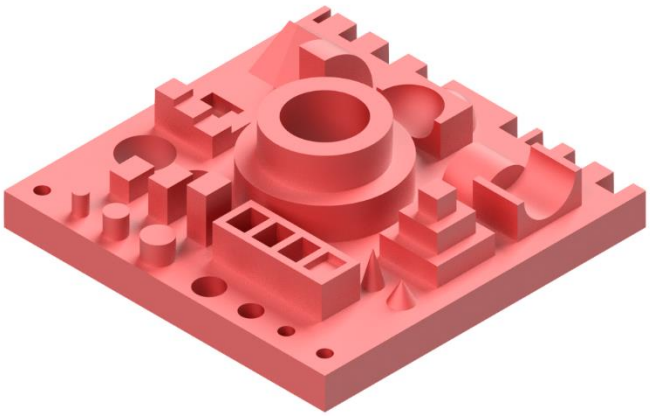

3.3.1 Dimensional Design

As seen in sections Benchmarking Type Considerations, Stereolithography (SLA) machine used and Digital Light Processing (DLP) machine used, each machine has dimensional limitations that must be considered within the artifact design. A first approach to the conception of a test part must be done regarding its principal outer dimensions. As seen in Chapter 3.2.3, the Digital Light Processing machine (Sharebot Rover) has a printing area of 62 x 115 x 100 mm. Therefore, the Rover is composed by the smallest available build platform, and this will be the main dimensional restriction of the test piece.

Since additive manufacturing processes are based in a successive deposition of material layers, most times there is a necessity for the use of supporting structures, which can be considered in artifact design. A model may contain bridges – structures that are not supported and connect two sides of the same part – or overhangs – non-supported, drawn-out extremities (Figure 19). However, it is a general rule of thumb that not all overhangs and bridges require supports. Considering that there is an imperceptible offset in the stacking of consecutive layers, it is possible to produce overhangs that are not overly tilted with respect to the vertical axis. Any geometry that has an angle below 45 degrees to the Z axis can be supported by previously produced layers [46]. Therefore, it is important to consider a potentially tilted artifact when establishing artifact dimensions.

Figure 19 – Comparison between 45° and 90° overhangs and supporting necessities.

Source: [46]

Additionally, an angled artifact and even the prioritization of using support structures may be an interesting consideration in some resin-based additive manufacturing processes.

Having stated these boundary conditions for the sizing problem of the artifact, it is finally possible to consider its outer dimensions and design. A rectangular shaped base was arbitrarily selected for simplicity and clarity of dimensional calculation.

Figure **20** illustrates the dimensional analysis for the artifact part being positioned in a generic arrangement, and (1) states the length $L_i = L(i)$ as a function of a possible axis $i = \{x, y, z\}$, where it is assumed $x \geq y \gg z$:

$$L_i = i * cos(\theta) + z * cos(\theta - \frac{\pi}{2}) \quad (1)$$

Figure 20 – Generic arrangement of the part with regards to the build tray.

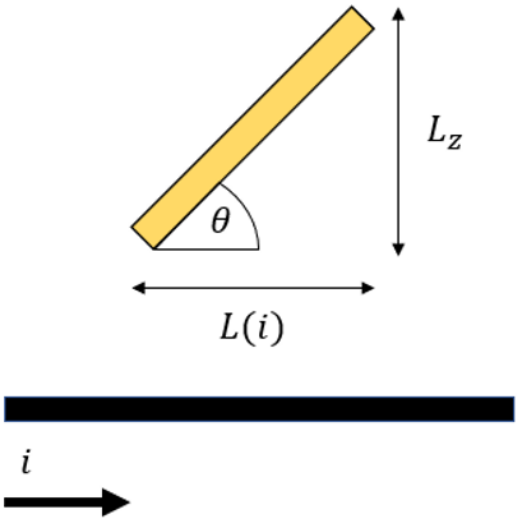

$$L_x = x * cos(\theta) + z * cos\left(\theta - \frac{\pi}{2}\right) < 115\ mm \quad (2)$$

$$L_y = y * cos(\theta) + z * cos\left(\theta - \frac{\pi}{2}\right) < 62\ mm \quad (3)$$

$$L_z = x * sin(\theta) + z * sin\left(\theta - \frac{\pi}{2}\right) < 100\ mm \quad (4)$$

It is desired that artifact design is planned out regarding outside dimensions lower than those accepted by the Sharebot Rover and the equations (2) to (4) presented above. Since the minimum dimensional limitation is of $62\ mm$ according to the y-axis of the Sharebot Rover, it will be arbitrarily defined that the principal outer dimension of the test part will be of around 80% this coordinate measure. Therefore, the square-shaped artifact will be proposed as a $50\ x\ 50\ mm$ part. According to (2), (3) and (4), calculations were made for a $50\ x\ 50\ x\ 15\ mm$ part, and results can be seen in Table below.

Table 6 – Main dimension calculations according to Equations (1) to (4).

x (mm)	50
y (mm)	50
z (mm)	15
θ (deg)	45

Lx (mm)	45.96
Ly (mm)	45.96
Lz (mm)	24.75

In Chapter 3.1.2 the Moylan *et al*. common practices for artifact design were presented. According to what was formerly listed, the proposed $50\ x\ 50\ x\ 15\ mm$ square-based part respects various aspects of the proposed "rules":

- The part's base is composed of a simple geometrical shape, which will allow for simple and satisfactory coordinate measurement machine calibration, positional precision and geometrical control;
- The simplicity of the geometry in itself allows for ease of measurement. When dealing with the principal dimensions, a planar structure will allow for accessibility to the various geometric elements that compose the artifact;

- Despite the fact that all machines allow larger artifacts in the z-axis (as seen in Eq. (4)), the design proposes a height of only 15 mm, which will preserve the artifact's small sizing, allowing for faster build times and low consumption of material.

Lastly, regarding the dimensions and limitations of machinery that will be involved in the analysis of this artifact, it is important to also consider the measurement equipment. The Poli Light Man CMM machine mentioned in Chapter 3.2.5 will use a 1mm Renishaw Probe. Therefore, it is important to secure that all gaps and openings within the artifact and its geometries will have a large enough tolerance margin to avoid undesired contact of the probe. The mentioned contact would cause incorrect readings and therefore the geometries would be incorrectly interpolated by the CMM's software. A breach allowance assimilated to the diameter of the probe $D_{probe} = 1\ mm$ to each side, resulting in a 3 x 3 mm clearance zone is a feasible solution that would allow for clear-cut readings, as presented in Figure 21.

Figure 21 – Probe Clearance Zone.

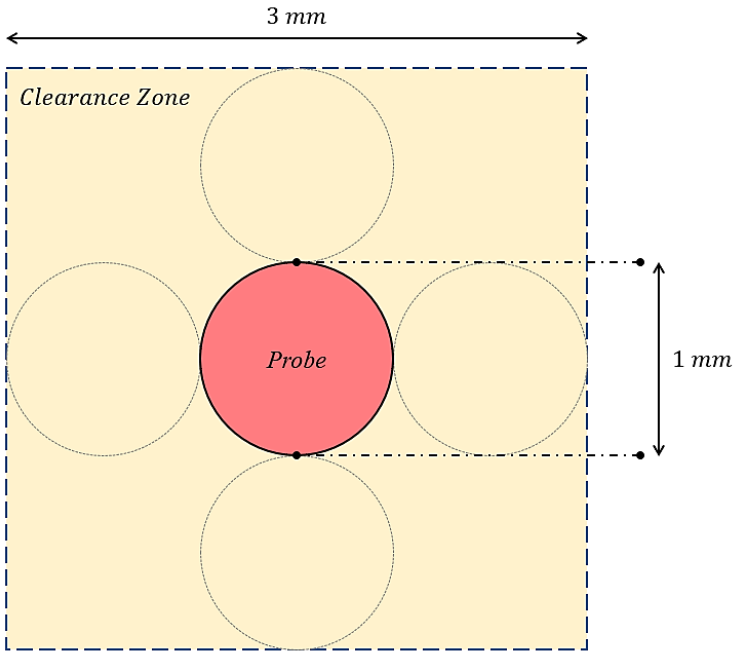

In other respects, it is also important to consider the effective working length (EWL) mentioned in Chapter 3.2.5 parameters and illustrated in Figure 15. The EWL that will be considered for the Renishaw probe is that of 7 mm in diameter, and therefore, all geometries to be measured within the z-axis must be designed with respect to these limitations. This will be further explored in the following chapter.

3.3.2 Selected Geometries

The type of study at hand is a geometric benchmark, and regarding this category of analysis, it is essential that the test artifact contains various classic geometries from which form error and geometric tolerances are derived. Amidst the geometries presented in Table 5, classic configurations (planes, cylinders, cones, spheres, prismatic features) will be included as both positive (embossed, or "boss" parts) or negatives (hollow and convex elements; holes) as a way of optimizing the available area of the artifact. Table 7 specifies the chosen geometries that have been chosen and will be observed throughout this section. A detailed approach to each geometries subcategory and label can be found in APPENDIX A – at the end of this document.

Table 7 – Geometry listing of the proposed test part.

ID	Family
A	Concentric Cylinder Boss
B	Cylinder Boss
C	Pins
D	Hemispheres
E	Circular Holes
F	Square Boss
G	Horizontal Cylinders
H	Staircases
I	Inclines
J	Rectangular Boss
K	Cone
L	Outer Dimensions
M	Square Notches

3.3.2.1 Concentric Cylinder Boss – Family A

Concentric cylinder boss is a hollow cylindric feature family that is composed of two coaxial cylinders, labeled as A1 and A2, where their diameters are of 20 mm and 15 mm, respectively. The height of feature A2 is of 10 mm from the base, and A1 is only 5 mm from the same reference – therefore, from the annular plane formed on A1, A2 is only 5 mm higher. Both contain a hollow region, or a "punched hole" that passes the base of the part, forming the larger circular hole of the feature family E. This feature will be utilized in order to evaluate cylindricity, concentricity, circularity, flatness and a general overview of IT grades in each machine.

Figure 22 – Visual representation of the artifact highlighting the feature family A.

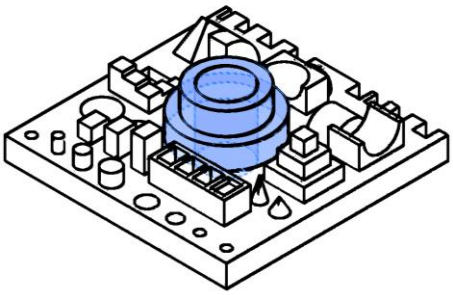

3.3.2.2 Cylinder Boss – Family B

Cylinder boss is a solid cylindric feature family that is composed of three separate cylinders, labeled as B1, B2 and B3, where their diameters are of 2 mm, 3 mm, and 4 mm, respectively. The height of all features is 3 mm, and they are located between the Rectangular boss and Pins features. This feature will be utilized in order to evaluate cylindricity, flatness and a general overview of IT grades for heights in each machine.

Figure 23 – Visual representation of the artifact highlighting the feature family B.

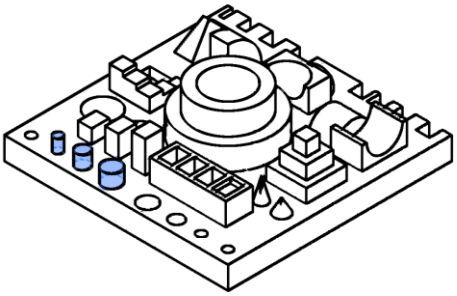

3.3.2.3 Pins – Family C

The Pins are a cylindric feature family that is composed of three separate holes or "hollow" cylinders, labeled as C1, C2 and C3, where their diameters are of 2 mm, 3 mm, and 4 mm, respectively. The height of all features is 3 mm, and they are located between the Rectangular boss and Cylinder boss features. This feature will be utilized in order to evaluate cylindricity and a general overview of IT grades for heights in each machine.

Figure 24 – Visual representation of the artifact highlighting the feature family C.

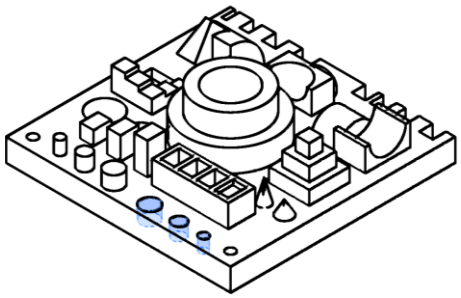

3.3.2.4 Hemisphere – Family D

The Hemisphere feature family is the representation of a half-sphere in both a positive (convex) and negative (concave) portrayal of the same size, making each feature effectively a quarter-sphere. The negative rendering of the feature is labeled as D1, whilst the positive version is D2. Both spherical features have a nominal diameter of 8 mm. This feature will be utilized in order to evaluate precision in the fabrication of spherical elements and a general overview of IT grades in each machine.

Figure 25 – Visual representation of the artifact highlighting the feature family D.

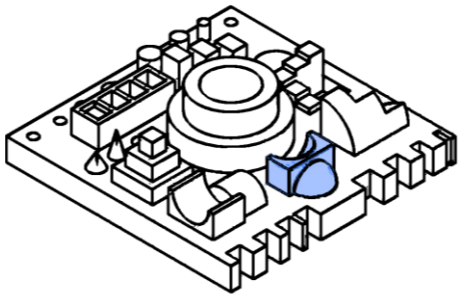

3.3.2.5 Circular Holes – Family E

The Circular Holes are a cylindric feature family that is composed of four separate passing holes onto the artifact base, labeled from E1 to E4 in crescent order. The diameters of each hole are of 3 mm, 5 mm, and 7 mm and 10mm from E1 through E4, in order. This feature will be utilized in order to evaluate cylindricity, circularity, concentricity, and a general overview of IT grades for heights in each machine.

Figure 26 – Visual representation of the artifact highlighting the feature family E.

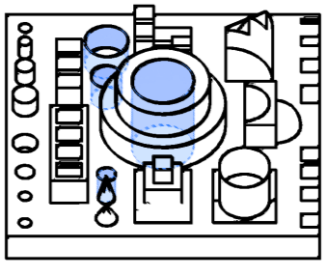

3.3.2.6 Square Boss – Family F

The Square Boss feature is composed of three square shaped prismatic extrusions, where each consecutive block is atop of the last. The features are labeled as F1, F2 and F3, whereas their edges are 3 mm, 6 mm and 9 mm long, respectively, and heights (Z direction) are all of 3 mm. This feature will be used in order to evaluate precision in all directions of the artifact (X, Y, Z) and contributes to the ISO analysis of IT grades.

Figure 27 – Visual representation of the artifact highlighting the feature family F.

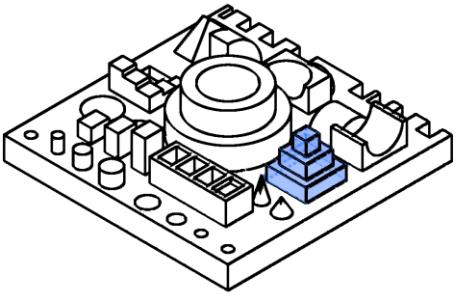

3.3.2.7 Horizontal Cylinders – Family G

Unlike the formerly described cylindric features, the feature family G is composed of hemicylinders with a horizontal axis – thus the name of Horizontal Cylinders. The set resembles the spherical family and consists of a convex hemicylinder (labeled G1) and its counterpart in concave form (G2). Feature G1 is a 6 mm long cylinder, while G2 is 7 mm long, and both cylinders have an 8 mm wide diameter. This feature will be utilized in order to evaluate cylindricity, a general overview of IT grades, and generate a comparison between vertically and horizontally oriented cylinders upon fabrication in each machine.

Figure 28 – Visual representation of the artifact highlighting the feature family G.

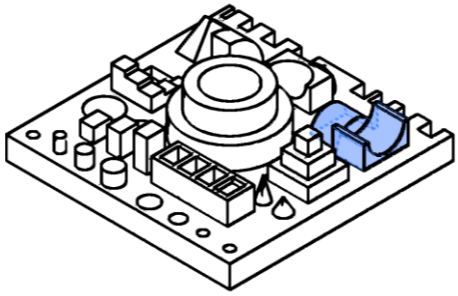

3.3.2.8 Staircases – Family H

The Staircase feature – label H – is composed of small 3x3 mm prismatic extrusions in different heights, forming a geometry similar to a staircase, ranging from -4 mm below the part's base, and up to 5 mm to reach an equal height to feature A1 on its tallest step. Each step is labeled from H1 (-4 mm) to H9 (+5 mm), and the height increment is of 1 mm for each consecutive change, except from H4 (-1 mm) to H5 (+1 mm), where there is a 2 mm increment.

Figure 29 – Visual representation of the artifact highlighting the feature family H.

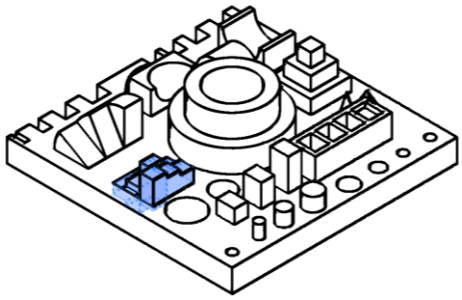

Figure 30 shows a cut-view representation of the part's staircase feature, where section D-D (left) intersects features H1, H4 and H8. Section E-E (right) demonstrates the "staircase" geometry more clearly, intercepting features H5, H6, H7, which are incremented by 1 mm from one to another. All formerly mentioned dimensions use the artifact's base plane as a reference for Z = 0. This geometry will contribute with many data points for the IT grade analysis and the inspection of precision in all directions (X, Y, Z).

Figure 30 – Sectioned representations of the staircase feature, viewed from the top of the part.

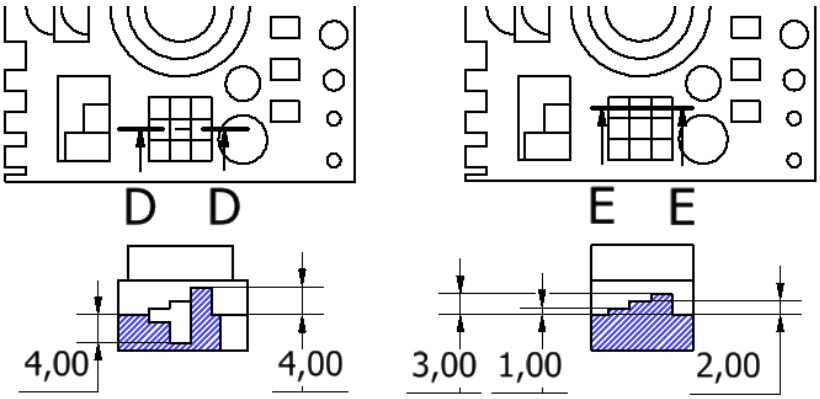

3.3.2.9 Inclines – Family I

The Inclines feature family is composed of a set of tilted planes built from slices of a cylindric feature. Inclines are labeled as I1, I2 and I3, where angles are nominally 30 degrees, 60 degrees and a quarter-cylinder incline of 90 degrees. The length of each "slice" is of 4 mm, and radii are of 7.5 mm (originally a 15 mm diameter cylinder), therefore the tilted planes of the feature are defined by a 7.5 x 4 mm inclined rectangle. This feature was designed to be utilized in the evaluation of angularity tolerances, and generate a comparison between each machine's ability to produce inclined planes. These features can also be used to evaluate flatness and cylindricity, if desired.

Figure 31 – Visual representation of the artifact highlighting the feature family I.

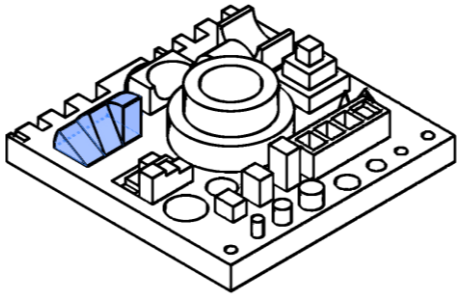

3.3.2.10 Rectangular Boss – Family J

The Rectangular Boss feature is a feature family inspired by the Minetola *et. al* test artifact, and it comprises a set of rectangular blocks and slots that are labeled from J1 to J7.

Each feature is composed of a 3x4 mm rectangular base that is either positive (embossed) – in features J1, J2 and J3 – or negative, inserted in a 17x6x5 mm block – features J4, J5, J6 and J7. All features have varying heights: J1 is 3 mm tall, J2 is 5 mm and J3 is 7 mm. Starting atop of the reference “slots block” (5 mm height from the base) J4 comprises a -7 mm height, J5 has -5 mm, J6 has -3 mm and the final slot is J7 with only -1 mm in height. This feature will be used in order to evaluate precision in all directions of the artifact (X, Y, Z) and contributes with a large amount of data points to the ISO analysis of IT grades.

Figure 32 – Visual representation of the artifact highlighting the feature family J.

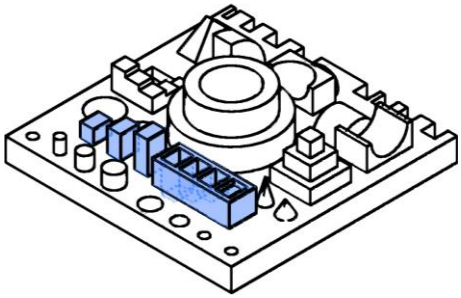

Similar to what has been done for the Staircase feature, a cut-view representation of the Rectangular boss set has been demonstrated in Figure 33. In the section (C-C) it is easier to understand the configuration, where the absolute maximum height of a positive or negative rectangular boss is 7 mm, and a “slot block” encompasses features J4 to J7, on the right side.

Figure 33 – Sectioned view of the rectangular boss feature, seen from atop of the part.

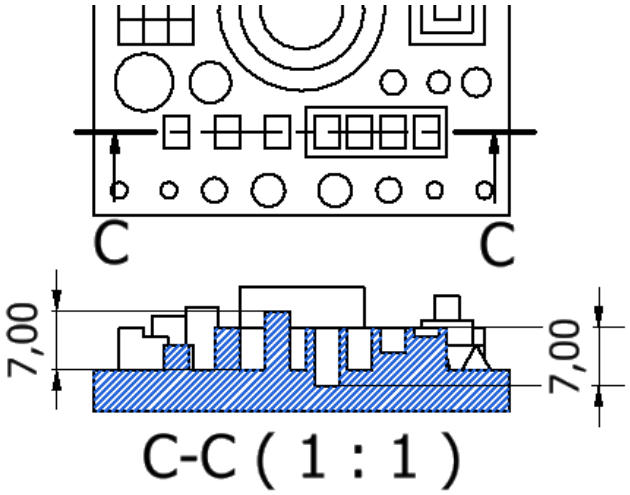

3.3.2.11 Cone – Family K

A set of two features composes the Cone family that is under the label K. A short 3 mm long right-angled circular cone is represented by K1, with a semi-vertical angle of 30 degrees at its tip. The featured right-angled circular cone in K2 is slimmer yet taller, with a 5 mm height and 15 degree semi-vertical angle. This feature will be utilized in order to evaluate precision in the fabrication of cones and their truncated elements.

Figure 34 – Visual representation of the artifact highlighting the feature family K.

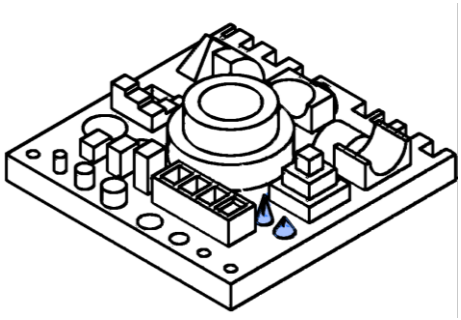

3.3.2.12 Outside Dimensions – Family L

As formerly mentioned in Chapter 3.3.1, the part base will be designed as a square of 50x50 mm, extruded by 5 mm in the Z direction – thus, a base block of 50x50x5 mm. The outside dimensions of the part will be labeled as L1 (X direction; smooth side) and L2 (Y direction; side etched by square notches).

Figure 35 – Visual representation of the artifact highlighting the feature family L.

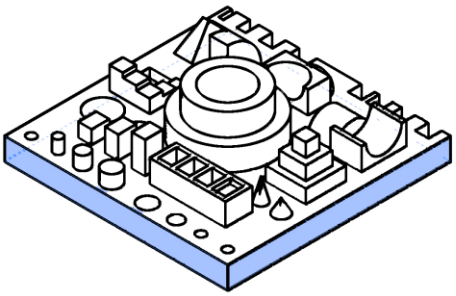

3.3.2.13 Square Notches – Family M

The Square notch feature is composed of 3x3 mm square-shaped indentations made onto one of the faces of the base. As per **Figure 36**, the right-sided notches are rendered square by irregular etches on the part, whilst the left-sided notches are even square-shaped etches engraved on the part. Features are labeled M1 to M7, from right to left. This feature will be used in order to evaluate the accuracy of edge-imprinted features in each machine, as well as to generate a large amount of data points for the ISO IT grade analysis.

Figure 36 – Visual representation of the artifact highlighting the feature family M.

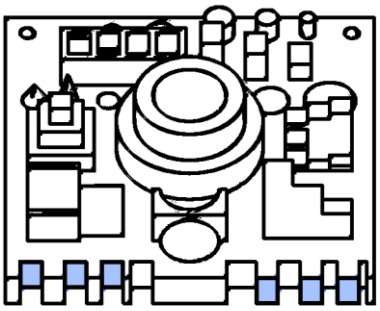

3.3.3 Analyzed Derivative Characteristics

A process planning study by Lynn-Charney et al. [47] in the field of accuracy models for manufacturing states tolerance, surface and orientation relationships between different types of geometries and the derivative characteristics that each one will produce – such as concentricity, positioning, circularity, etc. The affiliation of a geometry to a part's physical characteristics was initially detailed in Chapter 3.2.6.6 and the listing in Table 8 below states the chosen features to evaluate secondary, derivative aspects of the test part.

Table 8 – Derivative characteristic listing of the proposed test part

ID	Family
N	Vertical Cylinders
O	Concentricity
P	Planes

3.3.3.1 Concentricity and Vertical Cylinders – Family N and O

For measurement and analysis purposes a group of four features will be used to evaluate concentricity. All features used are fundamentally vertical cylinders, and the features selected are A1 and A2 from Concentric Cylinder Boss, B3 from Cylinder Boss, and E4 the Circular Hole located in the middle of the part. All features will be measured once again and labeled as "Vertical Cylinders" under the letter "N", and concentricity data will be labeled "O". Only features A1, A2 and E4 will be used for concentricity, and the label of each combination can be found in APPENDIX A – Geometric Labeling (Figure 85).

Figure 37 – Visual representation of the features that compose families N and O.

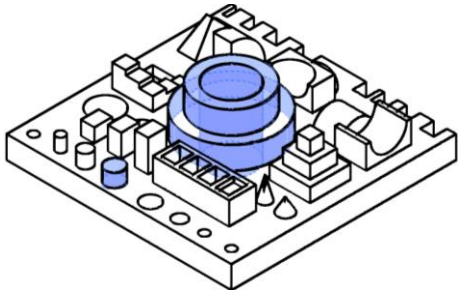

3.3.3.2 Horizontal Planar Surfaces of Interest – Family P

In order to evaluate flatness, parallelism, and surface irregularities it is necessary to define which planes will compose the measurement data. A set of 10 horizontal planes was selected for the evaluation of these characteristics, and Table 9 catalogues the selection by the feature from which the plane is originated.

Figure 38 – Visual representation of the artifact highlighting the planes selected for family P.

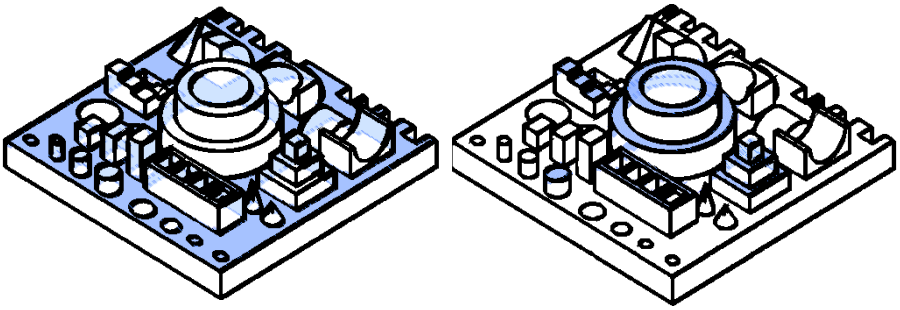

Table 9 – Detailed description of the selection of planes for feature family P.

ID	Related Feature	Description
P1	-	Plane of the base
P2	A1	Concentric cylinder boss
P3	A2	Concentric cylinder boss
P4	H7	Square step on Staircases
P5	H8	Square step on Staircases
P6	H9	Square step on Staircases
P7	F2	Superior plane of square boss feature
P8	F3	Superior plane of square boss feature
P9	B3	Cylinder boss feature
P10	J(-)	Superior face of the negative slot block

4. EXPERIMENTAL DEVELOPMENT

The experimental analysis explored within this chapter will cover both an overview of the experimental procedures, methodology and its conjectural background information. This material will deal with machine setup, instructions and the series of procedures taken in order to fabricate the replicas of the defined artifact part. On each of the compared machines, a single replica of the artifact part was manufactured using the same STL file that was designed throughout Chapter 3. Each machine had a specific slicing software that was used to prepare the numerical control file for printing.

4.1 Preparation procedures

The preparation of the additive manufacturing processes can be divided into two categories: 3D model preparing and machine setup. The first segment refers to the processing and conversion of the 3D CAD model into an adequate file format. When dealing with 3D systems, most models are likely to be produced in .STL or .OBJ formats. The artifact used in this study was initially produced in Autodesk Inventor (.IPT CAD format) and converted to .STL after the inclusion of supporting structures using CIMsystem's Pyramis 3D printing management software [48]. Furthermore, the STL file can be sliced with freeware slicing software or the machine manufacturer's own package, and the print path is converted into a standard ISO G-code file. This denotes that the machine will promptly be able to attain the file (via ethernet or USB) with instructions regarding position and orientation of the part, which will allow the commencement of fabrication.

Figure 39 – Support structure preparation in Sharebot's company-made software for the DLP Sharebot Rover.

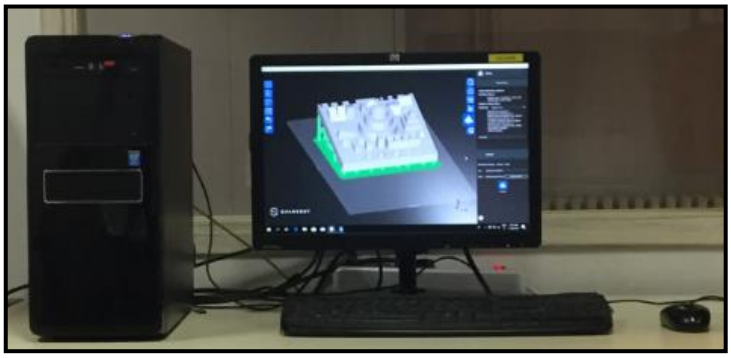

Machine configuration, however, is still necessary before initialization. Before usage of all three machines the build platform must be properly washed with isopropyl alcohol (IPA) in order to remove residual resin from other prints – IPA and TPM dissolve liquid resin, making them effective for washing [49] – or even unexpected filth.

Figure 40 – Sharebot Antares build platform when sanitized (left) and isopropyl used (left).

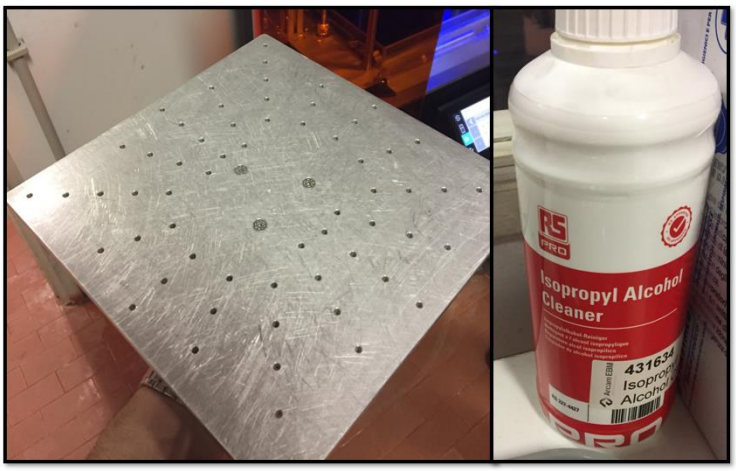

Once cleaning and software configuration has been finished, it is necessary to ensure the machine is properly calibrated. Photopolymerization machines that use a vat or container pool for resin such as the Sharebot Antares and Rover are calibrated through the positioning of the VAT into the build platform, according to layer heights. Proper calibration ensures that the first layer will stick onto the building platter, which promotes a lower chance of errors as a result of poor adhesion.

4.2 Fabrication of the replicas

As soon as preparation is finished, it is possible to initialize the machine and begin fabrication. The beginning of the manufacturing processes is generally slower, since layers that are produced first generally encompass a larger surface area, which results in a longer build-time for initial layers of the base, brims, rafts, and supports.

In this chapter the fabrication procedures and post-processing steps for the parts will be approached in each machine. Initially, both Sharebot machines will be analyzed since the stages of fabrication in SLA and DLP are remarkably similar, as these are naturally resemblant additive manufacturing processes. Afterwards, the more straightforward procedures of the Objet30 will be described for assessment of all manufacturing processes.

4.2.1 Sharebot Rover and Antares – Fabrication description and detail

Sharebot machines comprise VAT Photopolymerization processes, in which resin must be placed into the container in which the build platform will be submerged. The first part that was manufactured was the DLP replica on the Sharebot Rover. It is recommended that the entirety of the resin tank is filled for manufacturing, and around 18g of resin were consumed for each part. The resin used in DLP was the Sharebot S-Clear and the part was fabricated in approximately 16 hours with a layer thickness of 50 microns (initial estimates of the machine indicated a total of 14 hours, as seen in Figure 41). The resin costs 199.00 €/kg, which would indicate that the part had a cost of roughly 3.60 €, discounting occasional resin losses from filling the container [50]. A summary containing details about the S-Clear resin and its proprieties will be contained in “APPENDIX B – Summary of Resins”.

Figure 41 – Printing initialization of the Sharebot Rover for the DLP replica.

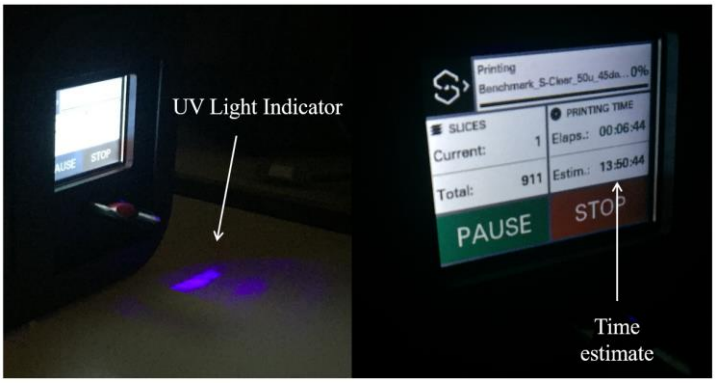

Figure 42 – DLP test part after printing completion.

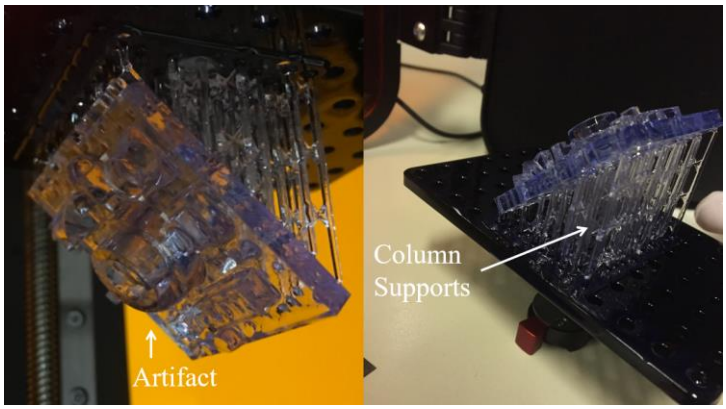

Both DLP and SLA parts were printed in a 45 degree angle, and column supports were utilized (Figure 42). Once manufacturing is complete, the part must be scraped from the build platform and delicacy is not mandatory since the elements that are in contact with the platform are disposable (supports and skirts; Figure 42). Since post-fabrication procedures are similar for all parts produced, this content will be presented in Chapter 4.2.3.

Figure 43 – Removal of the DLP part from the printing platform.

The stereolithography (SLA) part produced in the Sharebot Antares used another resin, the Sharebot PR-S high precision resin. Differently from the DLP resin, which was transparent, this photopolymer used in SLA is grey, with layer thickness of 50 microns and took roughly 4 hours to fabricate the reference part (considerably faster than the Sharebot Rover). The resin costs 149.00 €/kg, therefore, discounting eventual losses, the material price for manufacturing one test part is of around 2.80 € [51]. The Sharebot Antares uses an individual 3D management supporting and slicing software, and parts are transferred via an Ethernet connection. Further details about the material will be described in APPENDIX B – Summary of Resins.

Figure 44 – Sharebot Antares open for initialization.

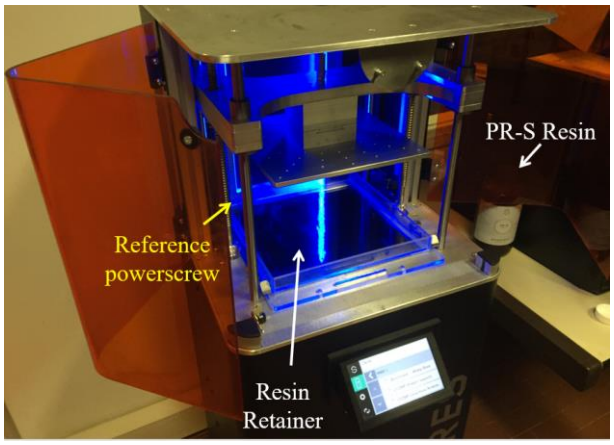

Figure 45 – Close-up photo of the Sharebot Antares during fabrication.

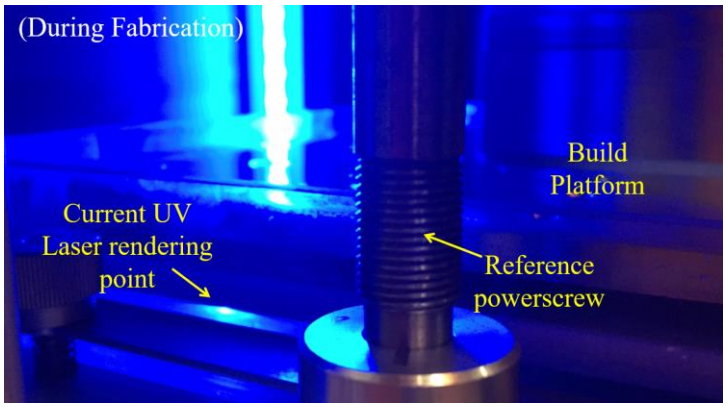

In Figure 45 a visual depiction of the main difference between SLA and DLP can be seen. On the bottom left corner of the image it is possible to notice the position in which the UV laser is curing the current layer of the part. The main difference between a DLP process and SLA is the operation of the light source; SLA uses a single UV laser, while the DLP machine uses light that is projected from a stationary source. In DLP, light source cures the complete layer of resin once at a time, while in SLA, the laser moves around the build platform, tracing the part's geometry [52]. After completion, both parts were successfully removed and prepared for their respective post-fabrication procedures.

4.2.2 Stratasys Objet30 – Fabrication description and detail

Fabrication of PolyJet on the Stratasys Objet30 was a much simpler procedure, where the machine's proper 3D management software is available and capable of qualitatively delivering a support structure and sliced layers of the STL file. Importing was also performed

directly via the Ethernet connection available between the Objet30 and the machine's dedicated computer.

A considerably more expensive resin was used for PolyJet: the VeroWhitePlus RGD835. This resin is white and opaque in color, and costs around 300.00 US$/kg [53]. The reference part was fabricated in roughly 7.5 hours, with a layer quality of 30 microns (Figure 46). Contrary to what is performed in the Sharebot machines, fabrication on the Stratasys PolyJet apparatus does not require an angled orientation of the part. This is due to the fact that there is no fluid tension from a vertically moving platform that requires submersion in liquid. The mechanism of PolyJet provides "on-demand" liquid jetting and curing (Figure 47), mimicking the fundamentals of an inkjet printer, but using liquid photopolymers instead of ink and solidifying them with UV light, layer-by layer [54]. Therefore, this mechanic allows the part to be produced in its designed orientation. The Objet30 also has a memorized initial setup, thus manual calibration was not necessary, which potentially contributes to better accuracy by decreasing the possibility of manual errors.

Figure 46 – Pre-print information and parameters of the Objet30 Prime.

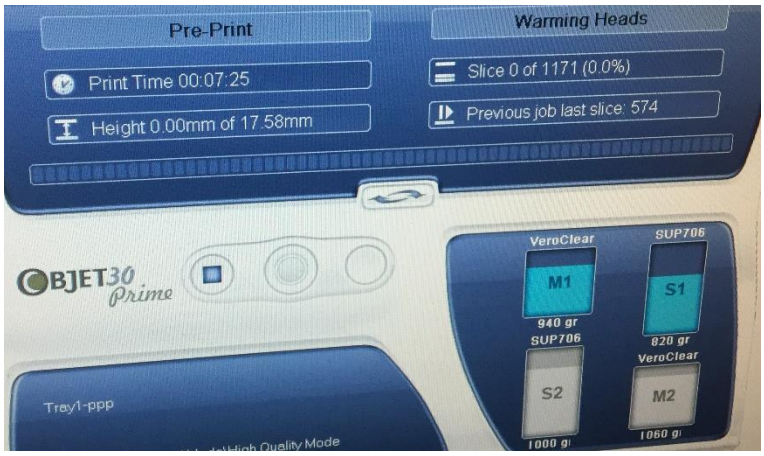

Figure 47 – Collection of frames from a recording of PolyJet fabrication.

4.2.3 Post-fabrication of the parts produced

Post processing in all of the manufacturing procedures presented thus far are composed of two possible steps: ultrasonic cleaning or washing; and UV curing. The first step after the removal of the part from the machine it to wash the part properly, in order to remove any residual liquid resin. Hence, the use of a solution such as the Isopropyl Alcohol (IPA) is once again necessary. For the Sharebot machine's reference parts, each artifact was placed in an ultrasonic bath.

A Digital Ultrasonic Cleaner (DUC) is a machine that uses vibration, fluid proprieties and heating to perform final conditioning of a resin-based AM part. In its interior, IPA is used in order to dissolve any lingering resin on the part. The heating effect was not available at RMLAB's DUC, therefore the ultrasonic bath was based only on wave emission and submerging the SLA and DLP parts, individually, in Isopropyl.

Figure 48 – Sharebot Digital Ultrasonic Cleaner.

Source: [55]

Furthermore, the second part of post-processing in the SLA and DLP procedures is the usage of a UV chamber or oven. As described by Sharebot, post-curing is a process that aims to stabilize a resin 3D model after printing, and to complete polymerization [55]. This ensures that the hardened models retain their structural characteristics and a uniform yield. Post-curing, however, can be done within a UV chamber or even through alternative methods such as exposure to sunlight. The Sharebot UV Curing Box (UCB) was used for curing of the SLA and DLP parts for 20 minutes each right after they were fabricated and thoroughly cleaned. A consumption of about 70W is used to power LED's of around 375 nm wavelength emissions.

Figure 49 – Sharebot UV Curing Box used in this study.

Source: [55]

Figure 50 – DLP (left) and SLA (right) fabricated parts while post-curing inside the UCB.

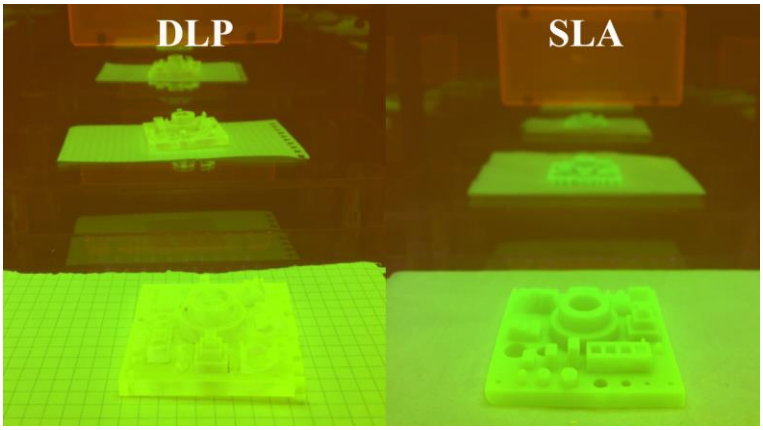

Finally, it is important to note that the replicas were not finished or polished, in order to not to alter their surfaces or dimensions. The manufactured condition should be considered for an accurate benchmarking of the AM machines. This is reinforced in the good-practices for artifact design of Moylan et. al [17], where it is recommended that the design does not require much post-processing, in order to preserve the fidelity of the manufacturing results for the model.

The procedures required for PolyJet were much simpler and faster than those realized in DLP and SLA. Parts produced by the Objet30 Prime also do not require any post-processing other than water jetting for washing and a following pressurized air drying (see Appendix C).

4.2.4 Finished parts and expected results

In this chapter a general overview and comparison of the manufacturing processes will be described. Additionally, general commentary and first impressions of the fabricated reference parts will be registered.

The first part was produced with the Sharebot Rover, and it was noticeable that the process took a particularly long time to manufacture the test artifact (16 hours). The machine requires manual intervention in calibration, and it is difficult to ensure layer adhesion in the early stages of fabrication. Within the first hour of initialization it is also not possible to discriminate whether or not the first print layers have attached themselves to the build platform. At first glance, the part seems well produced and finished, with well-defined basic features (squares, circles, cylinders etc.) to the naked eye. Conversely, it is also noticeable how the part seems to have retained and cured resin within some small openings, which will certainly contribute to inaccuracies regarding the CAD model. Overall, the part is visually satisfactory, and all geometries seem to have been well produced in the DLP machine.

Figure 51 – Photo of the DLP reference part produced in the Sharebot Rover.

In the second manufacturing process, the Sharebot Antares was used for fabrication of the SLA part. The interval of time that was necessary to fabricate the part was the shortest of all machines (only around 4 hours), which makes it feasible to correct setup errors promptly. Since calibration is also not automatic in the Antares, it may be challenging to obtain proper layer adhesion. It is also worth noting that this is a potential source of human error which may affect the geometric accuracy of the part. To the naked eye, the produced part seems to have better finishing characteristic than the DLP. However, some localized errors are very clear, such as a slight one-sided warping under the base, which opportunely is expected to not affect the

geometries contained on the upper side of the part. In terms of how costly it is to produce the part, since it is required to fully load the resin tray, the Sharebot Antares is subject to large resin losses which could vastly increase the cost of the part. Fortunately, the SLA resin is the least expensive and even with a hypothetical loss of 20% part volume, the part would still be less costly than the ones made in DLP and PolyJet.

Figure 52 – Photo of the SLA reference part produced in the Sharebot Antares.

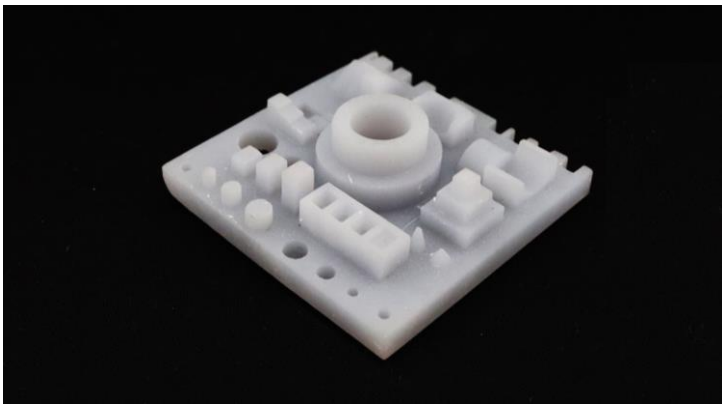

Lastly, the Objet30 is expected to produce the best results among all three machines. At first glance this seems to be the highest quality part fabricated thus far. The artifact presents a visually pleasing aesthetic, with seemingly well produced finishing and geometric accuracy. Such precision can be expected since the part had the best overall manufacturing configuration: there was no need for supports, the part was oriented without any inclination, and layering of 30 microns was used – which is the finest layer height used. This is expected to result in remarkably high quality finishing and accuracies. The VeroWhitePlus resin, however, is the most expensive used, costing roughly twice as much as the SLA PR-S. In terms of fabrication time, the part took only 7.5 hours since initialization, which points to high performance additive manufacturing within a time-frame that is not relatively long in comparison to DLP.

Figure 53 – Photo of the PolyJet reference part produced in the Stratasys Objet30.

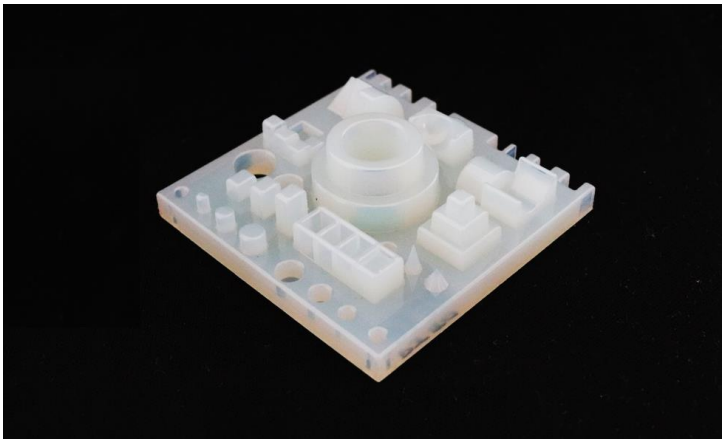

Figure 54 – Side by side photo of all three manufactured reference parts: DLP (left), SLA (middle) and PolyJet (right).

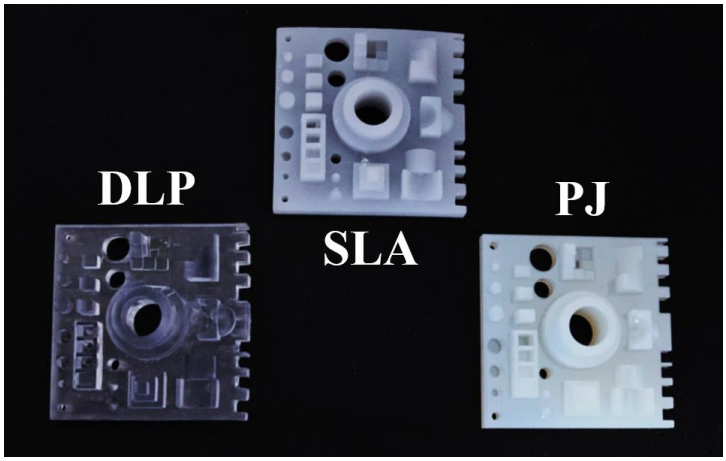

4.3 Measurement procedure of the replicas

The measurement procedure was conducted in the Poli Light Man coordinate measurement machine, as formerly mentioned in Chapter 3.2.5. In this chapter, the procedures and proper measurement practices of a benchmarking part will be described. The literature used for measurement instructions was the GEOSOFT Manual ("*Manuale di utilizzo*") available at Politecnico di Torino's RMLAB [56]. Further guidelines were presented in David Flack's Good Practice Guide for CMM Measurements [24]. The measurement capabilities and methodology presented in this document will follow the requirements of the Poli 3D GEOSOFT Measurement Software of the Poli Light Man.

4.3.1 Positioning and Fixation

When setting up the machine, the part must be placed in the Poli Light Man's measurement area. In order to the stability of the part, attribute height – a for ease of measurement – and position the part within a fixed reference position, a mechanical vise (or fixtures) is used to hold the measured part. When using fixtures it is necessary to ensure that they are clean, the workpiece is located correctly, clamping forces on the workpiece are not excessive, and that all features requiring measurement are accessible. In this case, the reference parts were placed atop of metal placeholders with its base parallel to the granite measurement board of the Poli Light Man, as indicated in Figure 55. In this setup, the workpiece is not over-constrained and all geometries are accessible.

Figure 55 – Positioning and fixation of a reference part on the Poli Light Man CMM.

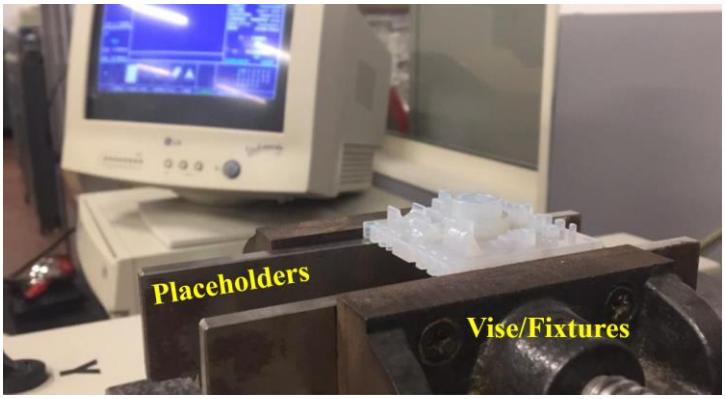

4.3.2 Measurement strategy for standard geometries

The workpiece at hand is composed of various different basic geometries, such as planes, holes, cylinders, squares, rectangles, cones, spheres etc. Mathematically, each geometry has a minimum amount of points (or data values) required to execute fitting of a geometric feature. The minimum number of contact points required for each type of feature to be measured and fitted is presented in Table 10 below, from David Flack's good practices guide.

Table 10 – Number of contact points required for feature measurement.

Number of contact points required		
Geometric feature	**Mathematical minimum**	**Recommended minimum**
Straight line	2	5
Plane	3	9 (Approximately three lines of three)
Circle	3	7 (To detect up to six lobes)
Sphere	4	9 (Approximately three circles of three in three parallel planes)
Cone	6	12 (Circles in four parallel planes for information on straightness) 15 (Five points on each circle for information on roundness)
Ellipse	4	12
Cylinder	5	12 (Circles in four parallel planes for information on straightness) 15 (Five points on each circle for information on roundness)
Cube	6	18 At least three per face

Source: [24]

In the Poli Light Man, the six most basic features that the machine is capable of determining are: points, lines, planes, circumferences, spheres, cylinders, and cones. Other features are “composed features”, such as parallelism, concentricity, distance, flatness etc. which can be evaluated only through the combination of multiple features. The measurement procedure of these geometries according to the GEOSOFT Manual will be presented in the following topics:

- Points: these are the most basic features available to any CMM. The coordinate system defines a contact value (X, Y, Z) for the point referencing the absolute origin that is defined during calibration. Calibration of the machine requires knowledge on how to measure specific features – including points – and therefore will be presented in subsequent sections. Points can be measured through a singular interception of the probing tool to the workpiece.

- Lines: This feature is obtained through a linear fit of data points, obtained through the coordinate system as mentioned in the previous topic. As per Table 10, this feature is evaluated at a minimum of 2 data points, and a recommended amount of 5. Lines are also a feature used in machine calibration.

- Planes: a planar feature can be defined through a minimum of three points, and in this work a minimum of 9 points will be used for small area finite planes. The Planes feature (“P” label; P1-P10) will be evaluated under these conditions, where small 3x3 mm planes such as P4-P6 will be sampled in 9 points, and other planes such as P1 may contain up to 30 data points (maximum collection of data points allowed in the Poli Light Man for a single measurement). Unlike the previous two features, a plane will return a mean deviation of its measurement (δ) and a maximum deviation observed (S_{max}).

- Circumferences: circular features and diameters can be evaluated through this feature in order to interpolate a circle that would fit through a minimum of 3 data points. It is recommended that this feature is measured with at least 7 points, and deviations such as those mentioned for planes are an output of this feature, such as all features that contain a minimum of at least 3 data points.

- Spheres: this feature will be used exclusively for the measurement of the Hemisphere set of the reference part (feature “D”). The sphere is the non-planar feature that can be evaluated in the CMM thus far, and it requires a minimum of 4 points in order to define a fitting combination of circumferences. A minimum of 6 points is recommended by the GEOSOFT manual, whereas David Flack’s manual suggests a more conservative approach of 9 data points. The GEOSOFT manual recommends that data points are measured in groups of three, where each group is contained at an equal latitude (or sectional diameter) of the sphere, as illustrated by Figure 56.

Figure 56 – Recommended distribution of data points on a sphere.

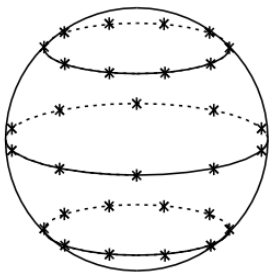

Source: [24]

- Cylinders: similar to spheres, the cylinder is a non-planar feature whose measurement emulates the measurement of circumferences at its different heights. A measurement of various circles parallel to the right-angle cylinder base, requiring a minimum of 6 points according to instructions of the Poli Light Man's GEOSOFT Manual. This geometry is present in various features, such as features A, B, C, E and G, among others. This feature will also be used for the analysis of concentricity; therefore, measurement must be performed with utmost concern.

Figure 57 – Recommended distribution of data points on a cylinder.

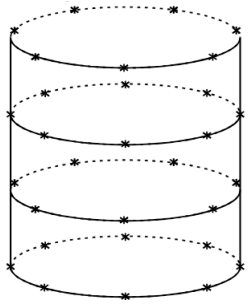

Source: [24]

- Cones: cones are also composed of a non-planar collection of data points. In this feature it is recommended that a minimum of 6 points is collected, in sets of three for different heights. This allows the CMM to evaluate the disparity in radii interpolated, and therein calculate tapering. Even using a 1 mm Renishaw Probe the measurement of features "K" (Cones) is to be challenging since due to tapering the radii of sectional circumferences will be very small. This effect allied to manual operation may cause the machine to interpolate small are circumferences that are not parallel, and therefore cannot compose a cone. Steadiness of measurement or axial fixation of the CMM is fundamental when measuring fine cone features in the reference part.

Figure 58 – Recommended distribution of data points on a truncated cone.

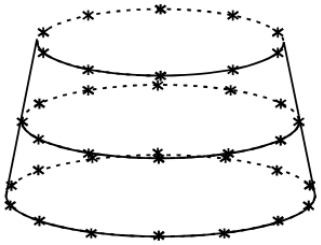

Source: [24]

Furthermore, it is possible to evaluate “composed measurements” in the Poli Light Man. This type of evaluation is used extensively since it is responsible for measuring dimensions such as the distance between two data points, distance between planes, parallelism, concentricity, angle between features and also to perform the calibration of the part.

- Distances: feature evaluated between two data points, resulting in a dimension value in mm. It is also possible to evaluate the distance between lines, planes and other features. This composed measurement is extensively used, and every measurement of length or height evaluated must be composed of two data points measured. Around 200 measurements of distances in X, Y, Z are conducted for each part, which means at least 400 data points have been collected for the part.

- Inclination: this function will be used in features “I”, of Inclines (tilted planes). For this feature a plane will be attributed to each incline (I1, I2 and I3) for each measurement. The angle between this plane and plane P1 (base of the reference part) will be compared in order to define inclination.

- Concentricity: In order to evaluate concentricity a group of vertical cylinders has been established (Family feature “N”). These vertical cylinders’ data points will be collected once again and saved into “cylinder” features of the CMM. Feature N1 and N2 will be evaluated at 20 points each, N3 at 10 and N4 with a total of 30 points. The permutation of the vertical cylinders N1, N2 and N4 will result in concentricity values, and N3 will be used for cylindricity and circularity purposes through another composed feature of “Intersection between planes and cylinders” available at the Poli Light Man.

- Parallelism: this can be obtained in two different methods in the Poli Light Man: composed feature number 14 or number 31. Essentially, the measurement encompasses the combination of two planes, and once again the feature “P” will be utilized. Function 14 returns the parallelism as a value in “mm/mt” indicating how much the interpolated planes distance themselves over a large distance. Function 31, on the other hand, utilizes an approach similar to what is expected in ISO standards, where parallelism is defined as a tolerance zone in mm to which all points of the “non-parallel” plane are contained.

4.3.3 CMM Calibration

In order to calibrate a CMM machine, an understanding of how features are measured is fundamental. The process of calibration in itself requires the measurement and definition of a plane, two lines, one point and a sphere.

The first part of CMM setup is the probe’s stylus calibration. This is performed through the use of a certified reference sphere of qualification. During this phase, the CMM will prompt the user to indicate which qualification sphere is being used, and the probe stylus should be driven perpendicularly to the sphere in several directions. This allows the CMM to compensate measurements for effects of pre-travel variation of the touch trigger, which can induce large errors to measurements [57]. In this analysis, a 16 mm reference sphere was used for calibration of the 1 mm probe stylus.

Figure 59 - Qualification sphere used in the Poli Light Man.

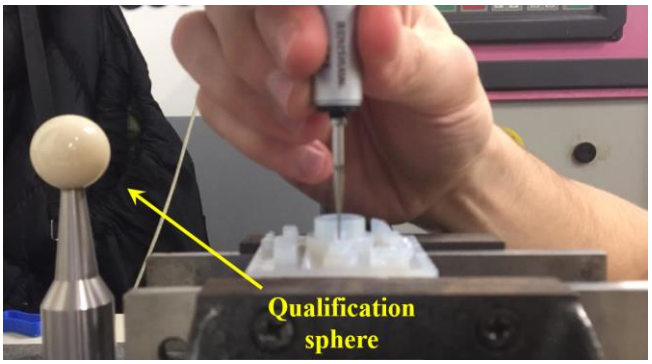

Once the stylus qualification is performed, it is necessary to define the global coordinate system (and origin) of the CMM through positioning calibration. In order to do this,

the reference part was fixed as formerly mentioned, and the parts superior base was adopted as the coordinate reference of Z = 0. Subsequently, it is necessary to define the position of both X and Y axes, and as seen in Figure 60, the dashed line (yellow) and full line (red) can encompass there axes, respectively. The GEOSOFT program of the Poli Light Man requests a primary feature, a secondary feature and an origin point. By definition, the primary feature used is the reference plane (in this case, feature P1). The secondary feature can be either axis formerly probed as a line-feature – for the sake of choice, assume a selection of the full line (red). Lastly, the machine requires an origin point that intersects both Z = 0 and Y = 0 in order to define the last remaining coordinate. The origin point (in green, Figure 60) is obtained as a "composed feature" of "intersection between two lines", resulting in the origin required for calibration. Once this is performed, the machine should identify the green point as [X,Y,Z] = [0,0,0]. Similar to what is seen in Figure 60, the following Figure 61 shows the setup on the actual reference part. Once calibration is completed, measurements can be succesfully conducted for analysis.

Figure 60 – Illustration of geometries necessary for part calibration.

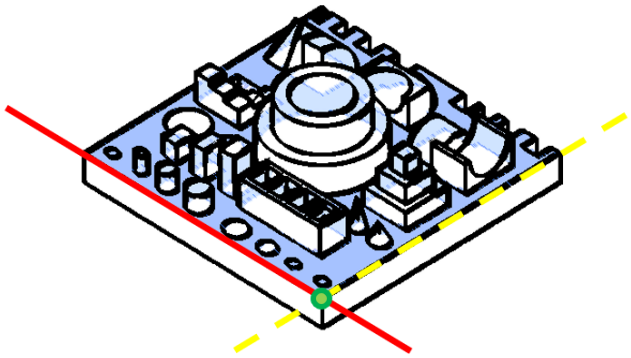

Figure 61 – Illustration of geometries necessary for calibration on a real reference part.

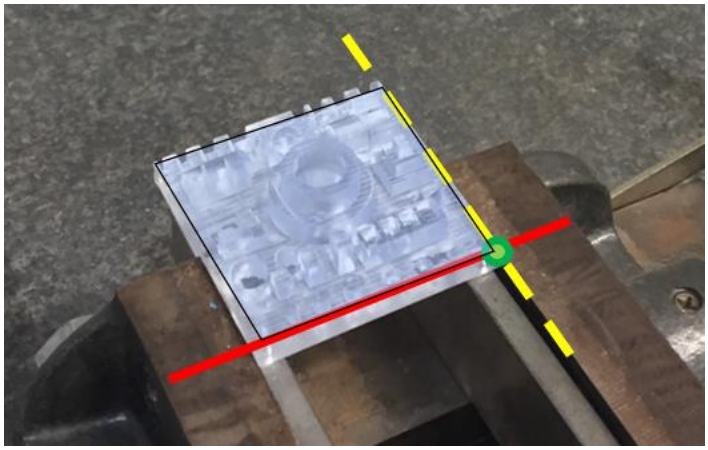

5. ANALYSIS AND RESULTS

A comparison of the three manufacturing systems described will be conducted within the following chapters. Initially, the analysis will be carried out within a framework established by the International Organization for Standardization (ISO) of basic dimensional ranges. Furthermore, a quality analysis will be realized: the collected data will be processed in order to evaluate the statistical distribution of measurements realized. Manufacturing results can therein be presented in terms of the probability of each process' machine and equipment of fabricating a qualitatively complying part.

It is important to have references as to which results are expected from the analysis. In a benchmarking analysis of fused deposition modeling systems (FDM) by Minetola et al. [58], it is possible to establish a correlation of expected results for additive manufacturing methods. In that case, however, it is possible to assume that the fused-polymer fabrication machines would produce less accurate parts than photopolymer UV-curing based processes such as SLA, DLP and PolyJet. According to Minetola et al., it is anticipated that the relative accuracy of a machine – established by ISO ranges – would increase as basic sizes increase. In other words, an additive manufacturing system will generally allow its user to manufacture smaller features with coarser accuracy, albeit an acceptable deviation for an IT grade not being constant and changing with the size of the feature by means of the standard tolerance factor, which will be further elaborated.

5.1 Dimensional accuracy in IT Grades

Every manufacturing process has a quantitative parameter to which its precision is correlated. According to ISO 286 [59], this value is referred to as an International Tolerance (IT) Grade. This grade identifies what is the expected tolerance value that a given process can create within a particular dimensional range. The values of standard tolerance grades for nominal sizes up to 500 mm are evaluated through the standard tolerance factor i that is expressed in micrometres according to the following formula:

$$i = 0.45 \cdot \sqrt[3]{D} + 0.001 \cdot D \qquad (5)$$

In equation (5) above, i is presented as a function of the parameter D, which is the geometric mean of the ISO range of nominal sizes, being D_1 and D_2 its lower and upper limits,

respectively. The equation that calculates D is presented in equation (6). Table 11 presents the values that correspond for each range, and the standard tolerance factor i calculated for each one.

$$D = \sqrt{D_1 D_2} \tag{6}$$

Table 11 – Ranges of ISO basic sizes and corresponding tolerance factor *i*.

Range			Basic Sizes					
Above	**D1**	(mm)	1	3	6	10	18	30
Up to and including	**D2**	(mm)	3	6	10	18	30	50
Std. Tolerance Factor	**i**	(μm)	0.542	0.733	0.898	1.083	1.307	1.561

Source: [16]

The International Tolerance grades are categorized according to the number of times (n_j) that the tolerance factor (i) fits into the dimensional deviation, which is the difference measured between the nominal value of a dimension ($D_{jn} = D_{CAD}$) and its corresponding measurement ($D_{jm} = D_{Measured}$). The equation below exhibits the calculation of this quotient, and the IT Grade division by n_j can be found in Table 12:

$$\mathrm{n_j} = \frac{1000 \cdot \left| D_{jn} - D_{jm} \right|}{i} \tag{7}$$

Table 12 – Classification of IT grades according to ISO 286-1:2010.

	Standard Tolerance Grades											
IT Grade	**5**	**6**	**7**	**8**	**9**	**10**	**11**	**12**	**13**	**14**	**15**	**16**
$n_j \cdot i$	7i	10i	16i	25i	40i	64i	100i	160i	250i	400i	640i	1000i

Source: [59]

In this chapter, the results for each feature will be presented and analyzed. All features will be categorized within an ISO range and compared to its respective tolerance factor, in order to allow for a standardized comparison within IT grades. Results will be discussed in terms of the mean expected deviation and average grades produced.

Having a range of basic sizes is an important factor for the analytical process. The range of ISO dimensions analyzed will contain measurements up to $50\ mm$, since the produced artifact is a $50\ x\ 50\ mm$ square-shaped test part. Additionally, the range of $i = 1.561$ μm (30

to 50 mm) involves only the outer dimensions of the artifact – features L1 and L2 – and the concentric cylinder boss feature A1. Therefore, the lower statistical relevancy of the data obtained for this ISO range must be accounted for. A general overview of the results can be seen in Figure 62, where the mean dimension accuracy for each machine is compared within a bar graph, and IT grades are set as horizontal baselines. The data analyzed is composed of approximately 300 measurements for each fabricated part, in which the dimensions of individual geometries were determined in at least three separate assessments of the CMM.

Figure 62 – Mean dimensional accuracy of the additive manufacturing machines in terms of IT Grades for different ranges of ISO basic sizes

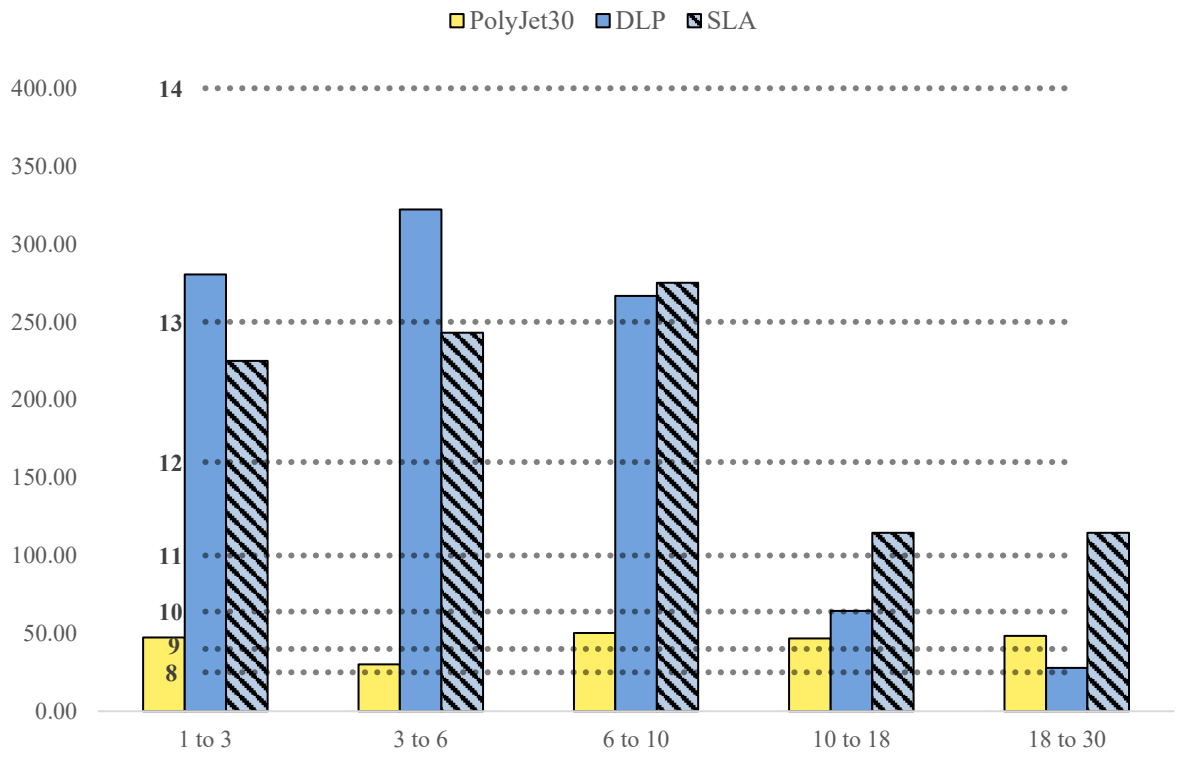

As formerly mentioned in this chapter, it is expected that an additive manufacturing system's accuracy increases as ISO basic sizes increase. As seen in Figure 62, the mean overall IT grade of each machine decreases as ISO ranges refer to larger dimensions, implying that there is a declining absolute dimensional disparity between the nominal value of the artifact part and that which was fabricated by the machine.

From the chart it is without question that the PolyJet part is the most accurate with regards to IT Grades, encompassing the process within a grade modal result of IT 9 for all ISO sizes. Overall, the PolyJet machine performs very well in all ranges, with a consistent value for

tolerances. This can be seen as a positive aspect as far as uniformity, however, with contrast to other machines, PolyJet is not relatively as accurate in larger ISO sizes.

Both DLP and SLA processes presented greater mean IT grades than the PolyJet part. This can be interpreted from various different points of view. Firstly, while the two processes are similar, they are also deviating from PolyJet's fabrication methodology. While the photopolymer machines of SLA and DLP used adopt UV projection onto a resin reservoir, PolyJet is composed of a jetting head that deposits material directly over a build tray. Additionally, both parts of the Sharebot Antares and Rover were produced over a 45° angle, whilst the Stratasys machine produced the PolyJet part in the originally designed orientation. These combined circumstances also imply the requirement of fabricating supports on the base of the Sharebot machines' artifacts, which is not an optimal arrangement, recalling good practices and orientation of Moylan et al. In the box plot diagram of Figure 63 it is possible to observe how data variance is considerably larger in DLP and SLA measurements than the values of the part fabricated in PolyJet.

Figure 63 – Box plot comparison of all three machines/processes according to ISO basic sizes and tolerance factor.

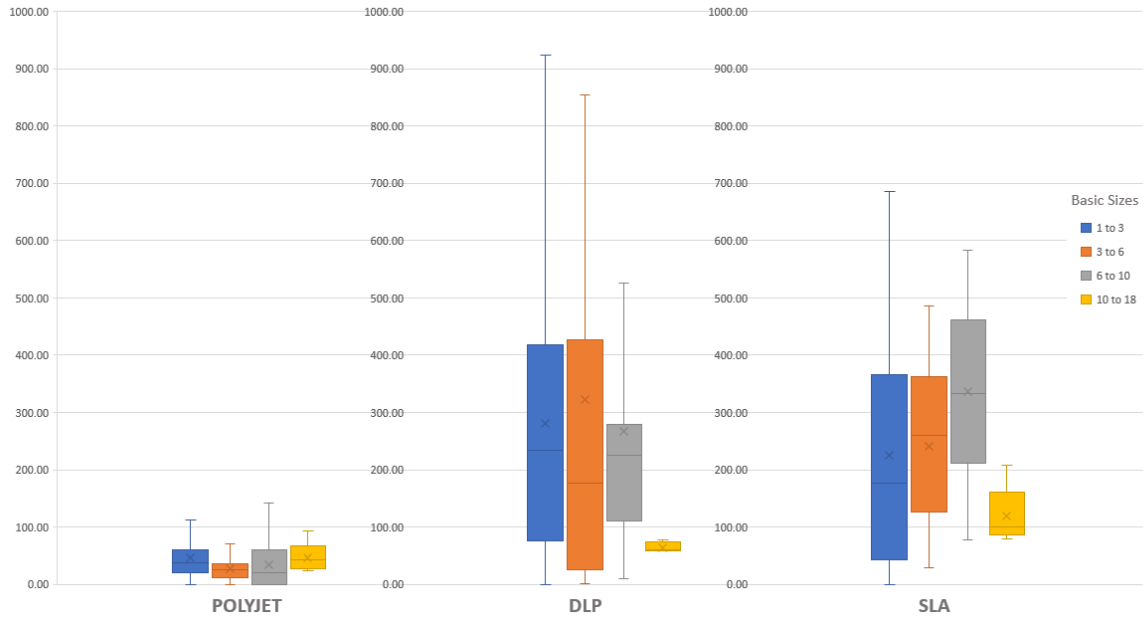

The remainder of this chapter will dissect the analyzed data with regards to each machine's capability of producing the individual geometries of the artifact. The analysis realized thus far limits itself to the format proposed by the ISO standards of IT Grades and approaches overall dimensions (D) as established in the standard tolerance factor calculations.

Forthcoming determined IT Grades will specify the features evaluated in the measurement process.

The data utilized for the following chapters discriminates each geometry in a label (letter and number from APPENDIX A – Geometric Labeling), and measurements will be divided in diameters (D), heights (h), lengths (L), dimensions regarding an axis of the part (X, Y, Z), or angularity (θ).

5.1.1 Stratasys Objet30 PolyJet – IT Grades for individual features

In both Figure 62 and Figure 63 it is clear that the Objet30 has the best overall performance of all machines analyzed in this study. This chapter, however, will observe the effectiveness of the machine in terms of fabricating the particular geometries of the artifact. A first analysis can be observed in Table 13, where features with diameters (D) have been dissected.

Table 13 – Dimensional accuracy of the Stratasys Objet30 in terms of IT Grades for different geometric features of the test part.

(Diameters)	Nominal	Avg. Measure	Avg. δ	Max. δ	Avg. IT Grade
A1	**20**	**19.864**	**0.006**	**0.032**	**9**
A2	**15**	**14.952**	**0.014**	**0.046**	**8**
B1	**2**	**1.969**	**0.008**	**0.029**	**9**
B2	**3**	**2.972**	**0.010**	**0.027**	**9**
B3	**4**	**3.960**	**0.009**	**0.049**	**9**
C1	**2**	**2.012**	**0.005**	**0.025**	**6**
C2	**3**	**3.008**	**0.007**	**0.034**	**6**
C3	**4**	**4.032**	**0.013**	**0.193**	**8**
D1	**8**	**8.049**	**0.014**	**0.059**	**9**
D2	**8**	**7.876**	**0.011**	**0.046**	**11**
E1	**3**	**3.016**	**0.007**	**0.028**	**7**
E2	**5**	**5.021**	**0.005**	**0.018**	**7**
E3	**7**	**7.028**	**0.008**	**0.028**	**7**
E4	**10**	**10.022**	**0.009**	**0.038**	**6**
G1	**8**	**7.833**	**0.017**	**0.069**	**16**
G2	**8**	**8.077**	**0.014**	**0.065**	**16**
Total			**0.009**	**0.193**	

With observation of Table 13, it is possible to conclude that the overall modal IT Grade for diameters of the Stratasys Objet30 is IT 9. For concentric cylinder boss features (A1, A2), the geometries conform to IT 8 and 9, with low mean deviation. With the difference of nominal

and measured values being greater in A1, this feature's nominal diameter of 20 mm places the cylinders within different ISO size ranges, and yet A1 presents itself in a less accurate IT Grade than A2. More delicate cylindric features labeled as cylinder bosses and pins (B1-3 and C1-3, respectively) also present themselves within a modal IT 9, and low measurement deviation, while also encompassing the largest outlier measurement point of all circular features, with $\delta_{max} = 0.193$ being the maximum. It is interesting to note how negative fine cylinders (pins) are more accurately fabricated than their embossed counterparts. Hemispheres (D1, D2) feature a comparable result, where it is observed that feature D1 – the "negative" sphere quarter – was measured above its nominal value in IT 9, while D2's measurement placed itself below CAD dimensions and at a much less accurate IT Grade (IT 11). Holes on the artifact (E1-4) have a lower tolerance grade of IT 7, and the measured diameter of all holes was larger than nominal value. Finally, the most inaccurate circular feature in PolyJet, Horizontal Cylinders place in IT 16, a range in which a much larger amount of tolerance factors (i) are able to fit within the gap value between CAD and measured dimensions. Additionally, similarly to what occurs in the spherical features, positive and negative cylinders seem to diverge from the nominal value in different manners.

Lengths (L) and heights (h) are "distance" type measurements in the Poli Light Man CMM. In the following tables, distance measurements will be analyzed for principal lengths and heights of each geometry. Since Table 13 previously evaluates the accuracy of circular features and diameters, the forthcoming material will cover heights and lengths as mentioned.

Table 14 – Principal distance dimensions of Cylinder Boss, Pins and Staircase geometries evaluated in terms of IT Grades for the Objet30.

Principal Dimensions	Nominal	Avg. Measure	Avg. IT Grade
Cylinder Boss (height)			
B features	**3.0**	**3.039**	**10**
Pins (height)			
C features	**3.0**	**2.953**	**10**
Staircases (height)			
H1	**-4.0**	**3.992**	**5**
H2	**-3.0**	**2.985**	**7**
H3	**-2.0**	**2.007**	**6**
H4	**-1.0**	**1.013**	**7**
H5	**1.0**	**0.998**	**4**
H6	**2.0**	**2.006**	**5**
H7	**3.0**	**2.983**	**7**
H8	**4.0**	**3.987**	**6**
H9	**5.0**	**5.006**	**5**

Above what has been previously observed in the Objet30's performance graphs, Cylinder Boss and Pins are similar features that achieve an equal IT Grade mean of IT 10 for lengths (Table 14). Meanwhile, staircases have a much more varied result in terms of the heights of each step, varying from IT 4 to IT 7. The Staircase feature consists of a very fine and small 3x3 mm square based step that may result in variation of the IT Grades obtained for the feature, even though results indicate performance with accuracy above the machine's average.

Rectangular bosses are a feature that is similar to staircases, but within larger dimensions and fabricated individually (non-bonded geometries). In this feature it is worth noting that dimensions in the x-axis have been fabricated with lower accuracy than in the other directions. This feature consists of a 3x4 mm rectangle, and varying heights, on negative and positive configurations. From Table 15 it is possible to observe low-value IT Grades in the ZY axes, whilst, as mentioned, the x-axis performs within IT 10. Larger rectangular bosses (absolute height of 7mm) performed with the best accuracy of the feature in PolyJet.

Table 15 – Principal distance dimensions of Rectangular Boss geometries evaluated in terms of IT Grades for the Objet30.

Rectangular Boss	Nominal	Avg. Measure	Avg. IT Grade
X	**3.0**	**3.007**	**10**
Y	**4.0**	**4.015**	**7**
Z			
J1	**3.0**	**3.014**	**8**
J2	**5.0**	**5.019**	**8**
J3	**7.0**	**7.010**	**6**
J4	**-7.0**	**7.019**	**7**
J5	**-5.0**	**5.018**	**8**
J6	**-3.0**	**3.021**	**8**
J7	**-1.0**	**1.055**	**11**

Finally, Table 16 presents the analysis for Square Boss geometries. In this feature, each height value resulted in a diverging mean IT Grade, however values range from IT 5 to 10, maintaining the geometric tolerances of fabrication within a maximum range of IT 10 and a deviation of 10 to 25 tolerance factor multiples. The major "square" dimensions of the artifact, evaluated as the base's dimensions L1 and L2 (Table 17), achieve IT 9 for the PolyJet manufacturing machine, which is interestingly large considering the artifact is a 50x50 mm part.

Table 16 – Principal distances of Square Boss geometries evaluated IT Grades for the Objet30.

Square Boss	Nominal	Avg. Measure	Avg. IT Grade
F1			
X	**3.0**	**2.972**	**9**
Y	**3.0**	**2.995**	**5**
Z	**3.0**	**2.984**	**7**
F2			
X	**6.0**	**5.929**	**10**
Y	**6.0**	**6.008**	**5**
Z	**3.0**	**3.019**	**8**
F3			
X	**9.0**	**8.930**	**10**
Y	**9.0**	**8.959**	**9**
Z	**3.0**	**3.002**	**5**

Table 17 – Test part outer dimensions evaluated in terms of IT Grades for the Objet30.

Outer dimensions	Nominal	Avg. Measure	Avg. IT Grade
L1 (X)	**50.0**	**49.924**	**9**
L2 (Y)	**50.0**	**49.944**	**8**
Grand Total	**50.0**	**49.934**	**9**

5.1.2 Sharebot Antares SLA – IT Grades for individual features

The overall performance of the Sharebot Antares (SLA) observed in Figure 62 ranges from an IT 12 or 13 grade in smaller sizes, up to an achievement of IT 11 in larger dimensions. This demonstrates that, contrary of what is seen in the performance of PolyJet, stereolithography IT grades exhibit a noticeable variance when set side by side in different ISO size ranges. In the same direction of the analysis that was performed for the Objet30, the Sharebot Antares' circular features have been evaluated as a primary result in Table 18 below.

Table 18 – Dimensional accuracy of the Sharebot Antares in terms of IT Grades for different geometric features of the test part.

(Diameters)	Nominal	Avg. Measure	Avg. δ	Max. δ	Avg. IT Grade
A1	**20**	**19.850**	**0.066**	**0.303**	**11**
A2	**15**	**14.876**	**0.061**	**0.213**	**11**
B1	**2**	**2.123**	**0.023**	**0.108**	**12**
B2	**3**	**3.108**	**0.025**	**0.094**	**12**
B3	**4**	**4.109**	**0.027**	**0.098**	**12**
C1	**2**	**1.685**	**0.015**	**0.043**	**14**
C2	**3**	**2.708**	**0.007**	**0.030**	**14**
C3	**4**	**3.734**	**0.007**	**0.033**	**13**
D1	**8**	**7.534**	**0.026**	**0.082**	**14**
D2	**8**	**7.710**	**0.015**	**0.052**	**13**
E1	**3**	**2.781**	**0.019**	**0.131**	**14**
E2	**5**	**4.693**	**0.010**	**0.054**	**14**
E3	**7**	**6.725**	**0.025**	**0.112**	**13**
E4	**10**	**9.589**	**0.022**	**0.099**	**14**
G1	**8**	**8.071**	**0.021**	**0.054**	**10**
G2	**8**	**7.712**	**0.056**	**0.291**	**13**
Total			**0.028**	**0.303**	

In the Sharebot Antares, circular feature fabrication is limited to a mean tolerance range of IT 13. Overall, the geometries are manufactured consistently with variation of only up to one IT grade between features of the same kind. Concentric cylinders (A1, A2) and cylinder boss (B1, B2) are produced consistently at IT Grades of 11 and 12, respectively – although it is feature A1 that has been measured with a major outlier of $\delta_{max} = 0.303$, which is significantly larger than the maximum irregularity in PolyJet circular features. Pins (C1-3) also perform regularly within the category, albeit having a lower modal accuracy of IT 14. All other features performed within ranges of IT 13-14, which is an acceptable result considering the overall evaluation from Figure 62 for small ISO sizes in SLA.

In a comparison of dimensional accuracies between SLA and Powder Binding, where a simple test part of concentric cylinders is used, Islam et al. found IT Grades in stereolithography up to a value of IT 10 [60]. The part, however, was much larger than the artifact used in this study, ranging up to a maximum diameter of 126 mm. From Politecnico di Torino, Ippolito et. al [20], in an accuracy benchmarking for rapid prototyping techniques evaluates SLA processes with a maximum tolerance grade range of IT 14 to IT 16. Therefore,

the results evaluated thus far follow a similar trend to what has been formerly evaluated in other stereolithography benchmarkings.

Since thus far results are coherent and akin to formerly developed work, it is justifiable to proceed with an analysis of linear dimensions – lengths and heights. As seen in Table 19 below, Cylinder boss (B) and Pin (C) heights conform to IT 12 and 13, respectively. This is an approximately equal result to the circular tolerance of these features. As for Staircases (H), within a similar frame to what has been observed in PolyJet, IT Grades vary vastly from IT 6-7 in smaller features, and generally increasing as absolute heights become larger – H1 and H9 obtained IT 13 and 12, respectively.

Table 19 – Principal distance dimensions of Cylinder Boss, Pins and Staircase geometries evaluated in terms of IT Grades for the Sharebot Antares.

Principal Dimensions	Nominal	Avg. Measure	Avg. IT Grade
Cylinder Boss (height)			
B features	**3.0**	**3.072**	**12**
Pins (height)			
C features	**3.0**	**2.826**	**13**
Staircases (height)			
H1	**-4.0**	**4.205**	**13**
H2	**-3.0**	**3.081**	**11**
H3	**-2.0**	**2.015**	**8**
H4	**-1.0**	**1.000**	**6**
H5	**1.0**	**0.988**	**7**
H6	**2.0**	**2.048**	**10**
H7	**3.0**	**3.018**	**7**
H8	**4.0**	**4.089**	**11**
H9	**5.0**	**4.879**	**12**

Since thus far results are coherent and akin to formerly developed work, it is justifiable to proceed with an analysis of linear dimensions – lengths and heights. As seen in Table 19 below, Cylinder boss (B) and Pin (C) heights conform to IT 12 and 13, respectively. This is an approximately equal result to the circular tolerance of these features. As for Staircases, within a similar frame to what has been observed in PolyJet, IT Grades vary vastly from IT 6-7 in smaller features, and generally increasing as absolute heights become larger – H1 and H9 obtained IT 13 and 12, respectively.

In SLA, Rectangular boss features (Table 20) perform lower accuracy than PolyJet. The Sharebot Antares performs with IT 13 for both direction in the XY plane, however for

heights it fabricates the features with a grade of IT 8, which is similar to that which is seen in PolyJet. With contrast to PolyJet, however, an observation about the SLA heights is that larger absolute lengths are less accurately produced – in stereolithography, J3 and J4 were the least accurately manufactured rectangular extrusions, whilst in PolyJet these were the most precise.

Table 20 – Principal distance dimensions of Rectangular Boss geometries evaluated in terms of IT Grades for the Sharebot Antares.

Rectangular Boss	Nominal	Avg. Measure	Avg. IT Grade
X	**3.0**	**2.942**	**13**
Y	**4.0**	**3.914**	**13**
Z			
J1	**3.0**	**2.981**	**8**
J2	**5.0**	**4.976**	**8**
J3	**7.0**	**7.055**	**9**
J4	**-7.0**	**6.926**	**10**
J5	**-5.0**	**4.972**	**8**
J6	**-3.0**	**2.989**	**7**
J7	**-1.0**	**0.982**	**8**

The results for Square boss can be found in Table 21, and Table 22 for Outer dimensions of the base. It is observed that similar to what is seen in "J" features of Rectangular Boss, heights of Square Bosses are produced very accurately, under IT 8. Equivalently, the accuracy within the XY plane is much lower, ranging to IT 12 and 13. As expected of larger ISO basic size, outside dimensions fall within IT 10 and 11, which are considerably more precise than the modal IT 13 grade observed throughout SLA (see Table 12).

Table 21 – Principal distances of Square Boss geometries evaluated IT Grades for the Sharebot Antares.

Square Boss	Nominal	Avg. Measure	Avg. IT Grade
F1			
X	**3.0**	**3.217**	**13**
Y	**3.0**	**3.132**	**12**
Z	**3.0**	**2.998**	**5**
F2			
X	**6.0**	**6.181**	**13**
Y	**6.0**	**6.063**	**10**
Z	**3.0**	**3.022**	**8**
F3			
X	**9.0**	**9.204**	**12**
Y	**9.0**	**9.150**	**12**
Z	**3.0**	**3.023**	**8**

Table 22 – Test part outer dimensions evaluated in terms of IT Grades for the Sharebot Antares.

Outer dimensions	Nominal	Avg. Measure	Avg. IT Grade
L1 (X)	50.0	49.852	10
L2 (Y)	50.0	49.795	11
Grand Total	50.0	49.824	11

5.1.3 Sharebot Rover DLP– IT Grades for individual features

The least accurate process studied, according to Figure 62, is the Digital Light Processing performed by the Sharebot Rover. Nonetheless, this machine is not vastly less performant than the SLA equipment analyzed, staying within a mean tolerance result of IT 13 for all low scale ISO basic sizes. On the other hand, the test part produced by the DLP equipment was the most accurate for the larger ISO dimensions available in the artifact, with a mean performance of IT 8. It is important to note, however, that this result has a lower statistical significance than those presented for small sizes, by reason of the sample space for larger ISO ranges containing a smaller amount of features.

Table 23 – Dimensional accuracy of the Sharebot Rover in terms of IT Grades for different geometric features of the test part.

(Diameters)	Nominal	Avg. Measure	Avg. δ	Max. δ	Avg. IT Grade
A1	20	19.964	0.045	0.309	7
A2	15	14.930	0.027	0.148	9
B1	2	2.092	0.025	0.080	11
B2	3	3.143	0.048	0.141	12
B3	4	4.152	0.051	0.234	12
C1	2	1.762	0.052	0.182	14
C2	3	2.704	0.043	0.238	14
C3	4	3.663	0.053	0.239	13
D1	8	7.769	0.020	0.091	12
D2	8	8.096	0.010	0.046	10
E1	3	2.777	0.031	0.044	13
E2	5	4.788	0.032	0.023	13
E3	7	6.815	0.023	0.112	12
E4	10	9.764	0.029	0.113	12
G1	8	8.011	0.020	0.124	6
G2	8	7.797	0.013	0.049	12
Total			0.033	0.309	

In the same analytical arrangement performed formerly performed, the results of the Sharebot Rover for circular features is presented in

Table **23** above. Other than Concentric (A) and Horizontal Cylinders (G), all circular features have been produced in the Sharebot Rover with tolerances above IT 11, yet averaging IT 13. In terms of measurement precision and surface roughness, the SLA and DLP machines have similar deviations (δ) in circular features, of 28 and 33 microns, respectively. This result, when compared to a 9 micron deviation in PolyJet, shows a lesser performance in accuracy of the Sharebot Rover and Antares machines when creating cylindrical components in AM.

Modifying the analysis to linear measurements, the lengths and heights of the Sharebot Antares present much better results in some features. As seen in Table 24, features such as Cylinder Boss (B) and Staircases (H1-9) have shown results better than those for SLA, where B-features performed at an IT Grade of 11, and Staircases demonstrated prominence by achieving grades as low as IT 5 and 6. The Staircase feature, however, did have a diverse performance as a function of step heights, since accuracy varies from IT 5 (H4) up to IT 10 (H6). The mean performance of excavated (or negative) features in Staircases is more accurate than protruding (or positive) features.

Table 24 – Principal distance dimensions of Cylinder Boss, Pins and Staircase geometries evaluated in terms of IT Grades for the Sharebot Rover.

Principal Dimensions	Nominal	Avg. Measure	Avg. IT Grade
Cylinder Boss (height)			
B features	**3.0**	**3.070**	**11**
Pins (height)			
C features	**3.0**	**2.245**	**> 16**
Staircases (height)			
H1	**-4.0**	**3.977**	**6**
H2	**-3.0**	**3.008**	**6**
H3	**-2.0**	**1.972**	**9**
H4	**-1.0**	**1.001**	**5**
H5	**1.0**	**0.971**	**9**
H6	**2.0**	**1.953**	**10**
H7	**3.0**	**2.978**	**9**
H8	**4.0**	**3.984**	**7**
H9	**5.0**	**4.966**	**9**

From Table 24 it is also noticeable that C-features, or Pins, have resulted in large imprecisions when measured, with a mean error of 25% with respect to nominal values of the artifact. The result of imprecision above IT 16 for Pins has been discarded from analysis, and highlights a qualitative complication of DLP manufacturing systems. Digital Light Processing

systems and resin reservoir AM methods in general are subject to problems and imprecision caused by unwanted resin curing. The Pins of the artifact consist of small 3 mm long openings, in which the largest diameter is that of feature C3, with 4 mm. Therefore, the feature is subject to unintended resin curing, that could be cause by inadequate washing of the part within post-processing, incorrect setup of the ultrasonic cleaning equipment, or even nonattendance of the part, being the last a likely hypothesis for the Sharebot Rover's fabricated part. The part produced turned out to have cured resin within small pockets, which was likely a byproduct of the long fabrication time of the unit – production of the DLP part required roughly 14 hours.

The same effect can be observed in Rectangular Boss feature (J), displayed in Figure 64, since there are also entries and gaps that can amass liquid resin remains. Therefore, data in Table 25 presents calculated tolerance grades particularly for outward rectangular features. Builds in the XY plane, however, remain unaffected, and can still be computed for data analysis. Finally, it is possible to observe that embossed rectangles produced by the Sharebot Rover are expected to present a minimum tolerance grade of IT 10, scaling up to IT 12 in its least accurate axis (X). Positive rectangular extrusions (J1-3; Z-axis), however, have been precisely produced features both in SLA and PolyJet, with a modal grade of IT 8, whereas the modal grade observed in DLP is considerably larger, at IT 10.

Figure 64 – Zoomed-in image of the DLP test-part's Rectangular Boss (J) and Pins (C) features where unintended curing had occurred.

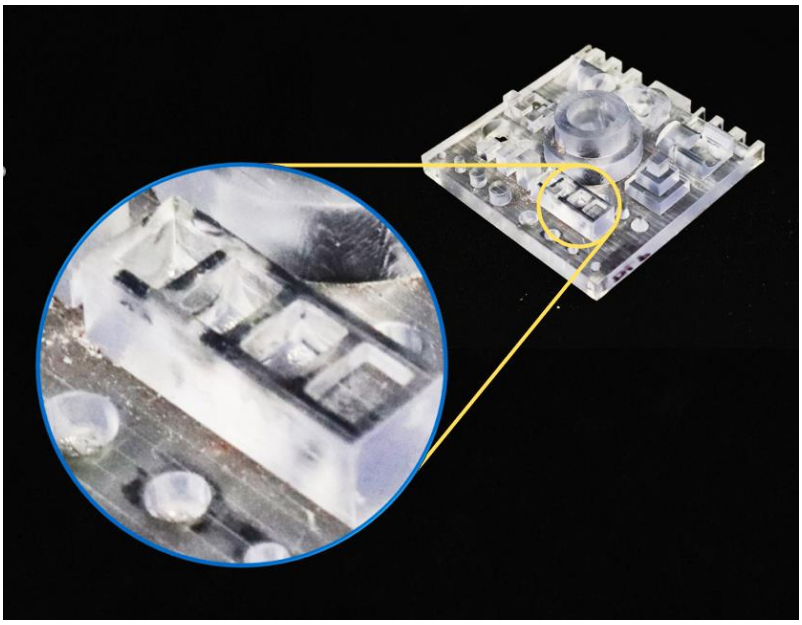

Table 25 – Principal distance dimensions of Rectangular Boss geometries evaluated in terms of IT Grades for the Sharebot Rover.

Rectangular Boss	Nominal	Avg. Measure	Avg. IT Grade
X	**3.0**	**2.945**	**12**
Y	**4.0**	**3.847**	**10**
Z			
J1	**3.0**	**2.984**	**8**
J2	**5.0**	**4.935**	**10**
J3	**7.0**	**6.926**	**10**
J4	**-7.0**	**2.809**	**-**
J5	**-5.0**	**3.651**	**-**
J6	**-3.0**	**2.844**	**-**
J7	**-1.0**	**0.824**	**-**

Finally, Table 26 presents the analysis for Square Boss (F) geometries in the DLP test-part. In this feature, it is noticeable how accuracy is affected as a function of manufacturing direction. The Z-axis demonstrates the best accuracy grade, in IT 8, whilst in the XY plane accuracy ranges from IT 14 to 15. Outer dimensions (L) for the Sharebot Rover achieved IT grades of 12 in the x-axis and 14 in the y-axis, which is quite inaccurate for a large basic ISO size.

Table 26 – Principal distances of Square Boss geometries evaluated IT Grades for the Sharebot Rover.

Square Boss	Nominal	Avg. Measure	Avg. IT Grade
F1			
X	**3.0**	**2.415**	**16**
Y	**3.0**	**2.487**	**15**
Z	**3.0**	**2.973**	**8**
F2			
X	**6.0**	**5.492**	**15**
Y	**6.0**	**5.550**	**14**
Z	**3.0**	**2.922**	**8**
F3			
X	**9.0**	**8.359**	**15**
Y	**9.0**	**8.501**	**14**
Z	**3.0**	**2.976**	**8**

Table 27 – Test part outer dimensions evaluated in terms of IT Grades for the Sharebot Rover.

Outer dimensions	Nominal	Avg. Measure	Avg. IT Grade
L1 (X)	**50.0**	**49.696**	**12**
L2 (Y)	**50.0**	**49.228**	**14**
Grand Total	**50.0**	**49.462**	**13**

5.2 Geometric feature accuracy according to GD&T standards

Machine tolerances are specified according to the type and value of tolerances and deviations produced, with respect to Geometric Dimensioning and Tolerancing (GD&T) standards. This system allows for predictability and forecasting of accuracy and precision in manufacturing processes when there is the necessity of controlled fabrication of a part or feature. Through GD&T, it is possible to define a range of dimensions in which manufacturing deviations are admissible. Various standards describe GD&T methodologies, each with particularities and geographic regions in which they are most commonly used, such as the ISO 1101 [61] and American Society of Mechanical Engineers (ASME) Y14.5 [62]. The ISO standards are also presented in individual norms that address control characteristics of features individually, in utmost detail.

The results of this benchmarking study will allow for tolerance synthesis in engineering projects that envision the usage of the Stratasys and Sharebot machines at hand. This process of tolerance synthesis, or tolerance allocation, refers to the controlled design of part features, where a purpose or parameter is established and clearances are mathematically planned to attain desired values after manufacturing [63].

The ISO 1101 standard classifies manufacturing variations into different tolerance classes and types. Geometrical characteristics are divided into class specifications of form, orientation, location and run-out. In this thesis, the analysis of form errors will be further classified in flatness, cylindricity and circularity (or roundness). Orientation tolerances considered will be parallelism and angularity, while location tolerances will be evaluated exclusively in terms of coaxiality and concentricity.

5.2.1 Form Specifications

Form specifications control only form deviations of a toleranced feature [61]. The classifications of form tolerances analyzed in this study are those of horizontal flatness (▱), roundness (◯) and cylindricity (⌭). These specifications are independent of a datum or reference feature, therefore representing surface deviation values of the measured data.

As formerly presented in chapter 3.3.3.2, a total of 10 planes (features P1-10) were selected in order to evaluate flatness of the part. Chapter 4.3 demonstrates the methodology of part measurement, according to ISO 12781 [64], where contact points are capable of establishing surface roughness and irregularities, and Figure 65 summarizes the concept which

will be indicated by the Poli Light Man's CMM as a deviation (δ) value for the measurement of planes, which has been formerly seen in the tables of Chapter 5.1.

Figure 65 - Two sets of parallel planes where an entire referenced surface must lie demonstrating the concept of flatness in GD&T.

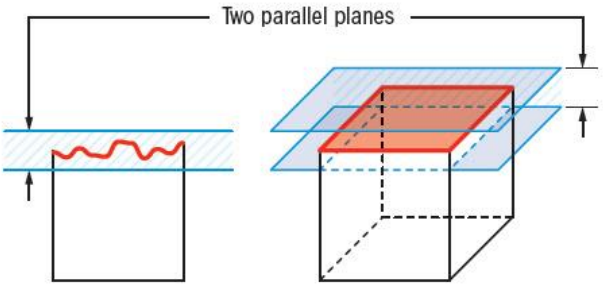

Source: [65]

Figure 66 – Comparison of horizontal flatness for the reference parts produced.

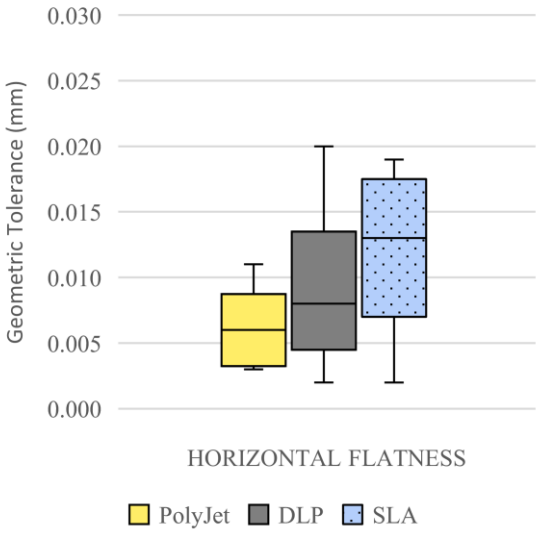

As expected from the data collected thus far, the PolyJet part performs very well as seen in Figure 66, with median flatness value of only 6 microns. This result is very similar to the performance of fused deposition modeling (FDM) machines seen in Minetola's benchmarking analysis, where median horizontal flatness would not surpass 10 microns, reaching even more accurate results than the ones observed in the box-plot above [16]. In comparison to Fahad & Hopkinson's benchmarking analysis of sintering-based additive manufacturing methods [66], all three machines (PolyJet, SLA, DLP) perform with

considerably greater accuracy, since the most flat HSS and SLS parts produced by Fahad & Hopkinson had deviations of 0.171 mm and 0.729 mm, respectively.

The Sharebot machines (SLA and DLP) did not perform as well as PolyJet, where the GD&T flatness value and tolerance zone of these test parts were roughly twice as large as the Objet30's fabricated artifact. Although the median value of DLP is smaller than SLA, its expected tolerance zone is slightly larger, and interestingly, the mean deviation for planar features is of 0.011 mm in both machines.

The circularity of the test artifact has been evaluated in terms of how closely its circular features approach the shape of a mathematically perfect circle, according to ISO 12181 [67]. Deviation values for GD&T are referenced as per what is measured by the Poli Light Man CMM, a root-mean-square deviation that is calculated upon each measurement of a circular feature. Therefore, the deviations or geometric tolerances of circularity for each machine in study can be seen in Figure 67 below. Once more it is notable that PolyJet performs with much larger accuracy than both DLP and SLA. In DLP, tolerance values can be up to eight times larger than PolyJet, and SLA's largest tolerance value is only approximately 20% more precise.

Figure 67 – Comparison of circularity for the reference parts produced.

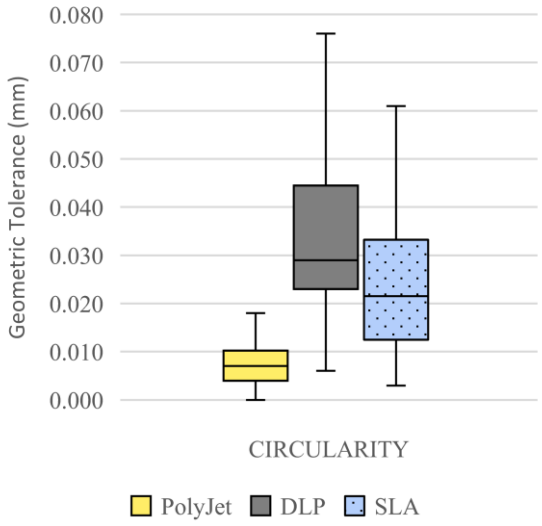

In cylindricity (ISO 12180), a surface of points is extracted from specific features in order to evaluate correlation to a mathematically cylindrical form that had been specified in part design, or CAD [68]. In order to evaluate the effect of commonly encountered errors in additive manufacturing, the test artifact was designed with cylinders in two types of orientations,

along both horizontal and vertical axes. Figure 68 presents a geometric tolerance analysis of cylindricity in terms of the measured deviation values of the CMM machine.

Figure 68 – Comparison of cylindricity for the reference parts produced as a function of feature orientation.

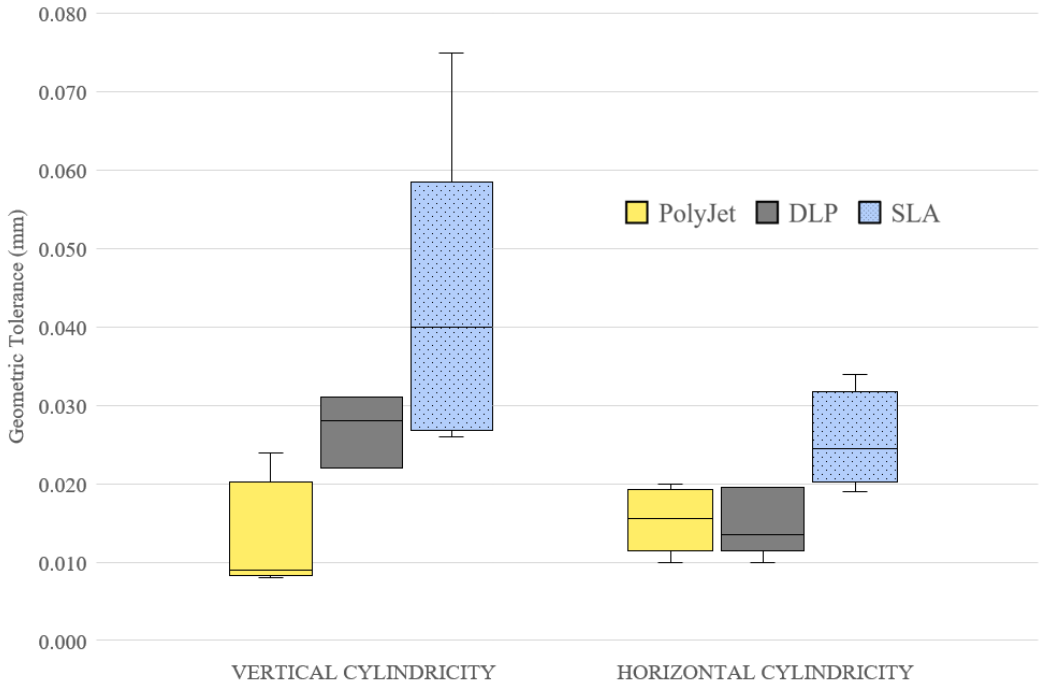

As observed in Figure 68, it is expected that horizontal cylinders have a smaller form tolerance in cylindricity. This is an interesting result, since in the IT Grade analysis realized in Chapter 5.1, features G1 and G2 (Horizontal Cylinders) had had bottom-tier performances in part accuracy. The GD&T feature of cylindricity, however, is not related to a datum, and therefore the results obtained represent only the expected surface deviations for any cylinder-like feature, independent of size. Once more, the Objet30 PolyJet machine performs at appealing and consistent accuracy rates, regardless of cylindrical orientation. Differently, the Sharebot machines of DLP and SLA perform with larger tolerance margin requirements, excluding the DLP results for horizontal cylinders, in which accuracy was evaluated closely to PolyJet.

5.2.2 Orientation and Location Specifications

An orientation specification controls orientation and form deviations of the toleranced feature but cannot control its location. Meanwhile, a location specification can control deviation of locations, orientation and form [61]. The classifications of orientation tolerances analyzed in this study are of parallelism (//) and angularity (∠), while for location tolerances, concentricity (◎) will be evaluated.

The Spain-based manufacturing company, Zorrotz, defines parallelism as "the absolute value of the maximum acceptable difference between dimensions X and Y" [69] and can be evaluated as an absolute value over a part's overall length, or can be given as a slope value in "mm/mt" (millimeters per meter). This approach to parallelism is commonly seen in GD&T, where the goal is to ensure that all points are contained within a specified tolerance from corresponding datum points of a reference plane [70]. Figure 69 shows the standard deviation obtained for the interpolation of P-features (Planes) in test parts produced by each machine. All machines perform very accurately in terms of the deviation of planar features, and all planar deviations without regards to a datum perform within 2 microns of mean accuracy. Datum points of maximum reference-to-peak deviation (S_{max}, in the Poli Light Man) do not surpass values of 40, 60 or 80 microns in PolyJet, SLA and DLP, respectively.

Figure 69 – Comparison of parallelism in P1-P10 for the reference parts produced.

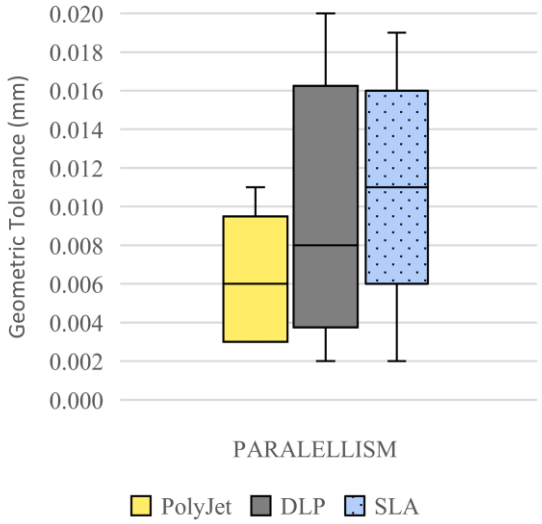

In Figure 70 another approach to parallelism is demonstrated, where the dimensional tolerancing can be measured by a sloping rate, through the millimetric

displacement obtained for every meter traveled along a part's reference length. All values calculated for the figure compare an arbitrary Plane feature (P2-P10) to a reference established by P1, the base plane of the part. Some datum points of the SLA part were not readable to the Poli Light Man, which explains the absence of P4-9 data for the Sharebot Antares' test part.

Figure 70 – Parallelism values for planes P2 to P10 in comparison to P1, in mm per meter.

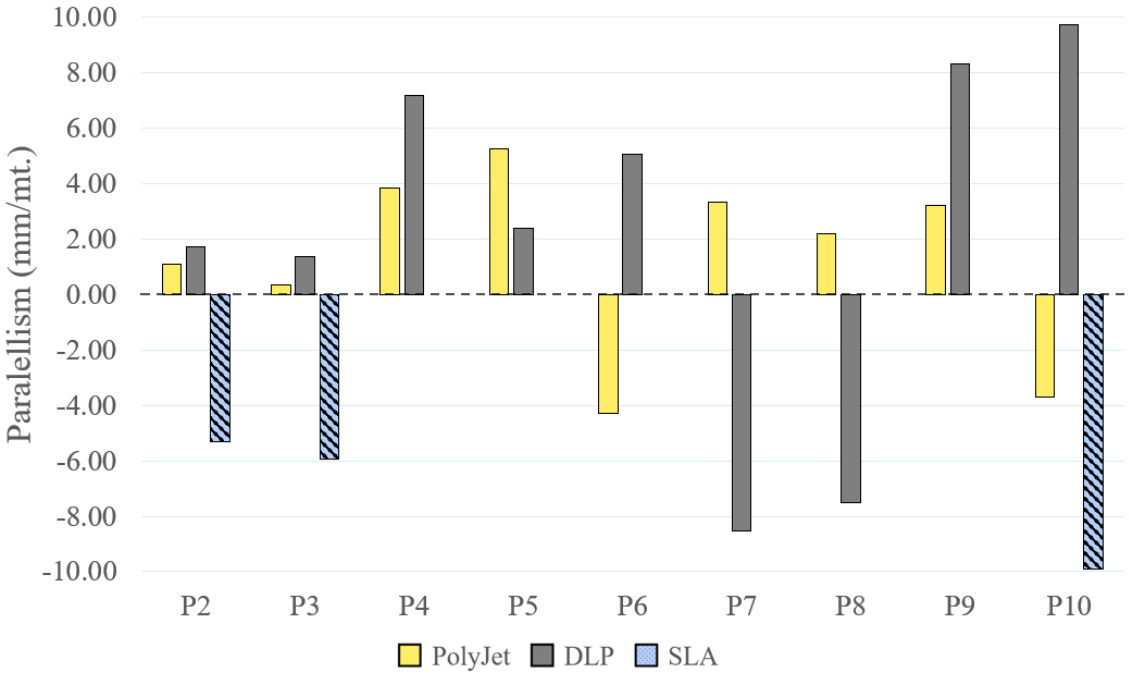

The analysis of Figure 70 demonstrates how each plane was sloped in regards to the part's basic plane, P1, demonstrating that the majority of planar features produced by the PolyJet and DLP parts were divergent to the orientation of plane P1. Planes P2 and P3 are associated to the Concentric Cylinder Boss (A) features, indicating that deviation in this kind of feature is very little. On the other hand, plane P9 the plane of Cylinder Boss B3, where deviation is much larger. This can be interpreted as the effect of a diameter's sizing into parallelism and local planar angularity – larger diameter features such as A1 and A2 perform well in parallelism, while a 3 mm diameter cylinder such as B3 does not.

Planes with relationships to square or rectangular features are the remaining P4-8 and P10. Planes P7 and P8 are linked to Square Boss (F), and it is possible to notice a similar performance both in terms of convergence direction and slope intensity. For the Staircases (H-features; planes P4, P5, P6), however, results are much more varied. This discrepancy is possibly justified in terms of sizing, since each step of the Staircase feature is composed of a

3x3 mm extrusion, which would lead to a similar conclusion of what has been seen in the contrast of planes P2-3 and P9. The final plane, P10, is associated to negative Rectangular Boss features (J4-J7). The results of parallelism in this plane are much less consistent, and greatly more sloped since the surface area of the block that holds features J4-J7 is composed of fine 1 mm walls, which likely contribute to an imperceptible curvature of planes that are included in the geometry. Accordingly, it is expected that the results of parallelism in plane P10 are composed of large tolerance margins and likewise a lower statistical relevancy.

Finally, the last point of interest in terms of location and orientation specifications lies within the latter and refers to the angularity of planes. In this study the benchmark of Incline features (I) is based on instructions and standards defined in ISO 1101. In GD&T, "Angularity" is defined as a parameter that does not control the angle of a referenced surface directly, but it controls the envelope or tolerance zone in which the entire surface must lie [71]. From authorial interest, the forthcoming analysis will contain a percentual error margin with regards to angular deviation. The measurement procedure realized in Chapter 4.3 consists of an angular comparison of the I-features' slope to the base (reference plane), and therefore data points will be sorted according to Equation (8), that can be visually understood from Figure 71.

$$(Angularity\ Tolerance) = 2R_I * \sin(\alpha_R - \alpha) \qquad (8)$$

Where:

- $R_I = 7.5\ mm$ is the general radius of all I-Features;
- α is nominal angle of the incline;
- α_R is real or measured angle of the incline.

Figure 71 – Outline of the adapted angularity tolerance zone calculated in this study.

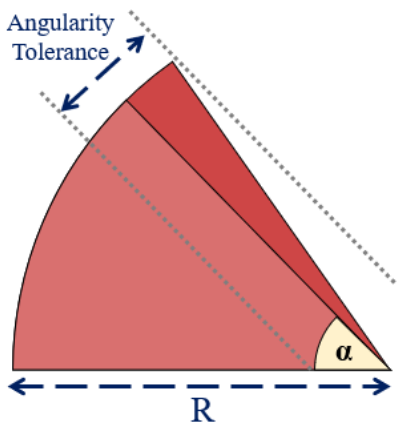

Table 28 – Angularity (mm) analysis of Inclines.

Inclines	Nominal α	Measured α_R	Error %	Angularity (mm)
PolyJet				
I1	**30.0**	**30.197**	**0.7%**	**0.052**
I2	**60.0**	**60.219**	**0.4%**	**0.057**
I3	**90.0**	**90.121**	**0.1%**	**0.032**
DLP				
I1	**30.0**	**30.545**	**1.8%**	**0.143**
I2	**60.0**	**60.401**	**0.7%**	**0.105**
I3	**90.0**	**89.585**	**-0.5%**	**0.109**
SLA				
I1	**30.0**	**30.794**	**2.6%**	**0.208**
I2	**60.0**	**60.285**	**0.5%**	**0.075**
I3	**90.0**	**89.627**	**-0.4%**	**0.098**

Figure 72 – Angularity values as a function of design slope.

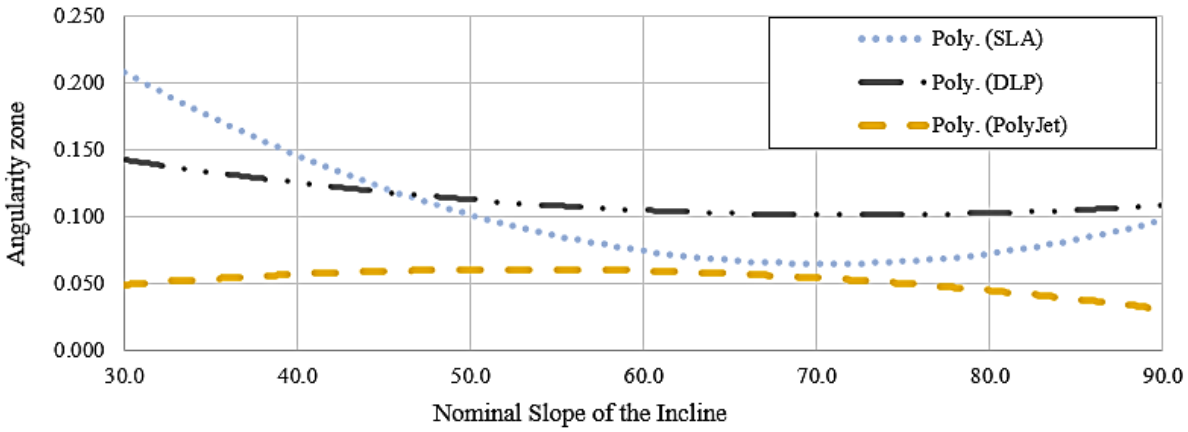

It is noticeable from Table 28 that error margins and angularity are proportional to one another, which is an expected result since in Equation (8) the tolerance should increase as the gap between α_R and α increases. From the results it is perceptible that PolyJet is once more the most accurate among the tested equipment, and that the angular accuracy of each feature depends largely on the process and particularly on the setup of fabrication. Assuming a simple quadratic interpolation for the behavior of angularity as a function of slope, it is possible to see in Figure 72 that in both SLA and DLP trendlines have an inflection minimum near the center of the nominal slope range. This can be interpreted as a balancing effect between the 45-degree fabrication setup to which both machines were subject, and the "staircase effect" that is expected from additive manufacturing processes. This is not observed in PolyJet since the part is printed without an inclination. Further detail will be included in Chapter 5.3 of Error Analysis.

5.2.3 Cones and spheres

There are no definitions for cones or spheres in ISO 1101 standards for GD&T, and therefore the deviation values evaluated for cones (K-features) and hemispheres (D-features) must be observed under instruction of different norms. For cones, the ISO 3040 norm, and spheres will be referenced through definitions contained in ISO 1132 of gauging and tolerancing principles, and ISO 3290 of steel spheres for roller bearings.

According to the ISO 3040, tolerancing of a cone is intrinsically defined by its angle, which can be defined through the cone's angle (α) or the rate of tapering (C). Additionally, for a fixed cone or finite geometry, a length (L_A) or height can be used; The concept presented is presented by the hypothetical cone of Figure 73.

Figure 73 – Intrinsic representation of a cone.

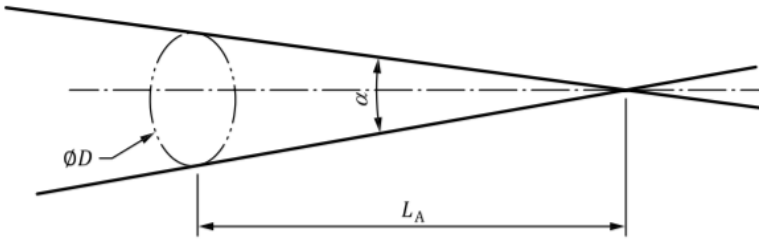

Source: [37]

Table 29 – Dimensional accuracy for cones in terms of angles and measure taper rates (mm).

CONE ANGLE	*Value of Angle*			*Taper Rates*	
	Nominal	**Avg. Measure**	**Error**	**$C_{NOM.}$**	**$C_{MEAS.}$**
PolyJet					
K1	**30.0**	**29.4**	**-1.88%**	**0.536**	**0.525**
K2	**15.0**	**14.5**	**-3.39%**	**0.263**	**0.254**
DLP					
K1	**30.0**	**30.9**	**2.97%**	**0.536**	**0.553**
K2	**15.0**	**15.5**	**3.54%**	**0.263**	**0.273**
SLA					
K1	**30.0**	**29.7**	**-0.93%**	**0.536**	**0.531**
K2	**15.0**	**18.2**	**21.27%**	**0.263**	**0.320**

Table 29 presents an error comparison between the angles that have been produced and their CAD nominal values. The ration of C_{MEAS}: C_{NOM} portrays roughly the same error

margin as seen in the category "Value of Angle", and therefore was not included. Interestingly, the angular values do not deviate much from design dimensions, remaining within a maximum mean error of 3.54%. The most irregular result lies in SLA's K2 feature, corresponding to the most acute cone in the artifact. The most likely cause of such result lies within a combined effect of the CMM and the feature. Coordinate measurement machines utilize an inspection method for cones that requires a 6-point measurement, where 3 points of contact are acquired in 2 different heights of the cone. Therefore, since the base of the 15 degree cone has a diameter of 2.68 mm, both 3-point circular features that compose the measurement will be interpolated with $d_{int} < 2.68$ mm, which opens space for low correlation or inaccurate readings from a 1mm wide Renishaw measurement probe on such a fine feature. Equivalently, the results obtained for cone heights are noticeably imprecise, and within an IT Grade analysis would reach grades above IT 16.

Table 30 – Dimensional accuracy for cones in terms height (mm).

CONE HEIGHT	Nominal	Avg. Measure	Error
PolyJet			
K1	**3.0**	**2.830**	**-5.68%**
K2	**5.0**	**4.650**	**-7.00%**
DLP			
K1	**3.0**	**2.589**	**-13.72%**
K2	**5.0**	**4.256**	**-14.89%**
SLA			
K1	**3.0**	**2.611**	**-12.98%**
K2	**5.0**	**3.973**	**-20.54%**

A ball gauge is a parameter defined by the amount in which the mean diameter of a sphere differs from the nominal sphere's diameter, allowing for an analysis of spherical tolerance through ISO standards. A first perspective of this result has been approached in Chapter 5.1's results of IT Grades for circular features (Table 13, Table 18, Table 23), therefore the nominal diameter of 8 mm and measured values will be omitted for the purpose of conciseness in further analyses of Hemispheres. The amount of deviation observed in each machine for D-features is the largest in SLA, and peak-to-reference maximum deviation is dependent of the feature. The "negative" feature D1 has a large outlier in DLP, whilst its mean deviation is low in the latter, and D2 has similar peak values, with SLA being only slightly larger. In terms of ball gauge, it is observable that SLA performs least accurately, and the sphericity observed in PolyJet and

DLP is very similar, having only an apparently opposing behavior in shrinkage, where this effect occurs in D2 for PolyJet and in D1 for DLP.

Table 31 – Ball gauge and error margins calculated for Hemispheres.

Hemispheres	Avg. δ	Max. δ	Ball Gauge	Error %
PolyJet				
D1 (-)	**0.014**	**0.059**	**0.296**	**0.62%**
D2 (+)	**0.011**	**0.046**	**-0.747**	**-1.56%**
DLP				
D1 (-)	**0.020**	**0.091**	**-0.694**	**-2.89%**
D2 (+)	**0.010**	**0.046**	**0.289**	**1.20%**
SLA				
D1 (-)	**0.077**	**0.082**	**-2.796**	**-5.83%**
D2 (+)	**0.045**	**0.052**	**-1.738**	**-3.62%**

5.3 Error analysis and inspection

In Chapter 3.2.7 a classification and description of potential errors is planned for artifact design and employment of the benchmarking analysis, based on an analysis by W. Cheng et al. [40]. According to a categorization proposed by Ameta et al. the error sources classified by W. Cheng et al. are “Process Driven Issues”, which include the effects of orientation, shapes, sizes, layering, etc. Effects classified as inherent to manufacturing, such as “free-form tolerancing” and “internal tolerancing” of parts are disregarded in the study of the machines and processes of the present work. Following an analogous line of thought from what is stated in Ameta et al. it is significant to consider errors encountered while performing the measurement of the part, those of which will be categorized as “Inspection Driven Issues” within this chapter. Process errors will be sorted according to fabrication similarities, and given that there is a large similarity between fabrication procedures of SLA and DLP, these processes will be categorized as “VAT Photopolymerization” technologies in comparison to PolyJet.

5.3.1 Process Driven Issues

As formerly mentioned, process driven issues and errors are correlated to inaccuracies that may be generated along the steps of fabrication of the part, which would introduce physical geometric errors onto the desired part. It is important to note, however, that

error sources will be observed individually within this chapter, and in actuality the results observed are a combination of multiple effects onto the geometric features.

In terms of importing a CAD file, approximations are made so that the designed part is understandable to the manufacturing machines, thus the model is converted to a Standard Tessellation Language file (STL) [72]. This conversion from CAD to STL introduces an error commonly known as “chordal error”, which is the maximum deviation between an original CAD surface and a triangulation of a tessellated model [73]. This error is a potential cause of inaccuracies within the parts fabricated in RMLAB’s Sharebot and Stratasys machines, however it is expected that the influence of this effect would be of only a small margin of micrometers. Nevertheless, Tessellation errors can be avoided through the usage of different file formats from the common STL type. Recently, other file formats such as Jupiter Tessellation (JT) and Additive Manufacturing File (AMF) have been proposed [74][75]. Such formats, however, have not been extensively accepted by machine manufacturers due to the larger complexity involved in CAD surface slicing, in addition to how widespread and simple STL has become over time.

The effect entitled as “missing feature” by W. Cheng et al. is exhibited in Figure 74 and shows how geometries and features may be distorted in uniform slicing procedures [76]. The results of this effect are likely seen in features whose precision is evaluated in terms of heights on the Z-axis. Since the VAT parts produced in Sharebot machines are tilted at an angle of 45 degrees, it is expected that this effect would materialize larger inaccuracies than in PolyJet. The effect can be seen clearly when contrasting the results presented by Table 14 to its counterparts in VAT Sharebot machines. Not only is the layer thickness of PolyJet as fine as the VAP parts, but orientation allows for topology-optimized prints, in which the influence of the “missing feature” and staircase effects is not as expected. Furthermore, as seen in Table 30, the error in heights of Cones (K) in VAT features is much larger than PolyJet, where error percentages are roughly 2 or 3 times greater. It is also noticeable how the larger feature (K2) presents a higher error margin, which is likely to be a contribution of the “missing feature” effect, where a slimmer feature’s tip is more likely to be approximated to an absent piece in the layer.

Figure 74 – Uniform slicing; (a) original model, (b) resulting part.

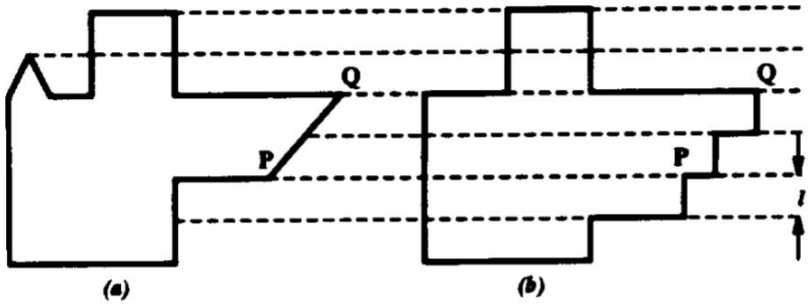

Source: [76]

Another source of errors is the "staircase effect", where inaccuracies are also caused by the difference between what is the designed part and the geometry that is realistically fabricated [40]. This effect appears over inclined surfaces creating cusps that would require post-processing in order to improve accuracy regarding the original design. Since the fabrication of parts is done in angled fashion, once more imprecision is introduced as a tradeoff to enabling the machine's production of the part. This source error can be observed in the results of various features, such as circularities specified in Chapter 5.2.1. As observed in Figure 67, the Sharebot machines are less likely to produce an accurate circular feature than the Objet30, whereas the least accurate circular feature of PolyJet is still more precise than the mean deviation produced in SLA and DLP. According to Dolenc et al. [76] the use of variable layer thickness slicers is a feasible method of handling both the staircase and "missing feature" effects. The slicer software must be given a range of working thicknesses such that the cusp height produced (c) is within a user-specified tolerance C_{max}. Post-processing is still a reasonable approach to handling these effects once slices are ready. Among various operations, offsetting allows for post-treatment that would require only material removal, such as the example seen in Figure 76.

Figure 75 – Staircase effect and cusp height c.

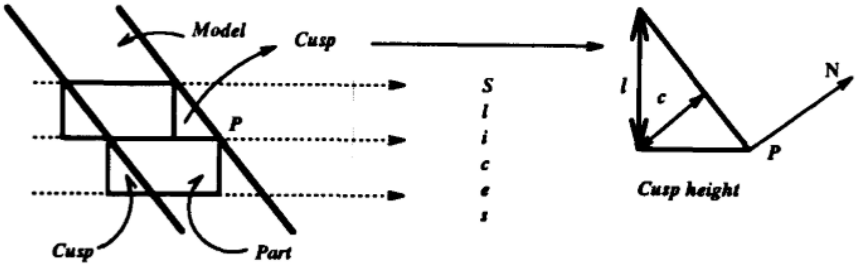

Source: [76]

Figure 76 – Compensation for post-processing that requires material removal.

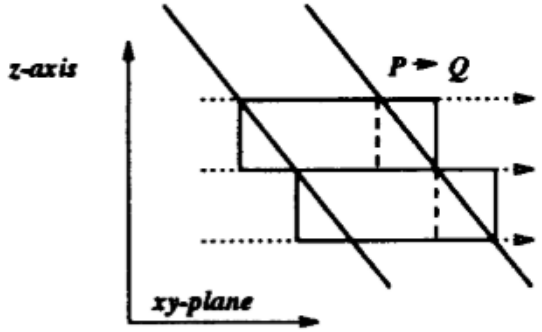

Source: [76]

Error sources related to undesired curing can be associated to the mentioned "container effect" and overcuring, cure-through, or the "back-side effect". The first effect mentioned is related to trapped volumes along the geometries of the part that can be categorized as small "containers". This effect was expected in SLA and DLP processes since they are VAT photopolymerization processes in which there is direct contact of the part to a pool of uncured resin. In PolyJet this is not an expected error since resin is precisely jetted onto the part with the objective of producing a singular layer. As formerly approached in Figure 64, the DLP fabrication process experienced a large amount of unplanned curing within negative non-passing features, such as Pins (C) and the Rectangular Boss (J). The process of SLA also undergoes the same effect, but under a lower intensity, since it is noticeable that Pin features had a mean deviation of around 0.2 mm in SLA, and up to 0.7 mm in DLP, for a 3 mm Pin feature. Most noticeably, the negative Rectangular Boss features (J4-J7) of the DLP part were disregarded from the data sample, since dimensions were largely affected by undesired curing. It is hypothesized that this is the result of a combined application of the container and back-side effects, where surface tension would retain resin that would be later cured by unaccounted-for light propagation. This can potentially be a result of a long print period (14 hours in DLP) combined to an incomplete control of light propagation in DLP since, unlike SLA, this process requires a large amount of simultaneous light emission.

Part shrinkage is a common problem in VAT processes due to the resin used. The manufacturing machine's software generally contains a compensation factor for shrinkage in all directions. However, it is still possible to observe shrinkage and warping of the part. This is the case observed in the part produced by the Sharebot Antares (SLA). The part contains a small

amount of warpage noticeable only on the bottom face of the part, as seen in Figure 78. Similar to the process observed in Mahesh et. al [21] the part displayed warpage on one side (Figure 77-b).

Figure 77 – Part warpage drifting towards edges (a) and only one side (b).

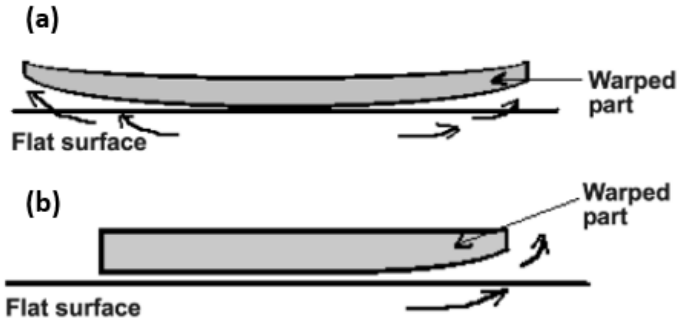

Source: [21]

Figure 78 – SLA part (left) and PolyJet (right) highlighting the warped edge of the SLA part.

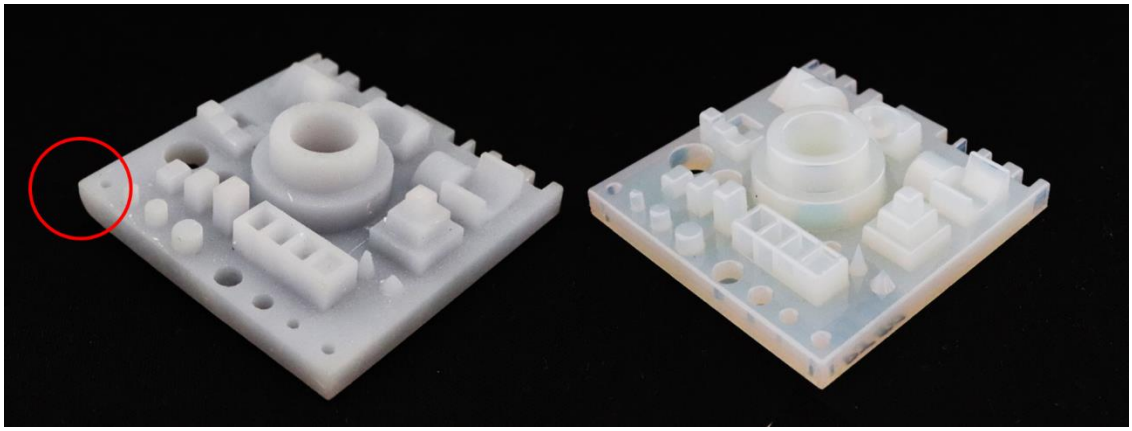

Shrinkage of resin during photo-polymerization is the major cause of errors during the SLA process. There are two types of shrinkage that occur due to the photopolymer's reaction. The first is caused by the formation of the polymer bond. Since the pre-polymer liquid resin state is less dense than the solidified (or already cured) polymer, the volume of the cured solid is smaller than the volume of liquid from which it was formed. The second cause of shrinkage is a thermal effect that results from the exothermic nature of photo-polymerization. Sudden heating causes the photopolymer to expand upon formation, and at the same time heat is lost to the surroundings, developing the shrinking effect. The combination of these types of shrinkage is known to result in internal stresses that lead to part warping [60] [77].

It is also possible that deformations in the edges and inferior base of the SLA test part were a result of insufficient supporting structures, since inverted stereolithography – as performed by the Sharebot Antares – requires larger support structures to keep the part attached to the build platform, and uncoupling could have been a cause to the distortion [78]. Also, in SLA sagging and unwanted bending are likely to occur since in this manufacturing method requires post-process UV curing for the parts to achieve full strength and become stable [79].

Conclusively, in order to ensure the absence of problematic warping and shrinkage, or even simply reduce distortion if it is significant enough, the user must factor the orientation of the part, its position on the build platform, power of light emission, temperature of the build platform, supporting sufficiency and the feasibility of brims and rafts. It is worth mentioning that the SLA part evaluated in this study had a minor one-sided warping effect that had negligible influence on the accuracy of geometries contained on the upper face of the part.

5.3.2 Inspection Driven Issues

Considering the aforementioned sources of error, it is also important to understand that inspection may also be a source of errors and uncertainties. As mentioned in Chapter 3.2.5, the Poli Light Man has a maximum permissible error (MPE), and this parameter of a CMM must be accounted for when considering possible sources of inaccuracies. The machine has a declared volumetric length measuring uncertainty of MPE 5 + 10*L, where L is the measured length.

A typical stylus used for CMM measurements is composed of a spherical tip at the end of the stylus shaft, as formerly seen in Chapter 3.2.5, in order to maintain a uniform shape in all relevant directions. Measurements and the dimensions of a workpiece are calculated based on the probing coordinates, therefore calibration of what is called the “form error” of a probe tip is essential in 3D measurements by a coordinate measurement machine. The order of form error in styli, however, is very minor, with a range of tens of nanometers when tests are performed on gauge blocks with ultra-flat surfaces [80]. Therefore, the effect of stylus error is negligible in this study, since the artifact features contain geometries in the range of millimeters, and precision is evaluated in a scale of micrometers.

6. CONCLUSION

The benchmarking study that was conducted in this thesis depicts the qualities of each machine analyzed, highlighting the performance in geometric accuracy of the Stratasys Objet30 Prime PolyJet printer, over the Sharebot Antares and Sharebot Rover. The IT grade analysis quantifies the discrepancy in performance, indicating that the Stratasys machine is capable of performing within grades of IT 8 to 9, whilst the Sharebot equipment manufactures at a range of IT 11 to 13.

Such difference in performance can be attributed to multiple factors, such as having a more advanced and costly machine in the Objet30, with various automated features provided by Stratasys. Moreover, the part is produced without the inclusion of supporting structures, in its designed orientation and with a fine layering quality, which are factors capable of ensuring higher accuracy and detail to an AM part. The absence of a resin vat – in contrast to the Sharebot machines – also contributes to a minimization of error sources originated from fluid tension and layer adhesion, preventing some possible distortions and warpage of the workpiece.

Regarding GD&T, the results indicate that the Sharebot machines are capable of performing closely in accuracy to that which can be manufactured in an Objet30, especially regarding the Sharebot Rover. Contrarily to what was initially expected, the Sharebot Rover outperforms the Antares in most geometries, and in some demonstrates a median accuracy range remarkably similar to what is fabricated in PolyJet. It is interesting that when ISO basic sizes of fabrication dimensions are compared, the Sharebot machines progress into better accuracies as the size of the part increases. On the other hand, the Objet30 performed consistently within its expected IT grade range, even when dimensions are in much larger basic sizes.

It is scientifically relevant to recognize improvement points of the study performed, and these can be categorized within the part design or experimental assessments. In terms of artifact design, perfecting of the test part includes the rearrangement and restructuring of features such as the square notch feature M1 and the enclosed spaces found in families C, H and J. The slim wall in the square feature mentioned had obstructed measurements, therefore it turns against initial design intentions. In the case of enclosed spaces, manufacturing with resins caused minor undesired curing, which disables features for measurement, and therefore removes their statistical relevancy in the analysis. This can be solved through the inclusion of punctures in the features, which would allow resin to escape the confinement whilst also not influencing the major geometry of the feature. It is also possible to include more inclines and planar features along main geometries, for a better utilization of space and material.

With regards to fabrication, measurements and overall experimental assessments, there is room for improvement of the study in different aspects. An alternative approach to that which was performed is to fabricate more than one test part per machine, either in a batch that is produced in the same session, or made in different moments, individually. This allows for a larger framework of data, in which the same geometry can be observed multiple times with regards to session or build platform area used. Another experimental enhancement that could increase statistical relevancy is fabrication of all parts in the same orientation. Since the PolyJet artifact was produced in design orientation, it is possible that the results observed for the Objet30 had been favored over the Sharebot machines, in which parts were inclined when fabricated.

Finally, it is important to note that data may have been influenced by the equipment used when conducting the measurement procedures. In particular, it is important to be wary of the CMM used, where manual measurement and calibration was conducted. The Poli Light Man used not only is manual but contains aging equipment that dates to 1992, and other newer, more precise, and advanced CMMs were not available for use at Politecnico di Torino. It is likely that more modern technology would be capable of minimizing human errors or measurement imprecisions that are propagated into the data.

The methodology presented in this dissertation has general applicability and can also be extended to other additive manufacturing systems that utilize photopolymers. As mentioned, over these first results it is possible to work towards an improvement of results, but the analysis performed is complete and allows for predictability when using the Stratasys and Sharebot equipment analyzed, which is the objective of the benchmarking analysis.

REFERENCES

[1] I. Newton and R. Hooke, “Isaac Newton letter to Robert Hooke,” 1675.

[2] J. Horn, L. N. Rosenband, and M. R. Smith, *Reconceptualizing the Industrial Revolution*. 2010.

[3] K. Pouspourika, “The 4 Industrial Revolutionso Title,” 2019. [Online]. Available: https://ied.eu/project-updates/the-4-industrial-revolutions/.

[4] J. S. Hyatt and J. W. Hyatt, “Improvement in Process and Apparatus for Manufacturing Pyroxyline,” US133229A, 1872.

[5] R. F. Jones, “Tools of the Trade,” *Astounding Science Fiction*, 1950.

[6] D. E. H. Jones, “Ariadne,” *New Sci.*, vol. 64, no. 917, p. 80, 1974.

[7] General Electric Additive, “ADDITIVE MANUFACTURING,” 2020. [Online]. Available: https://www.ge.com/additive/additive-manufacturing.

[8] T. Gornet and T. Wohlers, “History of Additive Manufacturing,” *Wohlers Rep. 2014*, pp. 1–24, 2014.

[9] MANUFACTUR3D, “A Comprehensive List of All 3D Printing Technologies,” 2018. [Online]. Available: https://manufactur3dmag.com/comprehensive-list-all-3d-printing-technologies/.

[10] S. Crump, “FDM Stratasys Patent US 5,121,329,” 1992.

[11] C. R. Deckard, “SLS Patent US 4,863,538,” Google Patents, 1986.

[12] L. J. Hornbeck, “SPATIAL LIGHT MODULATOR AND METHOD Patent US 4,662,746,” 1987.

[13] C. W. Hull, “Apparatus for Production of Three-Dmensonal Objects By Stereo Thography,” *Google Patents*, no. 19, p. 16, 1984.

[14] B. Kelly, I. Bhattacharya, M. Shusteff, R. M. Panas, H. K. Taylor, and C. M. Spadaccini, “Computed Axial Lithography (CAL): Toward Single Step 3D Printing of Arbitrary Geometries,” 2017.

[15] N. Sridharan and C. M. Petrie, “Ultrasonic Additive Manufacturing,” *Additive Manufacturing Processes*. pp. 247–260, 2020.

[16] P. Minetola, L. Iuliano, and G. Marchiandi, “Benchmarking of FDM Machines through Part Quality Using IT Grades,” *Procedia CIRP*, vol. 41, pp. 1027–1032, 2016.

[17] M. A. D. S.Moylan, J. Slotwinski, A. Cooke, K. Jurrens, “Proposal For a Standardized Test Artifact For Additive Manufacturing Machines and Processes,” *Solid Free. Fabr.*

Symp., pp. 902–920, 2012.

[18] E. P. Gargiulo, “Stereolithography process accuracy: user experience, Proceedings of the 1st European Conference on Rapid Prototyping,” 1992.

[19] J. P. Kruth, “Material Incress Manufacturing by Rapid Prototyping Techniques,” *CIRP Ann. - Manuf. Technol.*, vol. 40, no. 2, pp. 603–614, 1991.

[20] R. Ippolito, L. Iuliano, and A. Gatto, “Benchmarking of Rapid Protoyping Techniques in Terms of Dimensional Accuracy and Surface Finish,” 1995.

[21] M. Mahesh, Y. S. Wong, J. Y. H. Fuh, and H. T. Loh, “Benchmarking for comparative evaluation of RP systems and processes,” *Rapid Prototyp. J.*, vol. 10, no. 2, pp. 123–135, 2004.

[22] N. Decker and A. Yee, “A simplified benchmarking model for the assessment of dimensional accuracy in FDM processes,” *Int. J. Rapid Manuf.*, vol. 5, p. 145, Dec. 2016.

[23] F. A. Cruz Sanchez, H. Boudaoud, L. Muller, and M. Camargo, “Towards a standard experimental protocol for open source additive manufacturing: This paper proposes a benchmarking model for evaluating accuracy performance of 3D printers,” *Virtual Phys. Prototyp.*, vol. 9, no. 3, pp. 151–167, 2014.

[24] D. Flack, *CMM Measurement Stategies - Good practice guide No. 41*, no. 2. 2014.

[25] M. Fahad and N. Hopkinson, “A new benchmarking part for evaluating the accuracy and repeatability of AM processes,” 2012.

[26] N. P. Juster and T. H. C. Childs, “A comparison of rapid prototyping processes,” in *Proceedings of Third European Conference on Rapid Prototyping and Manufacturing*, 1994, pp. 35–52.

[27] Sharebot, “Sharebot Antares Technical Details Flyer,” *Technical Datasheet*, 2018.

[28] Sharebot, “Sharebot Antares: Professional SLA 3D printer with 15.000 cm3 of printing volume.” [Online]. Available: https://www.sharebot.it/en/sharebot-antares-3d-printer/.

[29] Sharebot, “Sharebot Rover DLP Printer Technical Details Commercial Sheet,” 2019.

[30] Stratasys, “Objet30 Prime Technical Datasheet,” 2016.

[31] Stratasys, “Specification Sheet Objet350 - Connex3,” 2018.

[32] K. America, “Measurement System Types and Characteristics | Measurement Fundamentals.” [Online]. Available: https://www.keyence.com/ss/products/measure-sys/measurement-selection/type/.

[33] Donato Pimazzoni, “Macchine usato – Pimazzoni Cmm Service.” [Online]. Available: https://www.pimazzonicmmservice.it/macchine-usato/.

[34] ISO 10360-2:2009, “Geometrical product specifications (GPS) — Acceptance and reverification tests for coordinate measuring machines (CMM) — Part 2: CMMs used for measuring linear dimensions,” 2009.

[35] Hexagon Manufacturing Intelligence, “All about CMM Styli,” 2014. [Online]. Available: https://www.hexagonmi.com/solutions/technical-resources/metrology-101/what-is-a-cmm-stylus#:~:text=All about CMM Styli,the component to be measured.

[36] E. W. Weisstein, “Cylinder,” *MathWorld -- A Wolfram Web Resource*. [Online]. Available: https://mathworld.wolfram.com/Cylinder.html.

[37] International Organization for Standardization, “Geometrical product specifications (GPS) — Dimensioning and tolerancing — Cones,” vol. 20, 2016.

[38] Bearing News, “Additive manufacturing of rolling bearings in innovative lightweight design by laser metal deposition,” 2019. [Online]. Available: https://www.bearing-news.com/additive-manufacturing-of-rolling-bearings-in-innovative-lightweight-design-by-laser-metal-deposition/.

[39] Oxford Learner’s Dictionary, “Sphere.” [Online]. Available: https://www.oxfordlearnersdictionaries.com/us/definition/american_english/sphere.

[40] H. T. Loh, “Optimization of Part- Building Orientation in Stereolithography,” vol. 1, no. 4, pp. 12–23, 2002.

[41] P. Kulkarni, A. Marsan, and D. Dutta, “Review of process planning techniques in layered manufacturing,” *Rapid Prototyp. J.*, vol. 6, no. 1, pp. 18–35, 2000.

[42] Z. D. Pritchard, M. P. de Beer, R. J. Whelan, T. F. Scott, and M. A. Burns, “Modeling and Correcting Cure-Through in Continuous Stereolithographic 3D Printing,” *Adv. Mater. Technol.*, vol. 4, no. 12, pp. 1–7, 2019.

[43] P. . Jacobs, *Rapid Prototyping and Manufacturing: Fundamentals of Stereo-Lithography*. Southfield, MI, USA: Society of Manufacturing Engineers, 1992.

[44] E. Yasa, O. Poyraz, E. U. Solakoglu, G. Akbulut, and S. Oren, “A Study on the Stair Stepping Effect in Direct Metal Laser Sintering of a Nickel-based Superalloy,” *Procedia CIRP*, vol. 45, pp. 175–178, 2016.

[45] H. Brooks, A. Rennie, T. Abram, J. McGovern, and F. Caron, “Variable Fused Deposition Modelling - analysis of benefits, concept design and tool path generation,” 2011, pp. 511–517.

[46] D. Chakravorty, “3D Printing Support Structures,” 2020. [Online]. Available: https://all3dp.com/1/3d-printing-support-structures/.

[47] C. Lynn-Charney and D. W. Rosen, “Usage of accuracy models in stereolithography process planning,” *Rapid Prototyp. J.*, vol. 6, no. 2, pp. 77–86, 2000.

[48] CIMsystem, “Pyramis - The easiest application for managing your 3D printing,” 2020. [Online]. Available: https://www.cimsystem.com/dental/products/pyramis-features.

[49] Formlabs Inc., “SLA basic finishing steps: Washing—soaking and moving parts in solvent,” 2020. [Online]. Available: https://support.formlabs.com/s/article/Form-2-Basic-Finishing-Steps.

[50] Sharebot, “S-CLEAR V2 1KG.”

[51] Sharebot, “PR-S 1KG.”

[52] MANUFACTUR3D, “The Difference between DLP and SLA,” 2018. [Online]. Available: https://manufactur3dmag.com/difference-dlp-sla.

[53] goengineer - Online Store, “VEROWHITE PLUS / RGD835 / 1KG,” 2020. [Online]. Available: https://store.goengineer.com/products/verowhite-plus-1kg-pack-of-2-fullcure-835.

[54] S. J. Jin, D. Y. Kim, J. H. Kim, and W. C. Kim, “Accuracy of Dental Replica Models Using Photopolymer Materials in Additive Manufacturing: In Vitro Three-Dimensional Evaluation,” *J. Prosthodont.*, vol. 28, no. 2, pp. e557–e562, 2019.

[55] Sharebot, “UV oven for post-curing resin prints,” 2020. [Online]. Available: https://www.sharebot.it/en/prod/uv-oven-for-post-curing-resin-prints/.

[56] GEOSOFT, “EL 1008 GEO SOFT 1 - Sistema di Misura Tridimensionale: Manuale di utilizzo,” vol. 6, 1993.

[57] W. Tyler Estler *et al.*, “Error compensation for CMM touch trigger probes,” *Precis. Eng.*, vol. 19, no. 2–3, pp. 85–97, 1996.

[58] P. Minetola, F. Calignano, and L. Iuliano, “Comparison of dimensional tolerance grades of AM systems,” pp. 9–11, 2019.

[59] ISO International Standard, “ISO 286-1:2010 (en) Geometrical product specifications (GPS) — ISO code system for tolerances on linear sizes — Part 1: Basis of tolerances, deviations and fits,” 2010.

[60] M. N. Islam, H. Gomer, and S. Sacks, “Comparison of dimensional accuracies of stereolithography and powder binder printing,” *Int. J. Adv. Manuf. Technol.*, vol. 88, no. 9–12, pp. 3077–3087, 2017.

[61] International Organization for Standardization, “ISO 1101:2017 Geometrical product specifications (GPS) — Geometrical tolerancing — Tolerances of form, orientation, location and run-out,” vol. E, 2017.

[62] ASME, “ASME Y14.5-2018 Dimensioning and Tolerancing.” New York, NY, 2018.

[63] B. C. Zhang, “Geometric modeling of dimensioning and tolerancing,” Arizona State University, 1992.

[64] International Organization for Standardization, “ISO 12781-1:2011(en) Geometrical product specifications (GPS) — Flatness — Part 1: Vocabulary and parameters of flatness,” 2011.

[65] GD&T Basics, “FLATNESS,” 2014. [Online]. Available: https://www.gdandtbasics.com/flatness/.

[66] M. Fahad and N. Hopkinson, “Evaluation and comparison of geometrical accuracy of parts produced by sintering-based additive manufacturing processes,” *Int. J. Adv. Manuf. Technol.*, vol. 88, no. 9–12, pp. 3389–3394, 2017.

[67] International Organization for Standardization, “ISO 12181-1:2011(en) Geometrical product specifications (GPS) — Roundness — Part 1: Vocabulary and parameters of roundness.” 2011.

[68] International Organization for Standardization, “ISO 12180-1:2011(en) Geometrical product specifications (GPS) — Cylindricity — Part 1: Vocabulary and parameters of cylindrical form.” 2011.

[69] ZORROTZ, “Machine Tool Slide-ways.” p. 16, 2019.

[70] GD&T Basics, “PARALLELISM,” 2014. [Online]. Available: https://www.gdandtbasics.com/parallelism/.

[71] GD&T Basics, “ANGULARITY.” [Online]. Available: https://www.gdandtbasics.com/angularity/.

[72] N. Panhalkar, “Hierarchical Data Structures for Optimization of Additive Manufacturing Processes,” 2015.

[73] J. Zhao, R. Xia, W. Liu, and H. Wang, “A computing method for accurate slice contours based on an STL model,” *Virtual Phys. Prototyp.*, vol. 4, no. 1, pp. 29–37, 2009.

[74] Siemens PLM Software, “JT File Format Reference Version 9.5 Rev-E.” 2010.

[75] ASTM, “Standard Specification for Additive Manufacturing File Format (AMF),” 2012.

[76] A. Dolenc and I. Mäkelä, “Slicing procedures for layered manufacturing techniques,” *Comput. Des.*, vol. 26, no. 2, pp. 119–126, 1994.

[77] W. Freed, Hull CW, L. CW, S. DR, S. ST, and V. WB, “Stereolithographic curl reduction,” 1989.

[78] Formlabs Inc., “The Ultimate Guide to Stereolithography (SLA) 3D Printing,” no. March, pp. 1–23, 2017.

[79] B. Redwood, “Dimensional accuracy of 3D printed parts,” *3D HUBS*. [Online]. Available: https://www.3dhubs.com/knowledge-base/dimensional-accuracy-3d-printed-parts/#sla.

[80] S. Ito, D. Tsutsumi, K. Kamiya, K. Matsumoto, and N. Kawasegi, “Measurement of form error of a probe tip ball for coordinate measuring machine (CMM) using a rotating reference sphere,” *Precis. Eng.*, vol. 61, no. Cmm, pp. 41–47, 2020.

APPENDIX A – Geometric Labeling

This appendix was developed in the interest of facilitating the identification of each geometry within its own category. A modified version of Table 7 and Table 8 from the document is included below, where each family category is once again listed and color coded.

Table 32 – Color coded appendix table with geometric family listing.

ID	Family
A	Concentric Cylinder Boss
B	Cylinder Boss
C	Pins
D	Hemispheres
E	Circular Holes
F	Square Boss
G	Horizontal Cylinders
H	Staircases
I	Inclines
J	Rectangular Boss
K	Cone
L	Outer Dimensions
M	Square Notches
N	Vertical Cylinders
O	Concentricity
P	Planes

Figure 79 – General location of each geometry throughout the artifact.

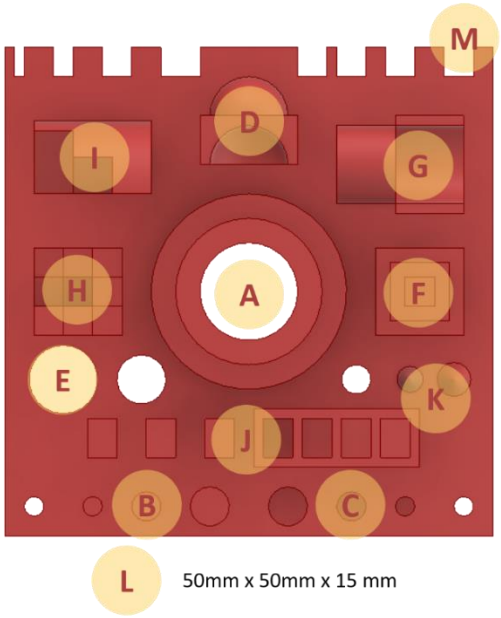

Figure 79 above associates the information presented in Table 32 to the physical location of each geometry in the artifact part. The following figures will discriminate and label each geometry within a specific category. Strictly speaking, each individual geometry will be designated a letter and number with which it will become distinguishable.

Figure 80 – Geometric labelling for A, B, C and L.

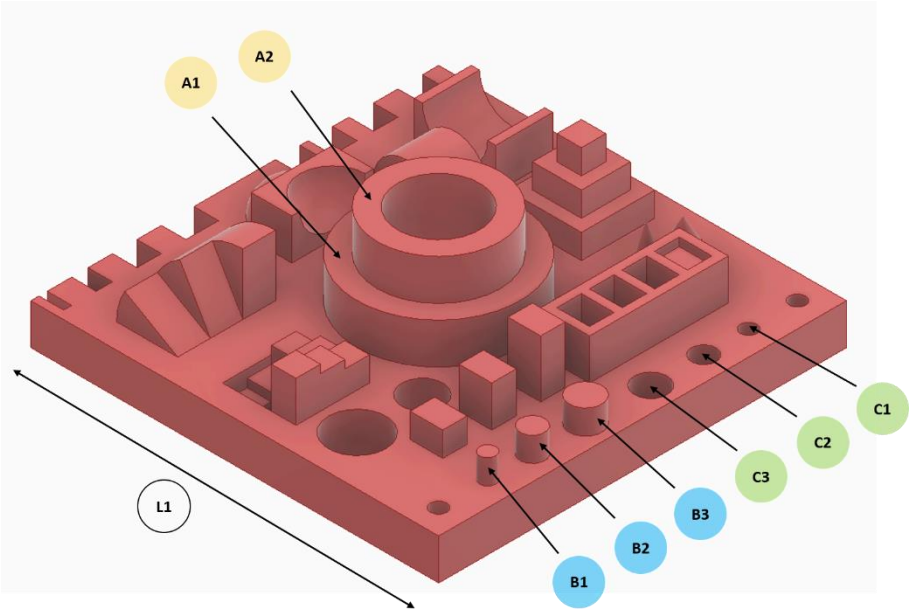

Figure 81 – Geometric labelling for D, E, I, K, G.

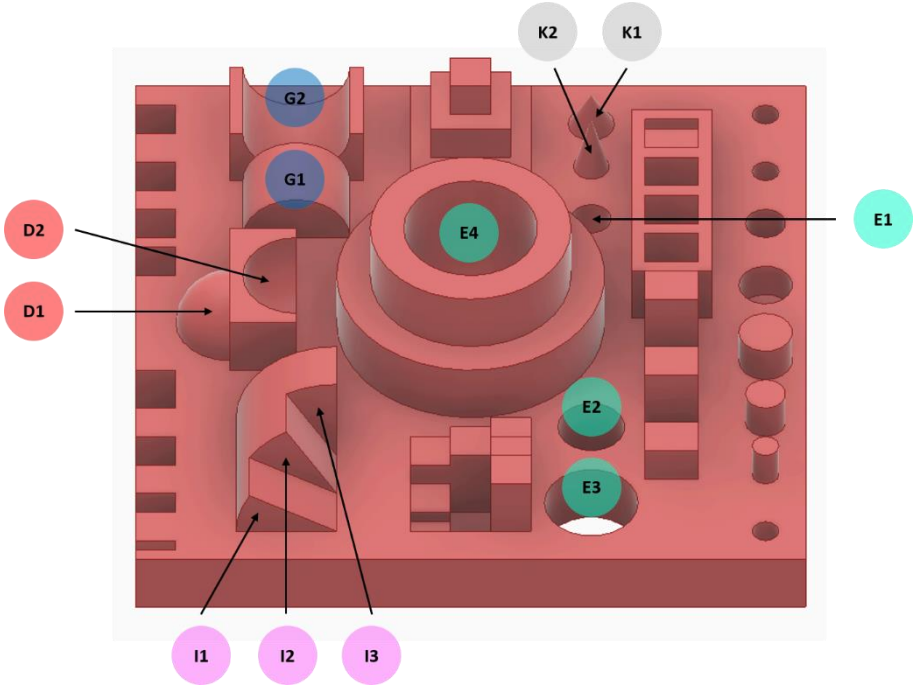

Figure 82 – Geometric labelling for F, H, J, M.

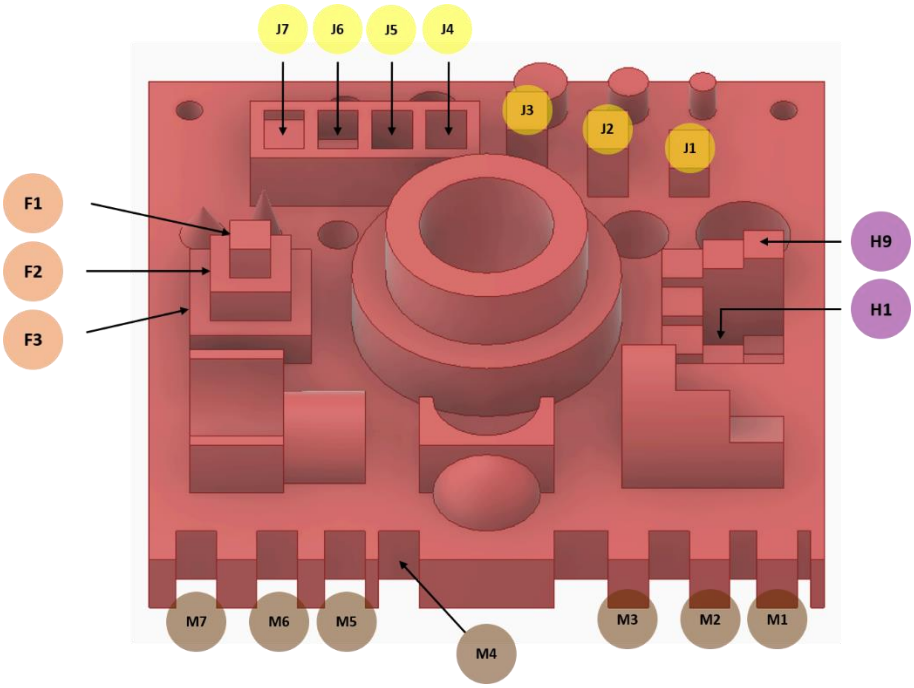

Labels were also assigned to some derivative geometric aspects: vertical cylinders, concentricity, and horizontal planar features. These features were assigned specific flags in order to organize the data and analysis worksheets. Horizontal planes are presented in Figure 83, while vertical cylinders and their combinations that are used to evaluate concentricity are indicated in Figure 84.

Figure 83 – Geometric labelling for horizontal planes (P).

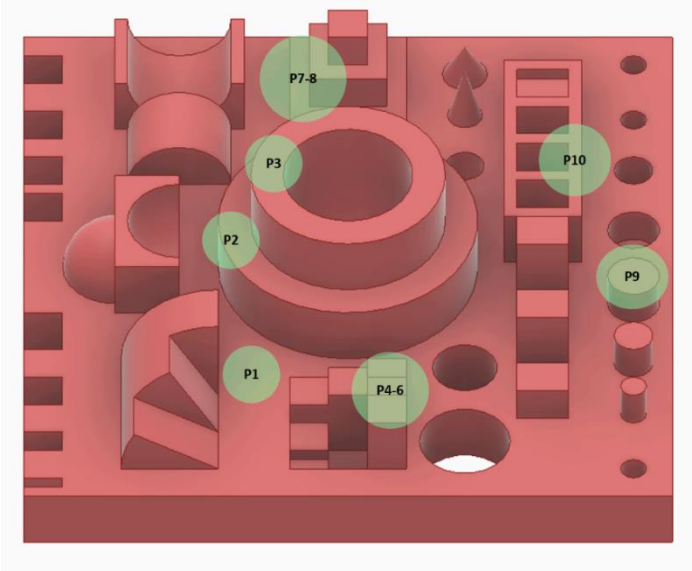

Figure 84 – Geometric labelling for concentricity (O).

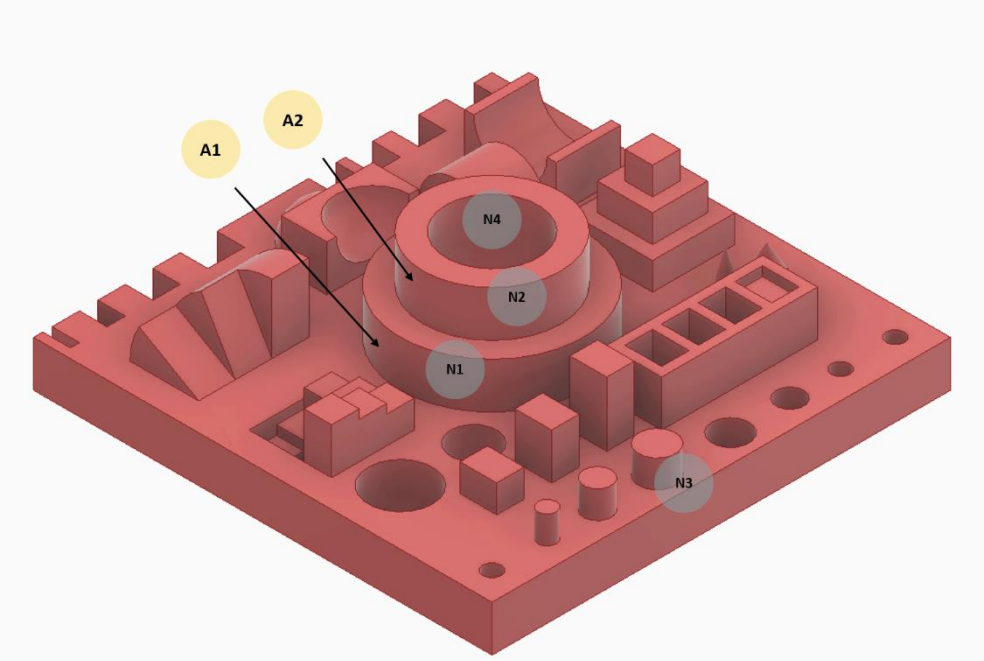

Figure 85 – Combination of labels regarding concentricity.

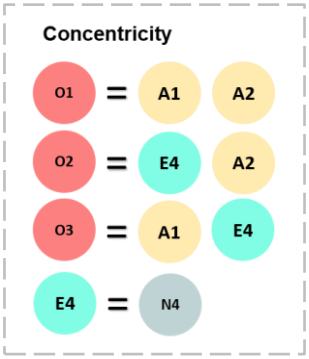

APPENDIX B – Summary of Resins

In this Appendix a summary of resins can be found. The following sheet-images contain a detailed description of each resin, with each name, price, quality, and machine in which it may be applied.

Figure 86 – Information sheet for the S-Clear Sharebot Resin (Rover).

DLP Fabrication

- **Machine name:** SHAREBOT ROVER DLP PRINTER
- **Material name:** SHAREBOT S-Clear Resin
  - Color: Transparent
  - Young's Modulus: 2310 MPa
  - Strength at break (Tensile; Flexural): (47,3 MPa; 71,04 MPa)
  - Hardness: SCALE D 81,7
  - Price: 199.00 €/kg
- **Support type:** Column Supports
- **Fabrication arrangement on bed:** 45° at 10mm from base
- **Initial spacing:** 0.3 mm
- **Layer quality:** 50 µm (0.05 mm)
- **Fabrication time:** about 14 hours

Figure 87 – Information sheet for the PR-S Sharebot Resin (Antares).

SLA Fabrication

- **Machine name:** SHAREBOT ANTARES SLA PRINTER
- **Material name:** SHAREBOT PR-S Resin (high precision resin)
  - Color: Grey
  - Young's Modulus: 1750 MPa
  - Strength at break (Tensile; Flexural): (30 MPa; 35 MPa)
  - Hardness: SCALE D 77
  - Price: 149.00 €/kg
- **Support type:** Column Supports
- **Fabrication arrangement on bed:** 45° at 10mm from base
- **Initial spacing:** N/A
- **Layer quality:** 50 µm (0.05 mm)
- **Fabrication time:** about 4 hours

Figure 88 – Information sheet for the VeroWhitePlus RGD835 Resin (Objet30).

PolyJet Fabrication

- **Machine name:** STRATASYS OBJET30 PRIME
- **Material name:** VeroWhitePlus RGD835
  - Color: Opaque White
  - Young's Modulus: 2500 MPa
  - Strength at break (Tensile; Flexural): (58 MPa; 93 MPa)
  - Hardness: SCALE D 85
  - Price: about US$300,00/kg
- **Support type:** No supports required
- **Fabrication arrangement on bed:** No required angle
- **Initial spacing:** N/A
- **Layer quality:** 30 µm and 15 µm
- **Fabrication time:** about 7,5 hours

APPENDIX C – Manufacturing Images

In this Appendix a group of images that refer to the fabrication of each replica have been attached. All images are of self-authorship and have been prepared in the laboratorial spaces of Politecnico di Torino.

I. SHAREBOT ROVER – DLP MANUFACTURING

Figure 89 – Sharebot Rover machine at Politecnico di Torino.

Figure 90 – Sharebot Rover details with respect to the build platform and resin vat.

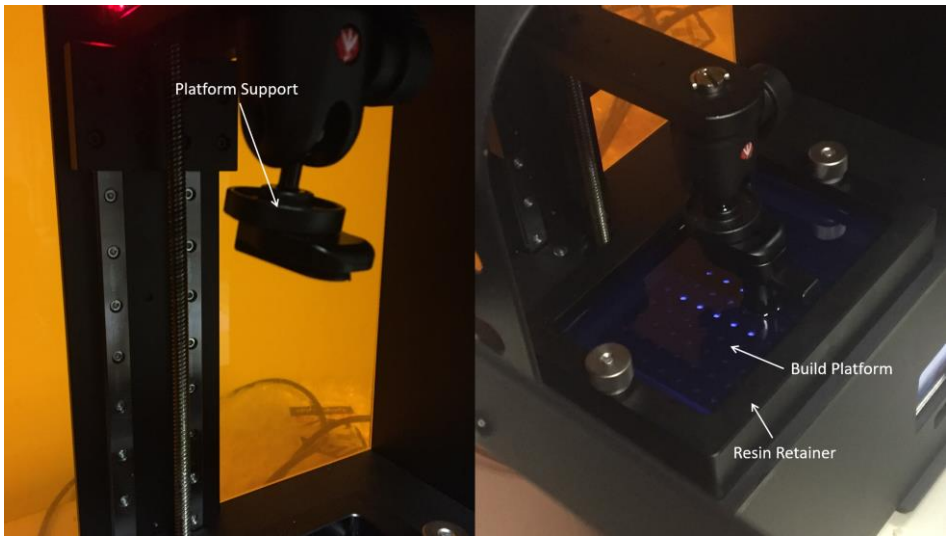

Figure 91 – Sharebot Rover upon initialization of the manufacturing process.

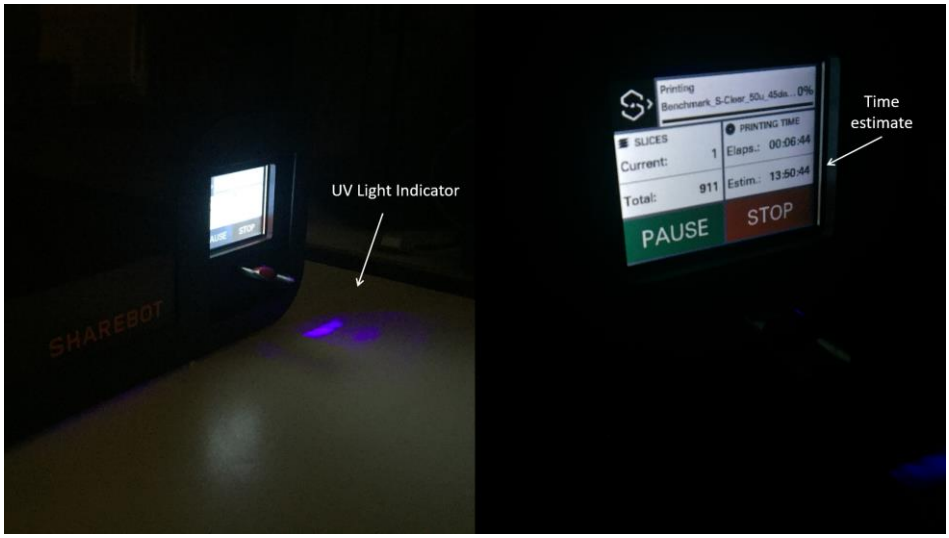

Figure 92 - Sharebot Rover after completion of the part; Highlights produced artifact and supports.

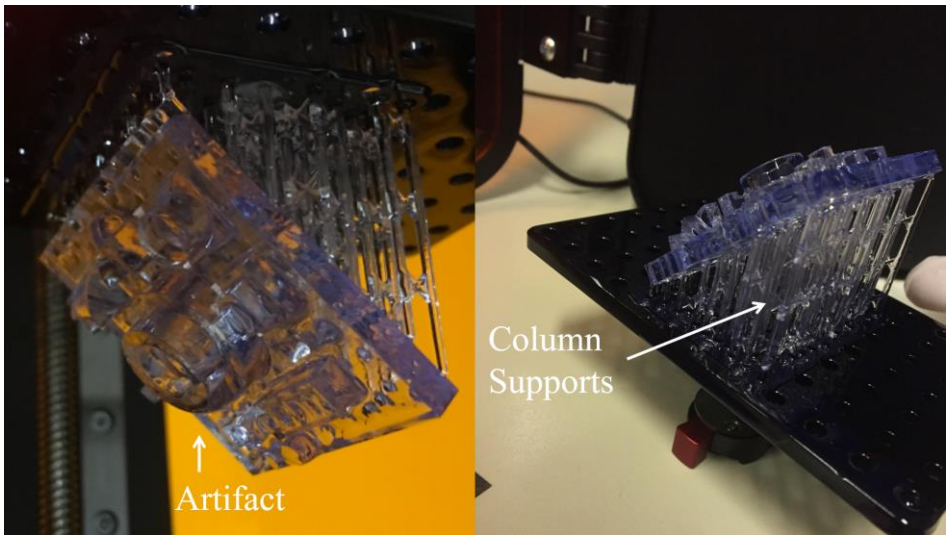

Figure 93 – Part removal from the build platform.

Figure 94 – Sharebot resins: S-Clear (DLP, left) and PR-S (SLA, right); Highlights the information on the label of the S-Clear resin.

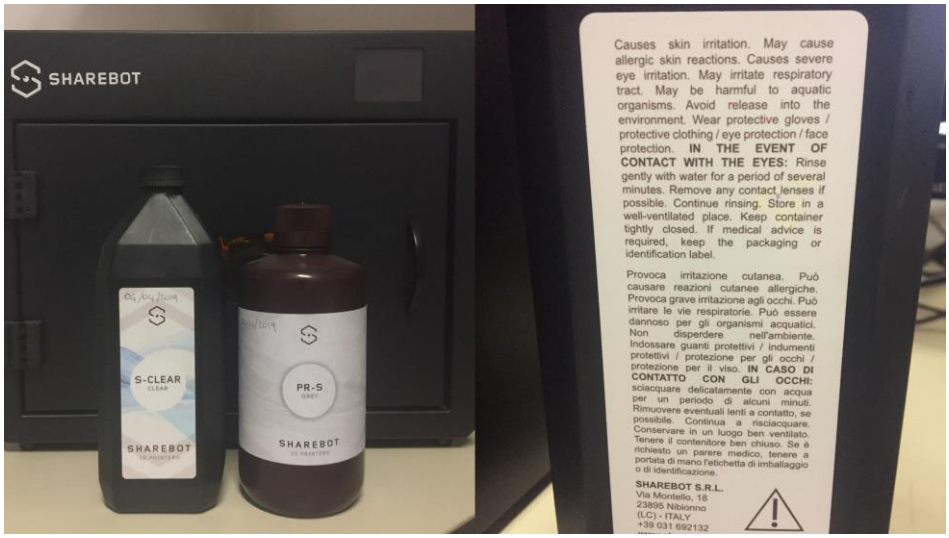

II. SHAREBOT ANTARES – SLA MANUFACTURING

Figure 95 – Opened Sharebot Antares and preparison; Highlights platform and establishes a reference of size (screw).

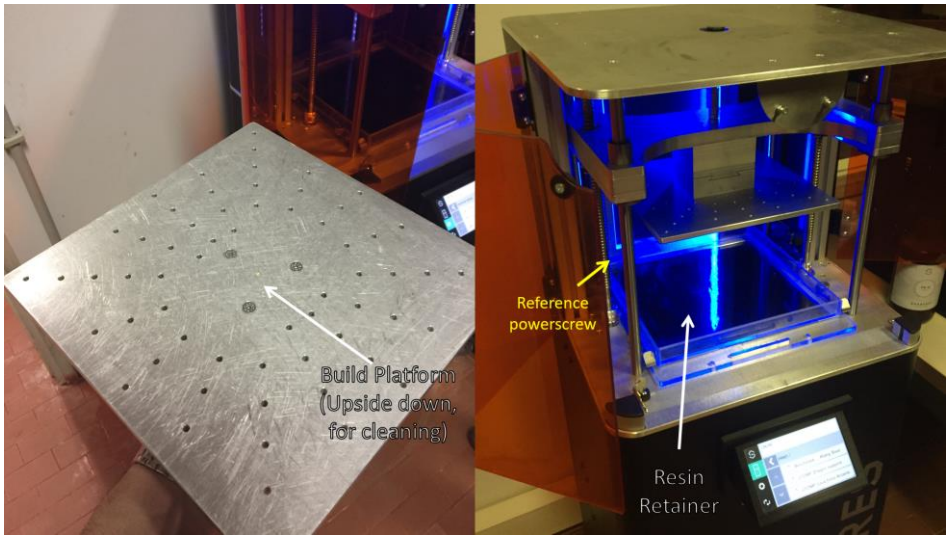

Figure 96 – Sharebot Antares interior during fabrication; Highlights the current UV curing point whilst referring to a reference of size (screw).

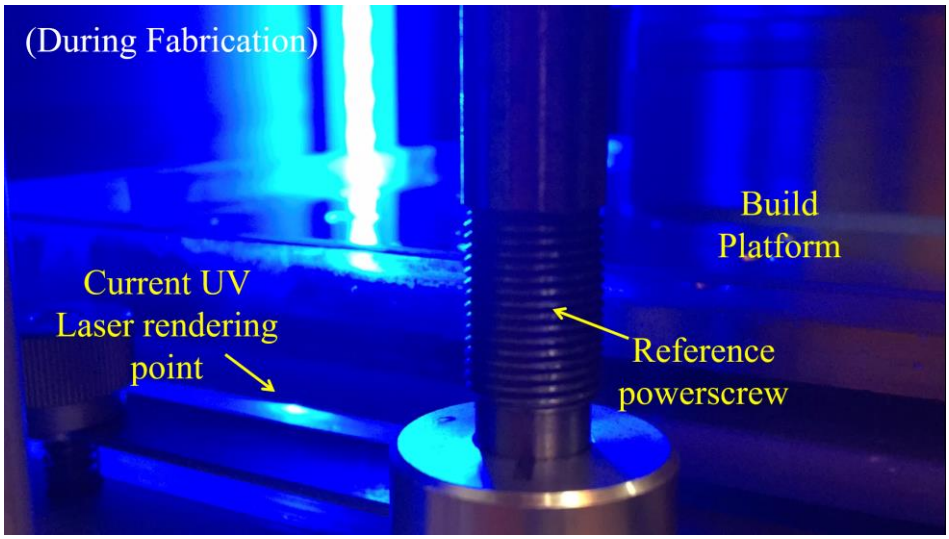

Figure 97 – SLA and DLP parts after fabrication.

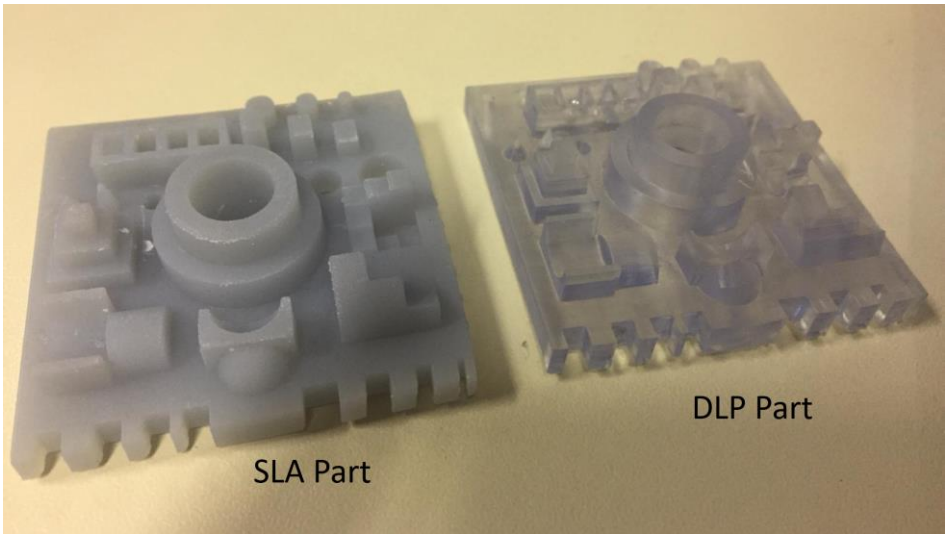

Figure 98 – Images of the post-processing equipment: Digital ultrasonic cleaner and isopropyl (left) and UV curing chamber (right).

Figure 99 – Image of the interior of the UV chamber whilst post-curing is occurring for the DLP and SLA parts.

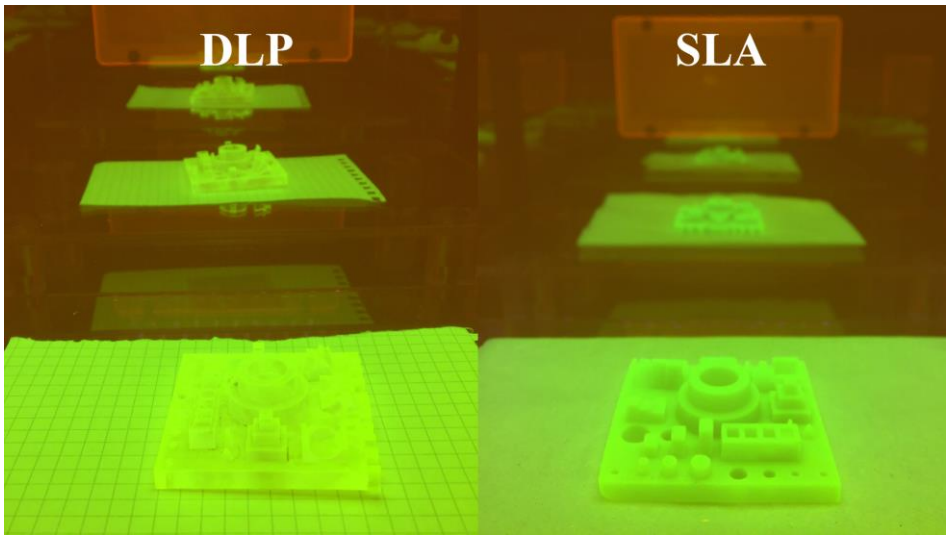

III. STRATASYS OBJET30 PRIME – POLYJET MANUFACTURING

Figure 100 – Stratasys Objet30 (left), VeroWhitePlus resin used (right, superior), and initialization data of the Objet30 with fabrication time estimate (right, inferior).

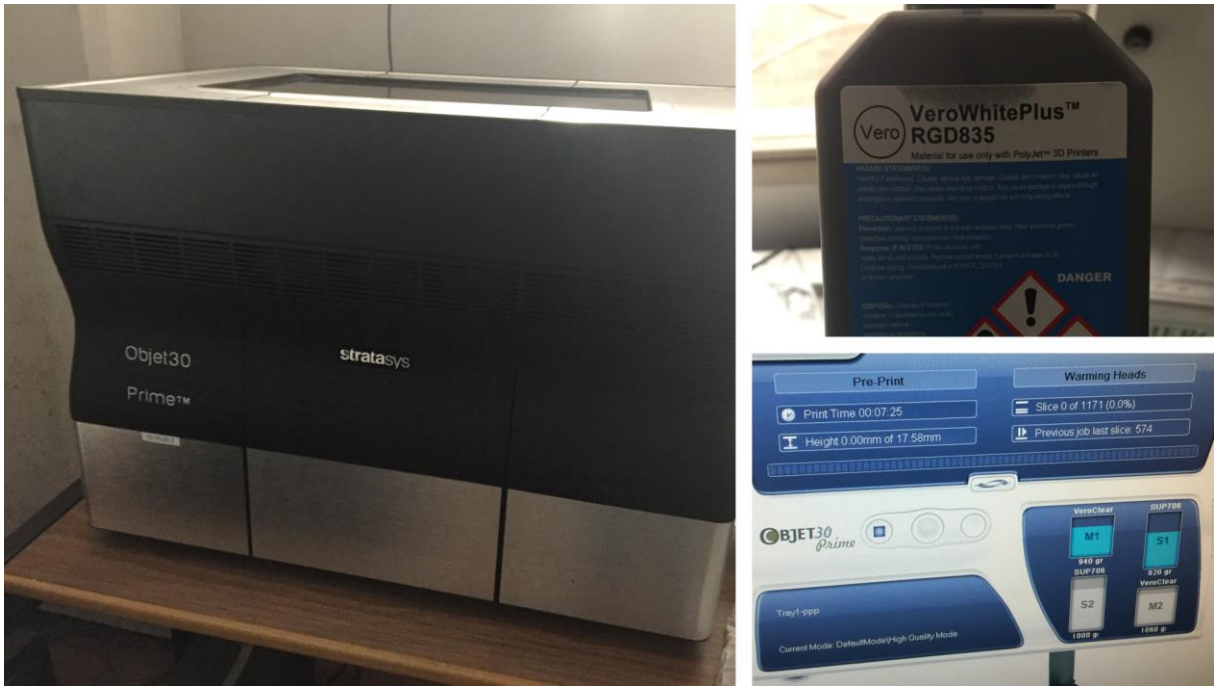

Figure 101 – Collection of frames from a recording of the PolyJet fabrication.

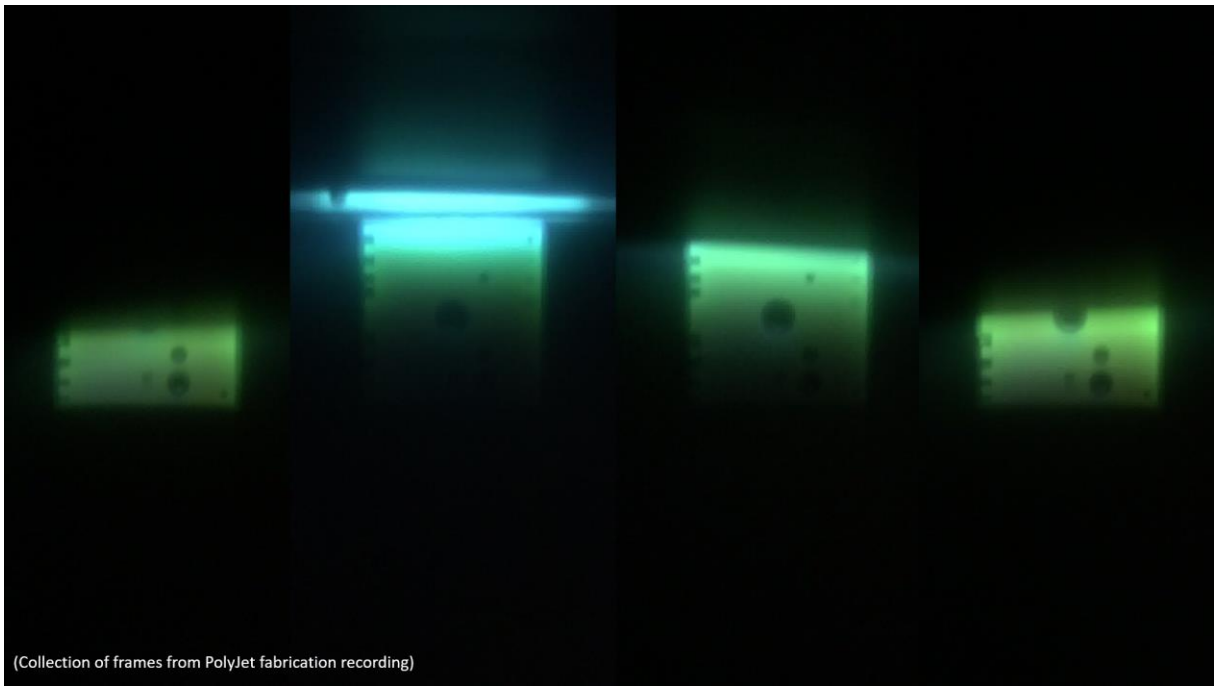

Figure 102 – PolyJet washing after fabrication in a cleaning tank with pressurized water.

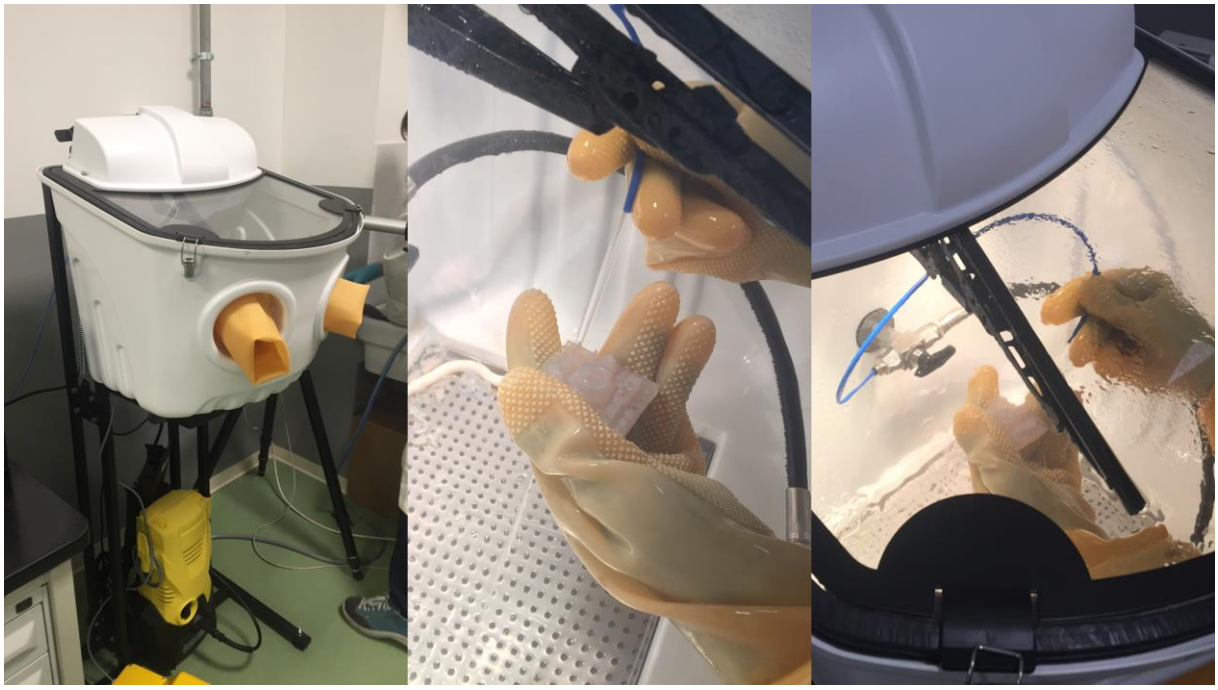

APPENDIX D – Photos of the produced reference parts

Figure 103 – Close range image of the PolyJet part for visual detail (lateral I).

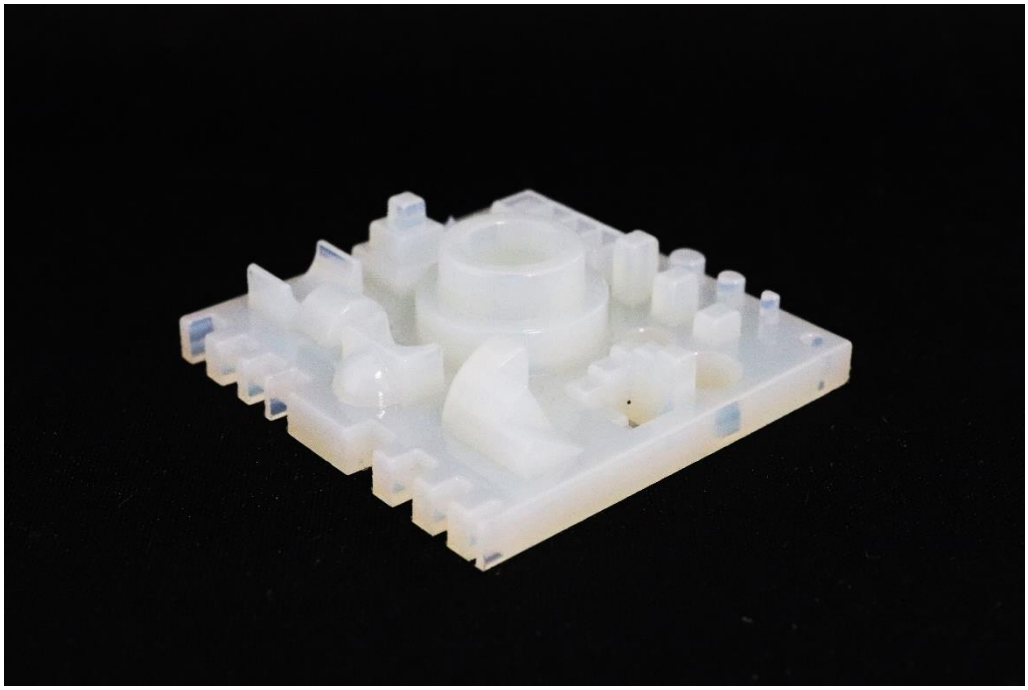

Figure 104 – Close range image of the PolyJet part for visual detail (superior).

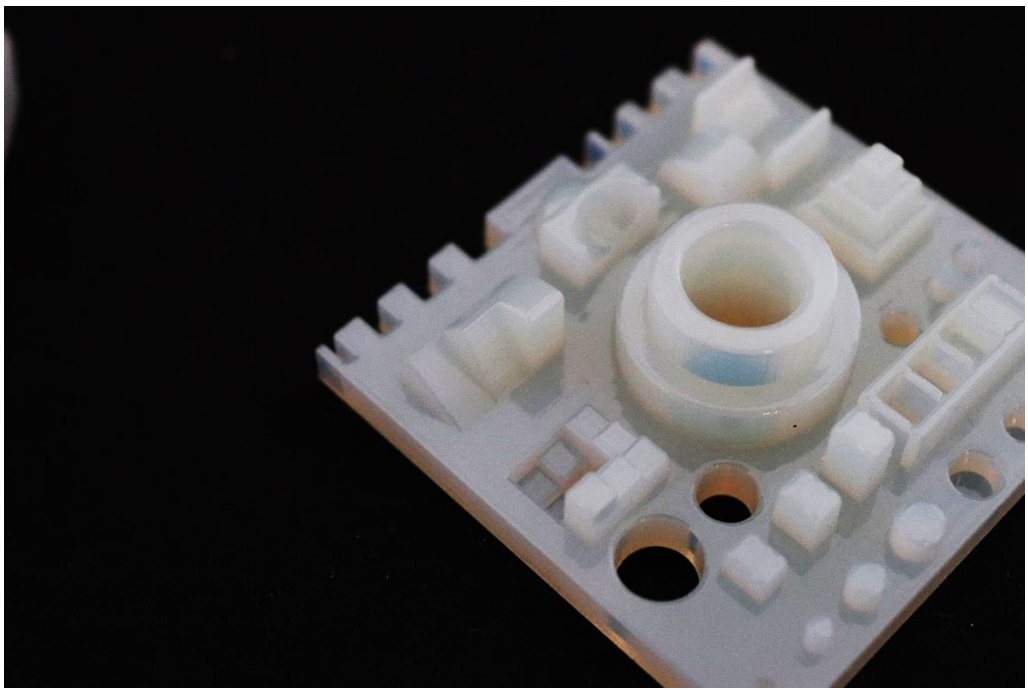

Figure 105 – Close range image of the PolyJet part for visual detail (lateral II).

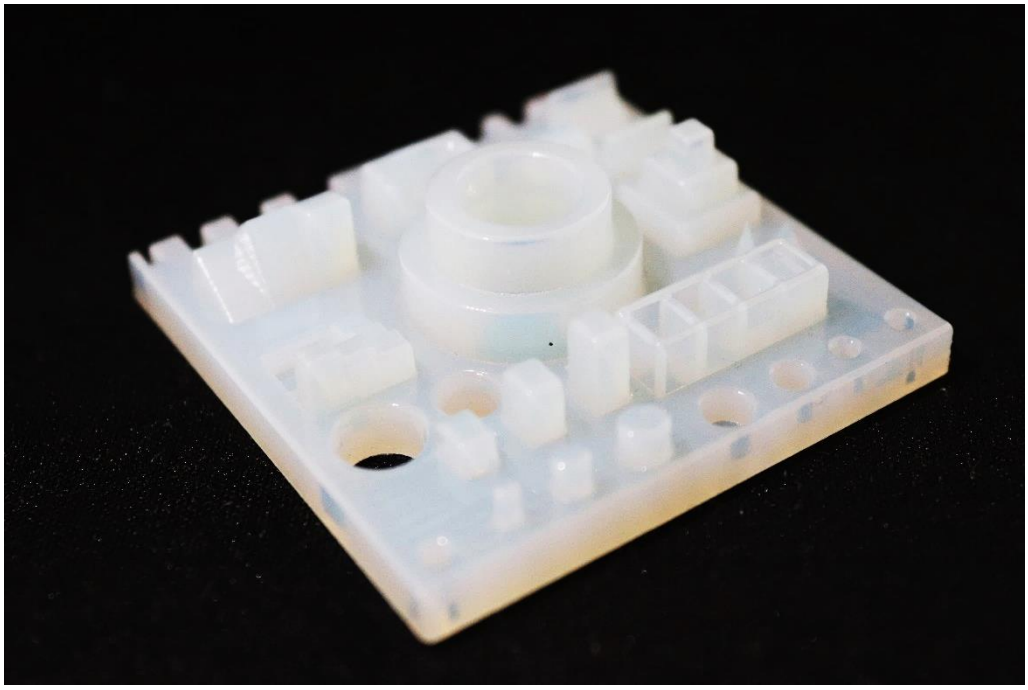

Figure 106 – Close range image of the PolyJet part for visual detail (lateral III).

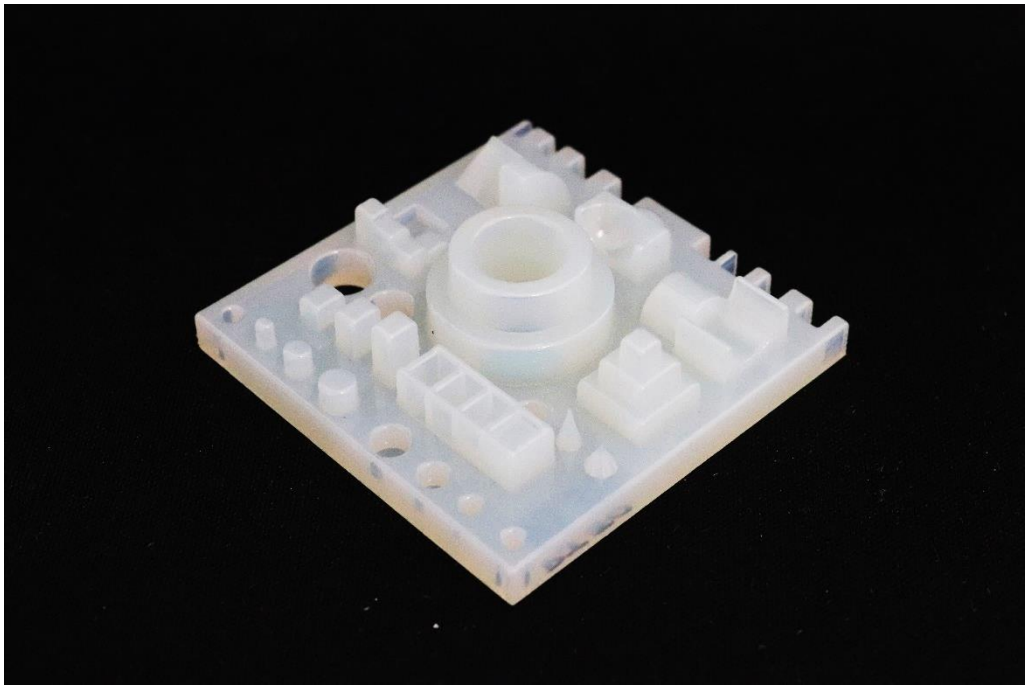

Figure 107 – Close range image of the PolyJet part for visual detail (lateral IV).

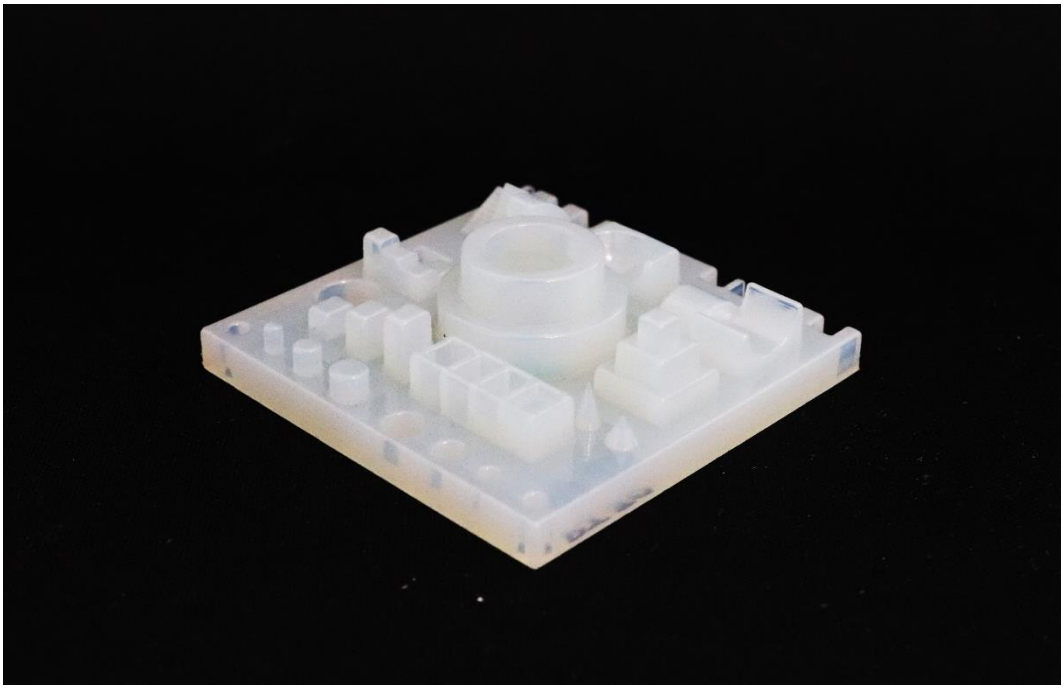

Figure 108 – Close range image of the DLP part for visual detail (lateral IV).

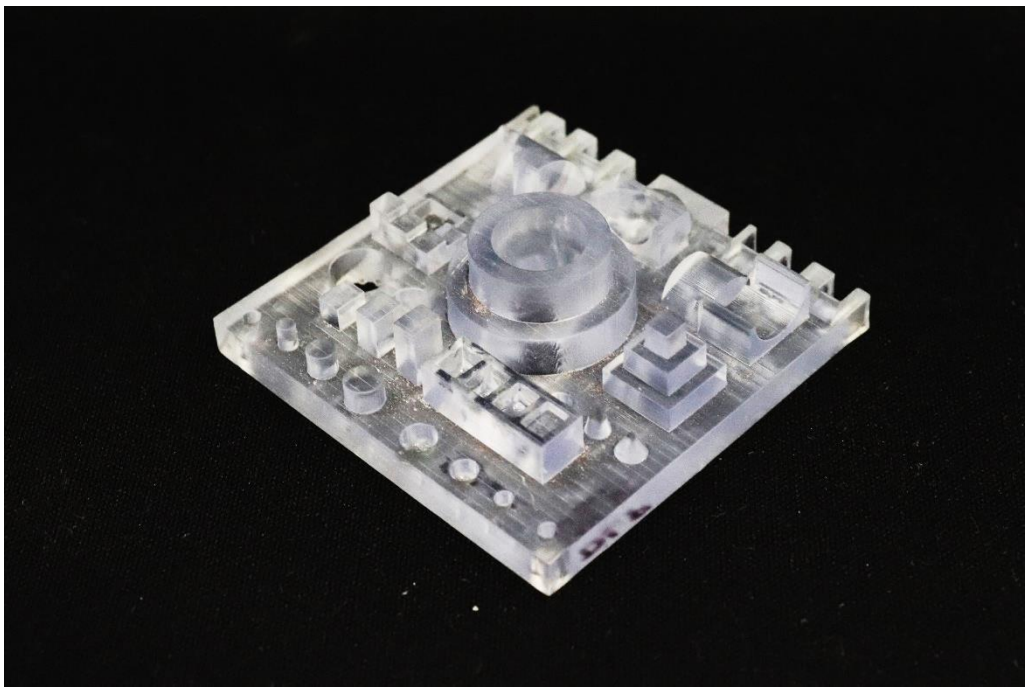

Figure 109 – Close range image of the SLA part for visual detail (lateral IV).